

Model membranes for drug- membrane interaction studies

by

Daniel K. Suhendro

Thesis

Submitted to Flinders University

for the degree of

Doctor of Philosophy

College of Science and Engineering

16 March 2018

Table of Contents

Abstract	iii
Declaration	iv
Acknowledgments.....	v
List of abbreviations.....	vi
Chapter 1 General introduction	1
1.1 The cell membrane.....	1
1.2 Model membranes.....	3
Chapter 2 Methods.....	8
2.1 Surface plasmon resonance spectroscopy	8
2.2 Electrochemical impedance spectroscopy	14
2.3 Ultraviolet-visible spectroscopy	21
2.4 Dynamic light scattering	21
2.5 Contact angle measurement	23
2.6 Zeta potential measurement	23
2.7 Fourier transform infra-red spectroscopy	25
2.8 Transmission electron microscopy.....	26
Chapter 3 Drug-membrane Interaction.....	27
3.1 Introduction	27
3.1.1 Drug-membrane interaction studies by techniques other than SPRS or EIS	28
3.1.2 Drug-membrane interaction studies using SPRS technique	32
3.1.3 Drug-membrane interaction studies using EIS technique.....	34
3.1.4 Previous research on CPZ interaction with membranes	35
3.1.5 Research aims and objectives	48
3.2 Experimental	50

3.2.1 Materials.....	50
3.2.2 Gold coated slides preparation and functionalisation	50
3.2.3 Formation of tBLM.....	51
3.2.4 Drug-membrane interaction	51
3.3 Results and Discussion.....	52
3.3.1 Monolayer self-assembly and bilayer formation	52
3.3.2 CPZ-tBLM interaction	56
3.3.3 EIS results	67
3.4 Conclusion and outlook	69
Chapter 4 Tethered liposome coated gold nanoparticles	70
4.1 Introduction.....	70
4.1.1 Research aims and objectives	72
4.2 Experimental	73
4.2.1 Materials.....	73
4.2.2 AuNP synthesis and functionalisation	73
4.2.3 Coating AuNPs with DPhyPC	75
4.3 Results and discussion	80
4.3.1 AuNP synthesis and functionalisation	80
4.3.2 Liposome coating of functionalised AuNPs	85
4.4 Conclusion and outlook	91
Chapter 5 Summary and outlook	93
Appendix: Chemical compounds and their chemical structures	95
References	104

ABSTRACT

Many model membranes have been developed and used to simplify the study of the processes that happen on the cell membrane. One of the processes is drug-membrane interaction. Studying drug-membrane interaction is important because many drugs have been designed to either interact with a cell membrane component or to pass through the membrane into the cell.

In the first part of this work drug-membrane interaction was studied using tethered bilayer lipid membrane (tBLM) as the model membrane and CPZ (Chlorpromazine) as the model drug. The aim of the study was to determine the mechanism of drug binding and accumulation on the membrane. The result of the interaction study showed that accumulation of drugs on the membrane did not depend on the free binding sites on the membrane but rather on the concentration of the free drug. This trend did not continue forever but there was a limit in which no more drugs could bind to the membrane. The limit was indicated by overshoots where at first the amount of drug binding to the membrane increase quickly but then decreased more slowly.

In the second part of this work, a three dimensional model membrane was developed. This three dimensional model was a spherical tBLM with gold nanoparticle core to anchor the tethered lipids. This model membrane, a tethered liposome coated gold nanoparticles should be more stable than liposomes. This is the aim of the second part in this work, to synthesise a novel model membrane consisted of gold nanoparticle core coated with liposomes in which the inner layer of lipids are tethered to the core by tethered lipid molecules.

The constructs were to be made in three stages: first is the synthesis of gold nanoparticle, second is the functionalisation of the nanoparticle with thiolipids and third coating the thiolipids with lipid. Although the aim was to make tethered lipid bilayer to the gold nanoparticle core, this cannot be fully realised. What was finally achieved was the assembly of gold nanoparticle functionalised with thiol molecules and coated with lipids. This work is still in the proof of concept stage and further work need to be done to synthesise the tethered liposome model membrane.

Overall, this thesis contributes to the research of drug-membrane interaction, particularly on the binding and accumulation of drugs to the membrane. It also contributes to the attempt to synthesise a novel model membrane that can further advance the research in drug-membrane interaction as well as drug carriers.

DECLARATION

I certify that this thesis does not incorporate without acknowledgement any material previously submitted for a degree or diploma in any university; and that to the best of my knowledge and belief it does not contain any material previously published or written by another person except where due reference is made in the text.

Daniel K. Suhendro

ACKNOWLEDGMENTS

I am very grateful to the Lord Jesus Christ who provided me with this opportunity to undertake a PhD degree at Flinders University. Without Your grace and love I would not be able to start and finish this study well.

I am also thankful to Ingo Köper for supervising me and giving good advice while I am in this journey. I am also grateful over the much assistance you gave whenever there were problems with the instruments used in the experiments. Thank you for many fruitful discussions during our weekly and even group meetings.

I would also like to thank Jakob Andersson and Julius Zieleniecki for the various help they gave regarding the preparation of the tethered bilayer lipid membranes, and methods to ensure reproducibility between batches.

I would like to thank Melanie Fuller for teaching me how to synthesise gold nanoparticles using the Turkevich method.

I am thankful to Ashley Slattery for taking the transmission electron photos of the amine capped gold nanoparticles.

I would like to thank my friend Abdulrahman Tuama because in asking me many questions, I learned more about surface plasmon resonance spectroscopy as a result. I also learned something about protein adhesion to surfaces.

I want to acknowledge Australian National Fabrication Facility who provided the thermal evaporator instrument which is one of the necessary equipment to do my experiments.

I am thankful to Flinders University for the Flinders University Research Scholarship which helped me greatly to focus on my studies without worrying about everyday living.

I am thankful for my father, mother, and sisters in Jakarta Indonesia who continually gave me support during my PhD candidature. I also want to thank Bethel International Church Adelaide for being my spiritual family here in Adelaide, especially Pastors John and Elvy Toming.

LIST OF ABBREVIATIONS

AC	alternating current
AFM	atomic force microscopy
AmB	amphotericin B
ANFF	Australian National Fabrication Facility
ATR	attenuated total reflection
AuNP	gold nanoparticle
C	capacitor, capacitance
CA	contact angle
CAD	cationic amphiphilic drug
CE	counter electrode
CHOL	cholesterol
CPE	constant phase element
CPZ	chlorpromazine hydrochloride
DCM	dichloromethane
DDTh	1-dodecanethiol
DLS	dynamic light scattering
DMPE	1,2-Dimyristoyl-sn-glycero-3-phosphoethanolamine
DMSO	dimethyl sulfoxide
DNA	deoxyribonucleic acid
DPhyPC	1,2-di-O-phytanoyl-sn-glycero-3-phosphocholine
DPhyTL	2,3-di-O-phytanyl-glycerol-1-tetraethylene glycol-D,L-lipoic acid ester lipid
DPPC	1,2-dipalmitoyl-sn-glycero-3-phosphocholine
EDC	1-Ethyl-3-(3-dimethylaminopropyl)carbodiimide
EIS	electrochemical impedance spectroscopy
EPC	egg phosphatidylcholine
EtOH	ethanol
F	Farad
FTIR	Fourier transform infrared spectroscopy
HAuCl ₄	chloroauric acid
HBM	hybrid bilayer membrane
HCl	hydrochloric acid
HDFDTh	3,3,4,4,5,5,6,6,7,7,8,8,9,9,10,10,10-Heptadecafluoro-1-decanethiol
HEPES	4-(2-hydroxyethyl)-1-piperazineethanesulfonic acid
His	Histidine
HNO ₃	nitric acid
HPLC	high performance liquid chromatography
Hz	Hertz
IR	infrared
IRRAS	infrared reflection absorption spectroscopy
I-V	current-voltage
LUV	large unilamellar vesicles
M	molar
MagI	magainin I
MDS	molecular dynamic simulation
MDZ	midazolam hydrochloride

mem	membrane
MilliQ	MilliQ water, ultrapure water
MPTS	3-mercaptopropyltrimethoxysilane
NaBH ₄	sodium borohydride
NaCl	sodium chloride
nD	refractive index
NHS	N-Hydroxysuccinimide
NSAID	nonsteroidal antiinflammatory drug
ODA	octadecylamine
PE	phosphatidylethanolamine
PL	phospholipid layer
PM-IRRAS	polarisation modulated infrared reflection absorption spectroscopy
Pol.	polariser
POPC	1-palmitoyl-2-oleoyl-sn-glycero-3-phosphocholine
Pt	platinum
ptBLM	protein tethered lipid bilayer membrane
θ	angle
R	reflectivity, resistor, resistance
RE	reference electrode
rotavap	rotary evaporator, evaporation by this instrument
SANS	small angle neutron scattering
SAXS	small angle x-ray scattering
sc	space charge
SCS	sodium cholesteryl sulphate
SEM	scanning electron microscopy
SLB	supported lipid bilayer
SM	sphingomyelin
sol	solution
SPR	surface plasmon resonance
SPRS	surface plasmon resonance spectroscopy
Synp	Synperonic
tBLM	tethered lipid bilayer membrane
TEM	transmission electron microscopy
TIR	total internal reflection
TX-100	Triton X-100
UV-Vis	ultraviolet-visible spectroscopy
Ω	Ohm
WAXS	wide angle x-ray scattering
WE	work electrode
Z	complex impedance
ZP	zeta potential

CHAPTER 1 GENERAL INTRODUCTION

The plasma membrane is the boundary that defines a biological cell [1]. It is an interesting area of research because many important processes happen at the membrane; one of them is molecular transport across the membrane. Plasma membranes also act as either the barrier for drugs that are designed to enter the cell or as the site of action for drugs that are designed to bind to membrane proteins.

The cell membrane is a very complex structure that consists of many types of lipids, proteins, and carbohydrates. Because cell membranes are very complex, a simpler system that still retains the important characteristics of the membrane is needed for systematic studies. These model systems have been used to study membrane proteins and drug-membrane interaction. Each of the model systems has its own advantages and disadvantages.

Here, two different model systems have been used and developed. First, a tethered membrane architecture has been employed to investigate drug-membrane interaction. Second, a new model membrane based on gold nanoparticles and liposomes has been developed. Before discussing these studies, the cell membrane and its models will be reviewed, followed by a description of the analytical techniques used in the second chapter. The drug-membrane interaction experiment and results will be discussed in the third chapter and the development of model membranes based on gold nanoparticles and liposomes will be discussed in the fourth chapter.

1.1 The cell membrane

There are two kinds of membranes in the cell, the plasma membrane and the membranes that define the cell's organelles [1, 2]. A cell's plasma membrane keeps dangerous substances outside the cell while it permits beneficial and nutritious substances inside and allows passage of waste from inside of the cell to the outside [2]. The plasma membrane, from now on referred as the membrane, also permits exchange of electrical signals between cells for communication [1].

The membrane is composed of various molecules but primarily it is composed of lipids/fats, proteins and carbohydrates (Figure 1.1). The lipids are the very basis of the membrane. They usually form a double sheet, called bilayers [3], but they can also form other structures than bilayers such as micellar, hexagonal, and cubic phases [4].

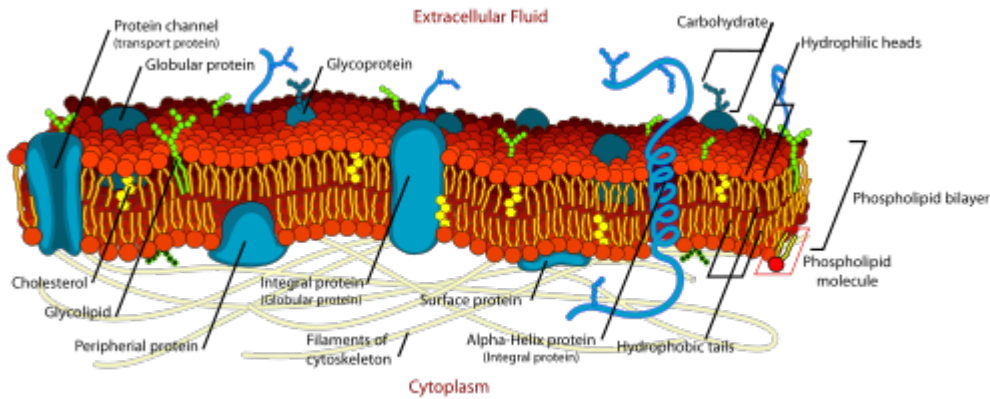


Figure 1.1 A simplified model of a cell membrane. The main components of the membrane are lipid bilayer, membrane proteins, and carbohydrates. There are many kinds of lipids, proteins, and carbohydrates in a cell membrane, and their composition depends on the kind of the cells.

The membrane bilayer is composed of several different types of lipids, forming domains. The types of lipids that form the bilayer structure include phospholipids, sphingolipids, glycolipids, and sterols [4]. Lipids are amphiphilic molecules with a hydrophilic head group and a hydrophobic tail group. The head group faces the outside of the bilayer while the tail group faces the inside of the bilayer. The proteins which are essential for cell functions are dispersed in the bilayer. Some proteins are adsorbed on the surface of the lipid bilayer and can be removed with relative ease; they are called the peripheral proteins [4, 5]. Some proteins have part of their structure buried in the membrane and even span the whole bilayer; these proteins are difficult to separate from the bilayer and are called integral proteins [4, 5]. Finally, the carbohydrates are covalently attached to the outside part of some of the integral membrane proteins [5].

The fluid mosaic membrane model proposed by Singer and Nicolson assumes that the proteins and lipids can freely diffuse across the whole membrane, which will cause a homogeneous distribution of these components [4, 6]. Recent research has shown that the diffusion of lipids and proteins is actually restricted, causing the membranes to have mosaic-like appearance with different microdomains [6-9]. This heterogeneity is actually important for the correct functioning of cells [6]. Each domain is composed of different lipids and proteins. The lipids and protein are free to move within the domain but they have difficulty passing from one domain to the other [9]. Aside from different lipid composition in each domain, the lipid composition in the inner and outer leaflet of the bilayer are usually different, this is called cross-sectional asymmetry [6, 9]. Certain cells also have a well-defined regions of membranes (apical, lateral and basal) with different lipid compositions [9]. The lipids themselves have different shapes and the shapes can influence the phases of the membrane. Lipids

which are roughly shaped like a cylinder usually forms planar bilayer phase but lipids which are roughly shaped like cones or truncated cones usually form a hexagonal phase [4, 6]. Even for the bilayer phase there are various forms of interdigitation between the inner and outer leaflet [9]. All these complexity made the cell membrane hard to study. A simpler model is needed to understand the basic properties of the membrane. The model's degree of complexity can then be adjusted to approximate the properties of real cell membrane as needed.

1.2 Model membranes

Some of the model membranes used to investigate membrane processes, including drug-membrane interaction, are vesicles, also called liposomes [10-12], freestanding bilayer lipid membranes, also called black lipid membranes [13, 14] and bilayers on solid support [2, 12, 15, 16] as shown in Figure 1.2. There are also tethered vesicles [17-19] (Figure 1.3).

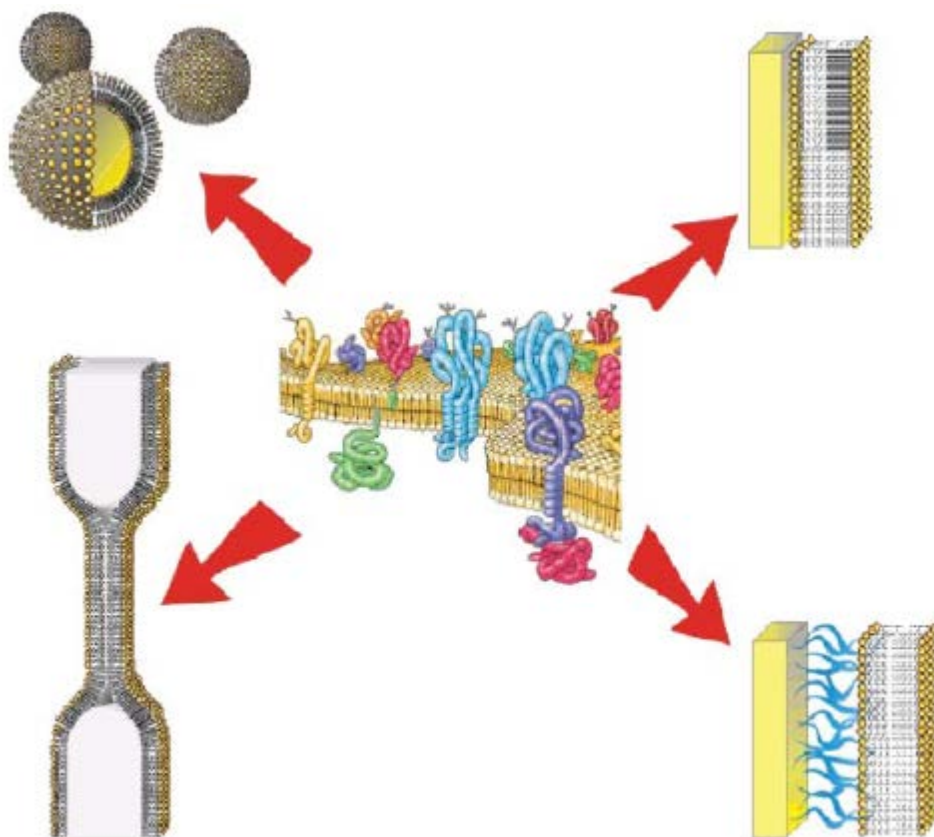


Figure 1.2 Some of the model membranes used in drug-membrane interaction studies. The top left corner is liposomes or vesicles, the top right corner is supported lipid bilayer membrane, the bottom right corner is tethered lipid bilayer membrane and the bottom left corner is freestanding lipid bilayer membrane or black lipid membrane. Reused from [13] with permission of the Royal Society of Chemistry.

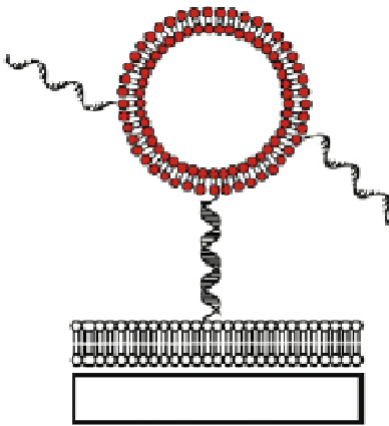


Figure 1.3 Tethered vesicle model membrane. The vesicle is tethered to a solid supported bilayer membrane by hydrogen bonding between the complementary strands of a DNA molecule. Reused from [17] with permission of Elsevier.

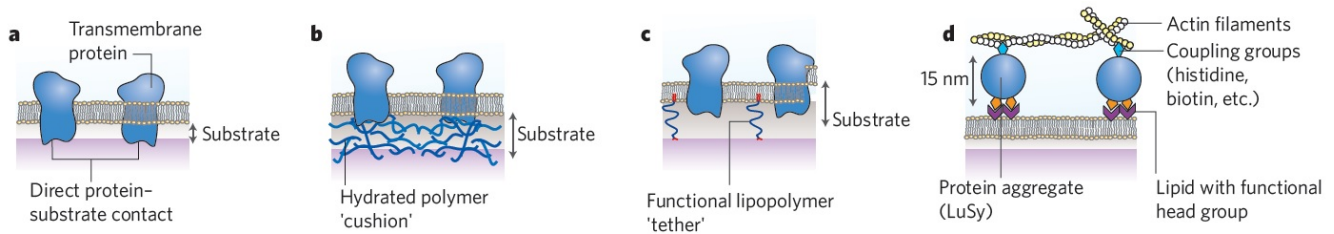


Figure 1.4 Several kinds of bilayers on solid supports. a is supported lipid bilayer, b is polymer cushioned bilayer, c is tethered bilayer and d is actin attachment on supported lipid bilayers using protein spacers. Reused from [2] with permission of Springer Nature.

Bilayers on solid supports are further divided into supported lipid bilayers (SLBs) [20-23], polymer cushioned lipid bilayers, [24] tethered bilayer lipid membranes (tBLMs) [25, 26], and supported membranes with spacers [27] (Figure 1.4). All these model membranes preserve the basic structure and component of the cell membrane, namely the lipid bilayers and they can be modified to the needed complexity level, for instance by incorporating proteins and transporters and maybe even carbohydrates.

There is one model system which resembles the supported lipid bilayer membranes but is not true lipid bilayer called the hybrid bilayer membrane (HBM) [16]. This membrane is actually composed of lipids as the upper leaflet and hydrophobic tethering molecules as the bottom leaflet. To form this membrane, vesicles are deposited on a substrate functionalised with hydrophobic tethers, causing the vesicles to burst and form a lipid monolayer on top of the tethers. The tethers are usually alkanethiol molecules (Figure 1.5).

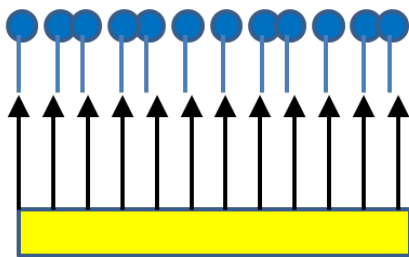


Figure 1.5 Hybrid bilayer membranes consist of a monolayer of lipid as the upper leaflet and tethering molecules as the bottom layer.

Each model membrane system has its own advantages and disadvantages. Liposomes and freestanding lipid bilayers have the advantage of being relatively easy to prepare compared to the rest of the model membranes. But they are less stable and cannot be characterised by surface sensitive techniques. Bilayers on solid supports are more robust and can be characterised by surface sensitive techniques [17]. But the formation of bilayers on solid support usually depend on vesicle fusion process that is kinetically uncontrollable.[28] Supported lipid bilayers that sit directly on the support have an additional disadvantage in that if transmembrane proteins are included, the proteins may lose their function as well as their lateral mobility because of the direct contact of the proteins and the support. One solution to the mobility problem is the use of proteins as spacers (Figure 1.4d). In this setup, the actin filaments which are representatives of the membrane protein are separated from the supported lipid bilayer by protein spacers. The filaments are attached to the spacers by coupling groups. The protein spacers themselves are attached to the upper leaflet of the bilayer and do not penetrate into the solid support. In this way the actin filaments retain their lateral mobility. Other solutions are polymer cushioned membranes and tBLMs (Figure 1.4 b and c). By introducing a cushion or tether between the membrane and the solid support, the protein does not change conformation and function and they do not lose their mobility. The tBLMs furthermore have an advantage in which the membrane-support distance and the fluidity/viscosity of the membrane can be controlled by choosing the length and the spacing of the tether molecules [2]. For the polymer cushioned membrane, these parameters are determined only by the type of the polymer [2]. The tethers also provide space for water and ions, acting as a reservoir [13]. In addition to these advantages, tBLMs are also easy to prepare and are robust up to several days. Yet another solution to protein-solid support contact problem is the tethered vesicles on solid supported bilayer. Here the proteins can be incorporated to liposomes which has one strand of DNA sticking out of it. The complementary strand is attached to the supported lipid bilayer and the two strand will bind together when the liposome is flowed on the bilayer. Although the model membrane shares the advantage with supported lipid bilayer that has spacers between the membrane

and the support in keeping the proteins from contacting the support, the model membrane is more difficult to make because of the need to attach oligonucleotides to the liposome and to the supported lipid bilayer. In addition to that, any membrane studies that can be done on tethered vesicles can be done also on lipid bilayers with spacers.

After surveying several model membranes, tBLM seems to have more advantages than disadvantages compared to other model membranes. Although it is more complex than liposomes, freestanding lipid bilayers and lipid bilayers that directly sits on the solid support, it is more robust than them. It is also simpler than bilayers with protein spacers or vesicles tethered to bilayers. And compared to cushioned bilayers, tBLMs have more significant submembrane space that can mimic the interior of cell membrane. Considering these factors, tBLMs are an indispensable platform to further drug-membrane interaction studies. Therefore, tBLMs were chosen as the model membrane for the first part of this work.

Rebaud et al [16] reviewed the use of tBLMs in membrane protein studies but mainly focusing on strategies to form tBLMs and incorporate proteins. The simplest and most common one is to use anchor lipid where the head group is modified with a functional tether to tether the proximal part to the substrate [29]. The bilayer is then completed by vesicle fusion. There are other strategies in tBLM formation. One strategy is to self-assemble peptide spacers on a substrate. One end of the peptide of course contains functional group that can covalently bind to the substrate surface. The free end of the peptide spacer is activated by EDC/NHS coupling so that they can bind lipids which have amines in their head group, e.g. DMPE. [30] After DMPE lipids bind to the peptides forming the bottom layer, the final layer of the bilayer is then formed by vesicle fusion. This form of tBLM has been demonstrated as suitable for protein incorporation.[31] Another strategy to form tBLMs is by direct fusion of vesicles containing spacer and anchor molecule on substrates functionalised with amino containing molecules. [32] By including the spacer and anchor molecules in the vesicles, the percentage of these molecules can be controlled more easily compared to the previous method. This allows for lower spacer density which will enable incorporation of proteins with large extramembrane domains. [16] A related approach is to use biotin/streptavidin coupling in which biotinylated vesicles is accumulated on streptavidin layer previously formed on biotin functionalised surface. [28] Vesicle fusion is triggered by adding polyethylene glycol, instead of uncontrolled spontaneous fusion, resulting in a continuous bilayer without defects. Yet another strategy involves proteins directly coupled to the functionalised surface before the formation of lipid bilayer around the protein, called a protein tethered

bilayer lipid membrane (ptBLM). First, nitrilotriacetic molecules are grafted to the substrate and activated by chelating Cu^{2+} or Ni^{2+} ions. Then His-tagged proteins solubilised in detergent solution are attached to the surface by the reversible binding of the His-tags and metal ions. Finally, the detergent solution is replaced with another detergent solution containing lipid micelles and the detergent is exchanged with lipids using dialysis. This will result in lipid bilayer forming around the immobilised proteins. [33, 34] This approach is only useful for studies where protein mobility is not important or the protein needs to be directly wired to the metal substrate. [16] The last strategy reviewed in this paper is making tBLM using DNA as spacers. DNA sense strands are printed on a patterned substrate and vesicles containing the antisense DNA strand are then deposited. [35] The sense and antisense strands will bind to each other and the vesicles fuse forming a bilayer. Rebaud et al. noted that one of the applications of tBLMs is the lab on a chip technology where proteins need to be immobilised on stable membrane platforms. [16] Despite the advancements of tBLM fabrication, they also noted that intracellular studies are still not feasible even with tBLMs. Also difficulties remain in making tBLMs composed of more than one type of lipids.

CHAPTER 2 METHODS

This work used several characterisation methods. For the drug-membrane interaction study, Surface Plasmon Resonance Spectroscopy (SPRS), Electrochemical Impedance Spectroscopy (EIS), Ultraviolet-Visible spectroscopy (UV-Vis), Dynamic Light Scattering (DLS), and Contact Angle measurement (CA) were used. For the liposome coated gold nanoparticle study, DLS, UV-Vis, zeta potential measurement (ZP), Fourier Transform Infra-Red spectroscopy (FTIR), and Transmission Electron Microscopy (TEM) were used. The following is a description of each of these techniques.

2.1 Surface plasmon resonance spectroscopy

Surface plasmon resonance spectroscopy (SPRS) is a surface sensitive technique that uses light and plasmon to detect refractive index changes in a thin film at the metal-dielectric interface [36, 37]. It is a label free technique that can be used to study the interactions of biological molecules, although the application is not limited to this. One of the advantages of label-free detection techniques is that the biological molecules studied can have their natural activity not compromised by the presence of labels either fluorescent or radioactive. This way, the conditions of molecules studied by SPRS closely reflect the *in vivo* condition. A surface plasmon is an excitation of electronic charge oscillations that occurs in the interface of metal and dielectric [36], typically air or water. The surface plasmon can be excited by a method called attenuated total reflection (ATR). The setup to achieve this method is called the Kretschmann geometry [36, 38] (Figure 2.1).

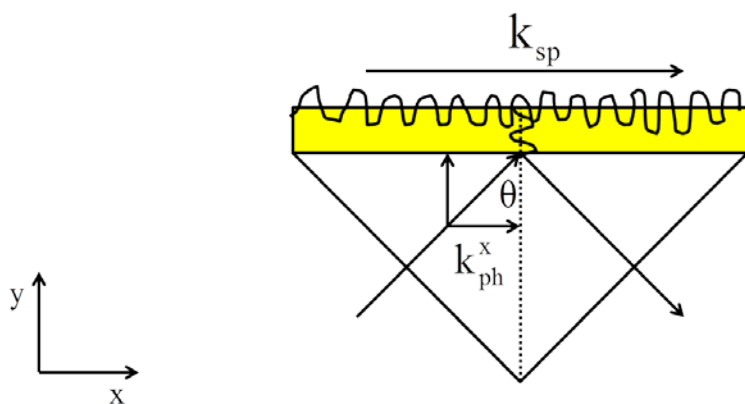


Figure 2.1 The geometry needed to excite surface plasmons. The evanescent part of the electromagnetic wave is indicated by the vertical wavy line across the gold layer. The horizontal wavy line indicates surface plasmon. The glass substrate is usually a prism. See text for definition of θ , k_{ph}^x , and k_{sp} .

The figure shows a layer of gold, on top of a glass substrate, usually a prism. The gold film is inside a flow cell. When a laser light is shone on the base of the prism above a certain incidence angle all the laser will be reflected in the prism with no transmission. This condition is called total internal reflection (TIR). During TIR, the tail part of the reflected light actually penetrates the thin gold film into the gold-dielectric interface. This part of penetrating light is the evanescent wave [36] and is responsible for the excitation of the surface plasmon. To excite the surface plasmon, the resonance condition of matching the x component of light momentum k_{ph}^x and the plasmon momentum k_{sp} must be satisfied. [38] Figure 2.2 shows how this condition can be achieved. The photons from a laser source have an angular frequency of ω_L . k_{ph}^x can be varied along the line ω_L by varying the angle of incidence θ ($k_{ph}^x = k_{ph} \sin\theta$). The momentum varies with incidence angle from zero, given by point 0 in Figure 2.2 to a maximum value at incidence angles near, but not including, 90° . The maximum k_{ph}^x of the photon at ω_L is given by the dispersion relation curve of the photons. The dispersion relation of reflected photons at a metal-dielectric interface without prism coupling is shown by the solid line. So, the value of maximum k_{ph}^x is given by point A. As can be seen from the figure, point A, even the entire dispersion relation curve, is always smaller than the dispersion relation of the surface plasmons given by the SP line in the figure. At low angular frequencies the SP asymptotically approached the solid line while at high angular frequencies the SP approached a maximum angular frequency ω_{max} . This frequency is dependent on the plasma frequency of the metal. The evanescent wave has momentum values higher than the simple reflected light, with the dispersion relation given by the dot-dash line in the figure. Because of the prism coupling to the metal-dielectric interface, now k_{ph}^x can vary from point 0 to C. This means that at a certain incidence angle, the resonance condition $k_{ph}^x \equiv k_{sp}$ will be fulfilled (point B in Figure 2.2). At this resonance angle, the evanescent wave resonates with the surface plasmon, causing its excitation and the reflected light is attenuated.

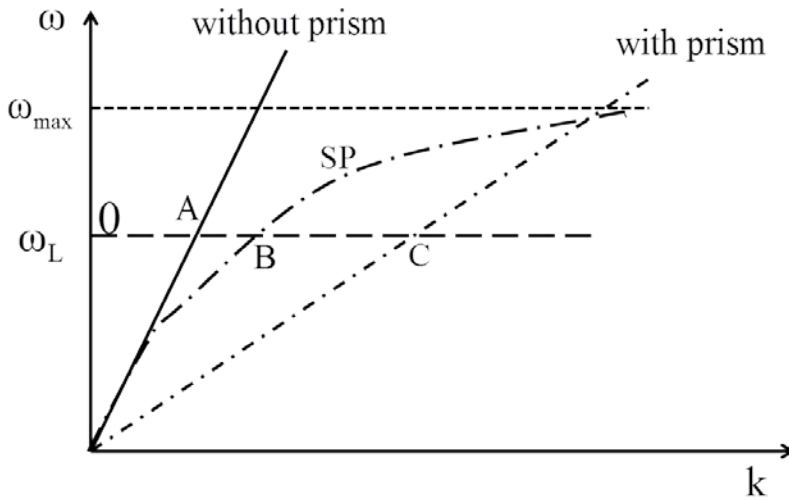


Figure 2.2 The dispersion relation between x component of electromagnetic wave and surface plasmon. SP refers to the surface plasmon dispersion curve, the straight line is the free photon dispersion and the dot-dash line is the photon dispersion in prism. ω_L and ω_{max} refers to the angular frequency of the photons and the maximum angular frequency respectively. See text for explanation of 0, A, B and C. Modified from [38] with permission from Annual Reviews.

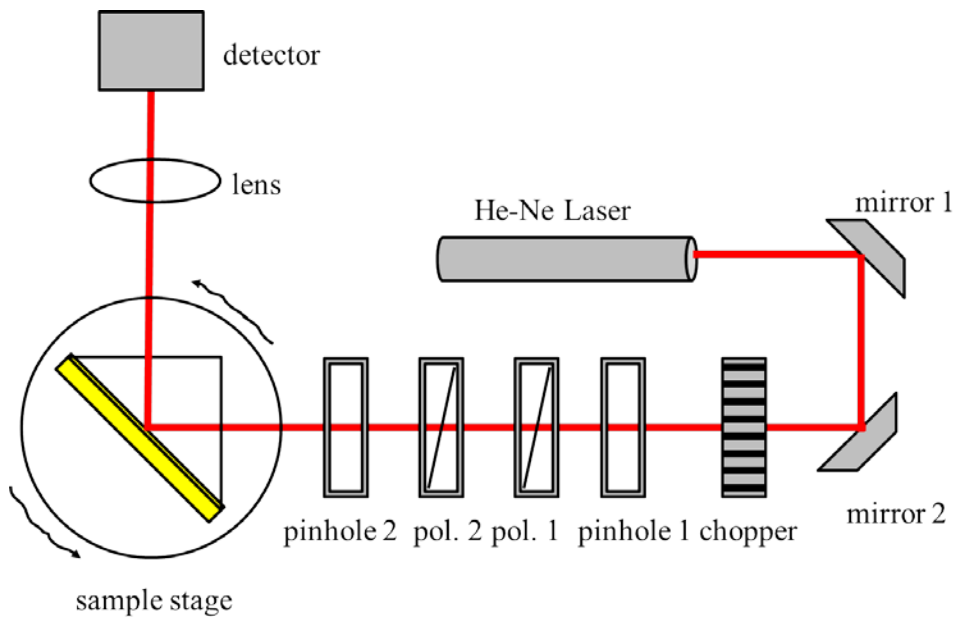


Figure 2.3 The instrumentation setup for SPRS experiments. Pol refers to polarisers. The sample mount can be rotated to change the angle of incidence and reflection.

The SPR instrument used in this work was custom made. The setup for a typical SPRS experiment is depicted in Figure 2.3 [39]. The laser light from a helium-neon source is passed through a series of

pinholes, polarisers and a chopper. The pinholes serve to align the laser pathway to the prism and detector. The chopper is connected to a frequency lock and serves to ensure that the SPRS instrument is measuring only at a single frequency. The chopper also filters out ambient light from detection. The first polariser's function is to convert the unpolarised laser to p-polarised because p-polarisation is a necessary condition for surface plasmon excitation [36, 38]. The second polariser controls the intensity of the laser. Finally the lens focuses the reflected light onto the detector. During an SPRS experiment, the whole assembly of prism, gold film and flow cell is mounted on a rotating goniometer and the reflected light is monitored by a detector. The sample goniometer is rotated simultaneously with the detector while the reflected light intensity (reflectivity) is measured as a function of the incident angle. The resulting reflectivity vs angle is depicted in Figure 2.4.

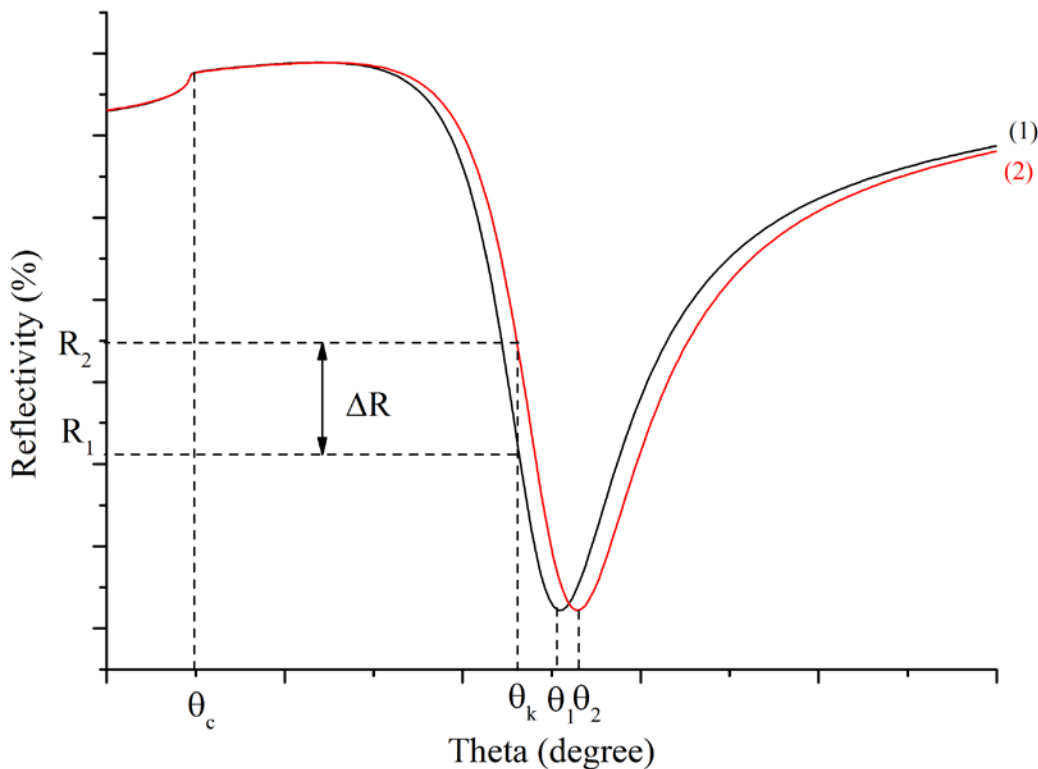


Figure 2.4 Diagram explaining the angle shift caused by the addition of a layer on top of the surface. (1) is the plasmon curve before layer addition and (2) is the plasmon curve after addition. ΔR is the reflectivity difference after addition of a material. R_1 and R_2 are the reflectivity before and after layer addition while θ_1 and θ_2 is the resonance angle before and after layer addition. θ_c is the incident angle in which TIR occurred. θ_k is the fixed angle where the changes in reflectivity are observed for kinetic measurement.

The θ_c is where the total internal reflection starts to happen. The resonance angle θ_1 is shown as a sharp dip in the reflectivity. At this angle the reflected light is extinguished because the light is absorbed to stimulate the surface plasmon. If a layer of material is deposited on top of the gold, the refractive index of the interface where the surface plasmon is located is changed because of the presence of the

additional layer and the resonance angle shifts to a higher value θ_2 . Reflectivity as a function of incidence angle is actually given by the Fresnel equations. The reflectivity curve can be fitted to the equations if the thickness and dielectric constant parameters are given [38] This is easily done by using Winspall software. By fitting the angle vs reflectivity curve and comparing the curve before and after layer addition, the thickness of the layer can be determined. This angle scan mode is useful to determine the thickness of the tBLM. The starting parameter values for SPRS curve fitting used in this work is listed in Table 2.1. The parameters include complex dielectric constants which are related to the complex refractive index. The real part of the dielectric constant corresponds to the refractive index and the imaginary part of the dielectric constant corresponds to the attenuation or absorption of the laser by the layer.

Table 2.1 Layer parameters used in SPRS curve fitting. Dielectric constant values for glass, chromium, gold, air, water, and lower layer lipid was taken from the SPR Quick datasheet (<http://www.res-tec.de/pdf/res-tec-optical-constants-database.pdf>). The upper layer lipid dielectric constant is taken from [25].

Layer	Optical thickness (nm)	Dielectric constant (real part)	Dielectric constant (imaginary part)
Glass (LaSFN9)	∞	3.4036	0
Chromium	2	-6.3	9.7
Gold	50	-12.3	1.29
Lower layer	2.5 - 5	2.25	0
Upper layer	5 - 6	2.1025	0
Air	∞	1	0
Water/ NaCl solution	∞	1.778	0
CPZ Buffer	∞	1.782	0

The shift of the resonance angle can also be monitored as a function of time; this is the time or kinetic measurement mode. In this mode, an angle near the resonance angle is chosen, typically an angle which gives 20-25% reflectivity. This is shown as R_1 in Figure 2.4. The detector and sample goniometer are then fixed at the corresponding angle θ_k , and as the resonance angle shifts because of addition of materials, the reflectivity value will increase with time to R_2 . This mode is useful to confirm drug binding or release from the membrane as well as studying the drug-membrane interaction kinetics. In the course of a drug-membrane interaction experiment, the reflectivity will increase or decrease with time when drugs are bound or released from the membrane. The typical kinetic curve from a drug-membrane interaction kinetic experiment is seen in Figure 2.5.

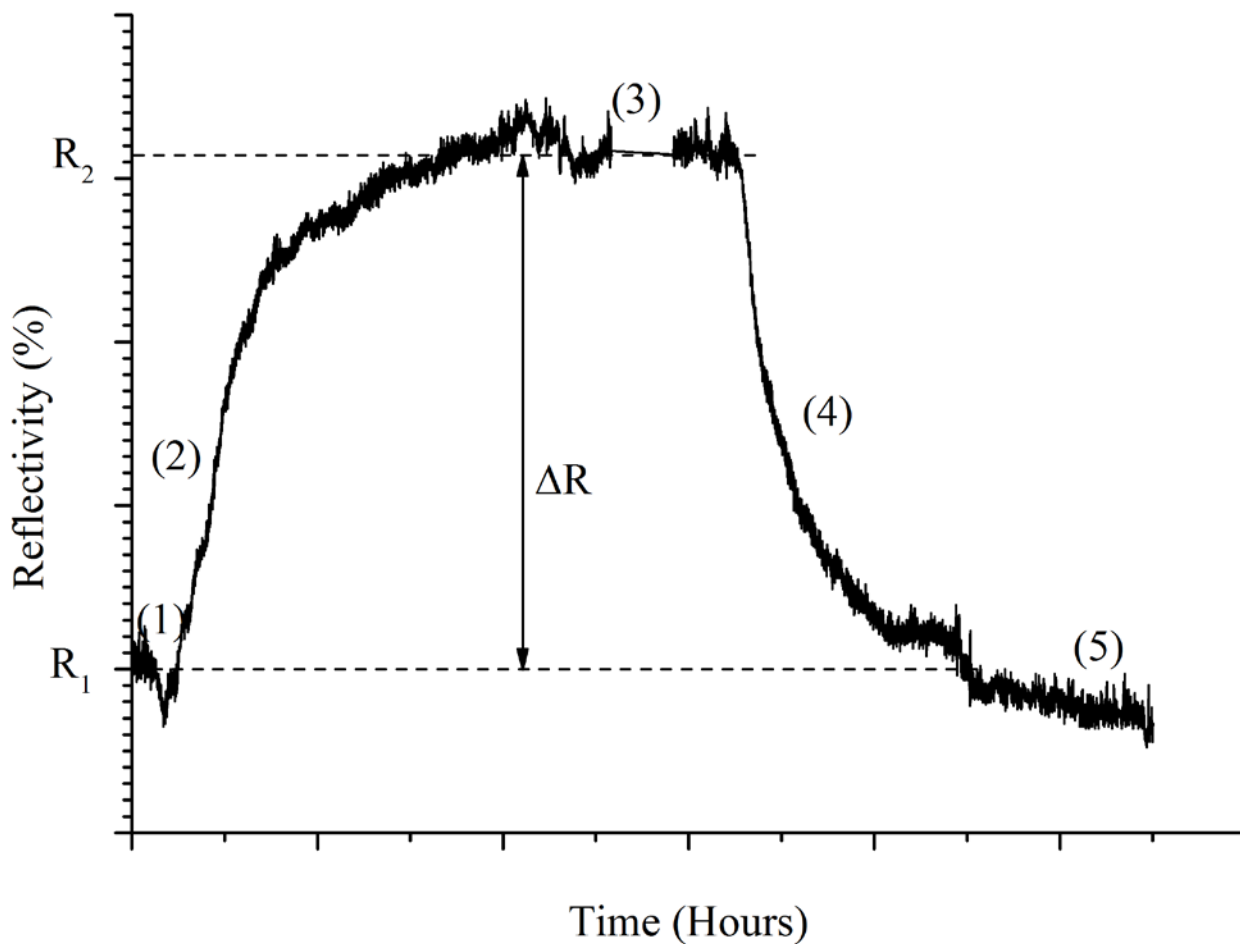


Figure 2.5 An example of drug-membrane interaction kinetic measurement result from SPRs. (1) is the baseline where no drug has been introduced. (2) is the drug association stage. (3) is the equilibrium stage where the amount of drugs that bind to the membrane is equal to the amount that is released into the solution. (4) is the drug dissociation stage and (5) is the final stage after no more drugs are released. R_1 , R_2 , and ΔR correspond to the same symbols in the previous figure.

In the figure there are 5 stages of drug-membrane interaction. The first stage, (1) is the baseline, the membrane without any drugs. When the drug is introduced and begins to bind to the membrane, (2), the reflectivity begins to increase and this stage is called the binding or association stage. After the rate of drug binding to the membrane is equal to the rate of drug release, equilibrium is reached and this is the maximum binding stage (3). If no more drugs are added and instead the buffer solution is added to wash the drugs away, the reflectivity will decrease as drugs are now released from the membrane (4). This stage is the dissociation or release stage. Finally the stage where no more drugs can be washed is reached (5). The reflectivity at this stage may be lower or higher than the baseline reflectivity. This would indicate that either some drugs cannot be washed away or some of the membrane material is washed with the drug. R_1 , R_2 , and ΔR correspond to the points in Figure 2.4.

There are some practical considerations in SPRS experiments. The first consideration is the modification of the Kretschmann geometry. In the ideal Kretschmann geometry, the gold film is directly laid onto the base of the prism, but this way is too expensive and it is difficult to do. The common modification then is to evaporate the gold on a glass slide and then put the prism on the backside. Before the prism is placed, a small quantity of index matching oil ($n=1.7$) is applied on the back of the gold coated slide. The common glass slides used are BK7 ($n=1.5$), but the index of BK7 is too low compared to the refractive index of the prism ($n=1.85$). This caused the SPR reflectivity vs incident angle curve to have a discontinuity around 62° . To improve the scan range, glass slides with refractive index similar to the prism, LaFSN9 glass, is used ($n=1.85$). With this glass, the usable range of angles can continue to 70° .

A second consideration is the limitation of the detector. As the goniometer and the detector moves from small to large angles the reflected laser spot also moves across the detector. If the medium in the flow cell is changed from air to water or any other solution, the resonance angle shift is big. In air, the resonance angle is between $20^\circ - 45^\circ$ while in solution the resonance angle is between $45^\circ - 60^\circ$. A detector with a small photodiode cannot keep track on the reflected laser the whole range from $20^\circ - 60^\circ$. A solution to this limitation is to adjust the detector differently for detection in air and detection in solution.

The third consideration is the adhesion of gold to glass which is weak. The gold can come off easily if it is immersed in water or any other solvent. 2 nm of chromium can be deposited before gold to improve the gold adhesion to the glass.

2.2 Electrochemical impedance spectroscopy

Electrochemical impedance spectroscopy (EIS) is a spectroscopy technique that lets one to study the electrical response or impedance of a system under alternating current (AC) with varying frequencies [40]. The working part of EIS is the electrochemical cell, consisting of at least two electrodes, the working electrode (WE) and counter electrode (CE) with electrolyte solution in-between. When a potential difference is applied between the electrodes, electron flows from the negative electrode to the positive electrode and if direct current is used, an electrochemical reaction will occur with the positive ions leaving the WE and depositing on the CE because of the electron flow. If a sinusoidal AC signal is used instead, net electrochemical reaction will not happen as the electrical current changes polarity every half cycle. This is one of the reasons why AC is better than DC for EIS as it avoids unwanted

electrochemical reactions.[41] Additional reasons to use AC rather than DC is with AC, only a relatively small external changing signal is needed to measure the electrical properties of the WE. A small signal ensures linear response of the electrochemical cell. With DC, a larger signal or perturbation is needed to measure electrical properties. AC can also be used for materials with low electrical conductivity while DC can only be used for materials with high conductivity. [42]

The EIS instrument used in this work was μ Autolab III/FRA 2 from Metrohm. The range of frequencies used in this work is from 2 mHz to 0.1 MHz. The system studied with EIS is the tBLM on a gold covered glass slide. The tBLM and the gold covered glass functions as an electrode in the EIS setup (Figure 2.6) and the whole flow cell acts as an electrochemical cell.

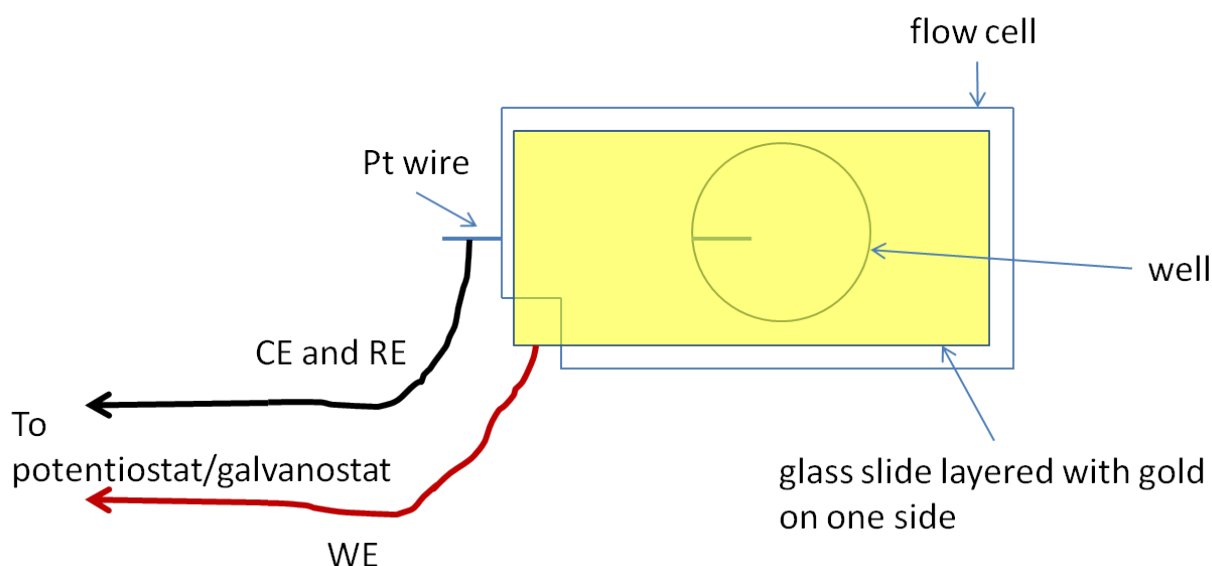


Figure 2.6 A flow cell modified for EIS experiments and the electrodes. CE is the counter electrode, RE is the reference electrode, and WE is the working electrode. Pt is platinum.

In this setup, a computer controlled potentiostat/galvanostat is connected to the gold covered glass slide and a platinum (Pt) wire. The gold covered glass slide and the attached tBLM forms a part of the working electrode (WE). The platinum wire functions as both the counter and reference electrode (CE and RE). The well in the flow cell will act as electrolyte reservoir. Since the flow cell is the same one used in the SPRS, both SPRS and EIS measurements can be made in one run. The potentiostat/galvanostat controls the current or voltage. During a measurement, a sinusoidal potential is applied to the electrochemical flow cell, which includes the tBLM, and the resulting current is measured. [40] Since this is an AC, the current and voltage are sinusoidal. The applied potential will vary according to the relation $E = E_0 \sin(\omega t)$ and the resulting current will vary according to the

relation $I = I_0 \sin(\omega t + \theta)$. [43] E_0 and I_0 are the amplitudes of potential and current respectively while ω is the angular frequency, t is the time and θ is the phase difference between the potential and the current. Since AC is applied to the electrochemical cell, the cell behaves as an AC circuit, where the components that can impede the current flow are resistors, capacitors and inductors. These components impede the current flow, causing phase difference between E and I . The impedance by these components is called the complex impedance, symbolised by Z . The familiar Ohm's law then become $E = IZ$ in the linear response range, which can be achieved by using small potential with small resulting current. From this equation the value of Z is

$$Z = \frac{E_0 \sin(\omega t)}{I_0 \sin(\omega t + \theta)} = Z_0 \frac{\sin(\omega t)}{\sin(\omega t + \theta)}$$

Where Z_0 is the magnitude of the impedance. Since Z is a complex function it can also be expressed as $Z = Z' + jZ''$ where Z' is the real part of the complex function, j is the unit imaginary, and Z'' is the imaginary part. In this form the magnitude of Z is given by $|Z| = \sqrt{Z'^2 + Z''^2}$ and the phase difference is given by $\theta = \arctan \frac{Z''}{Z'}$. Since the electrochemical cell consists of the tBLM which is anchored to a gold film, surrounded by electrolyte solution, these components acts as the components of the AC circuit that impedes the current response. The impedance of the solution is far smaller than that of the tBLM in most region of frequencies used except at the very high frequencies, so for practical purposes the EIS measures the impedance of the tBLM. There are several ways to plot the electrical response of the tBLM one of which is the Bode Plot (Figure 2.7).

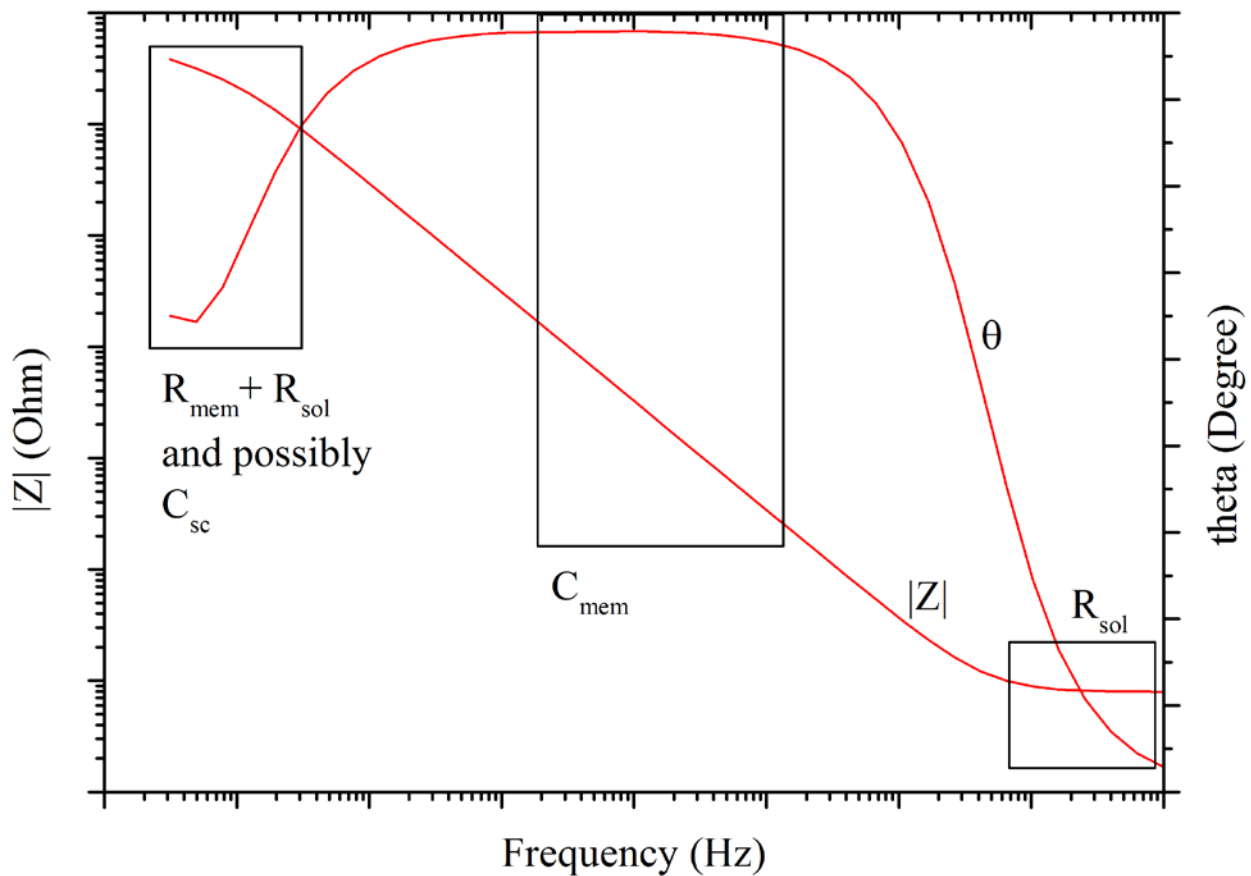


Figure 2.7 Example of Bode plot and areas corresponding to the equivalent circuit components. R_{sol} is the solution resistance. R_{mem} and C_{mem} is the resistance and capacitance of the membrane, while C_{sc} is the space charge capacitance. The symbol θ is the phase difference between current and voltage and $|Z|$ is the absolute value of complex impedance.

The Bode plot shows the relation between the frequency of the alternating current, the phase difference (θ) of the current and applied potential and the absolute value or magnitude of the complex impedance ($|Z|$). To extract useful information from the Bode plot, the tBLM has to be modelled with an equivalent circuit model. This is a model that treats the tBLM as a circuit composed of resistors (R) and capacitors (C). In this work, the tBLM has been modelled by two equivalent circuit models. R(RC) and R(RC)C (Figure 2.8).

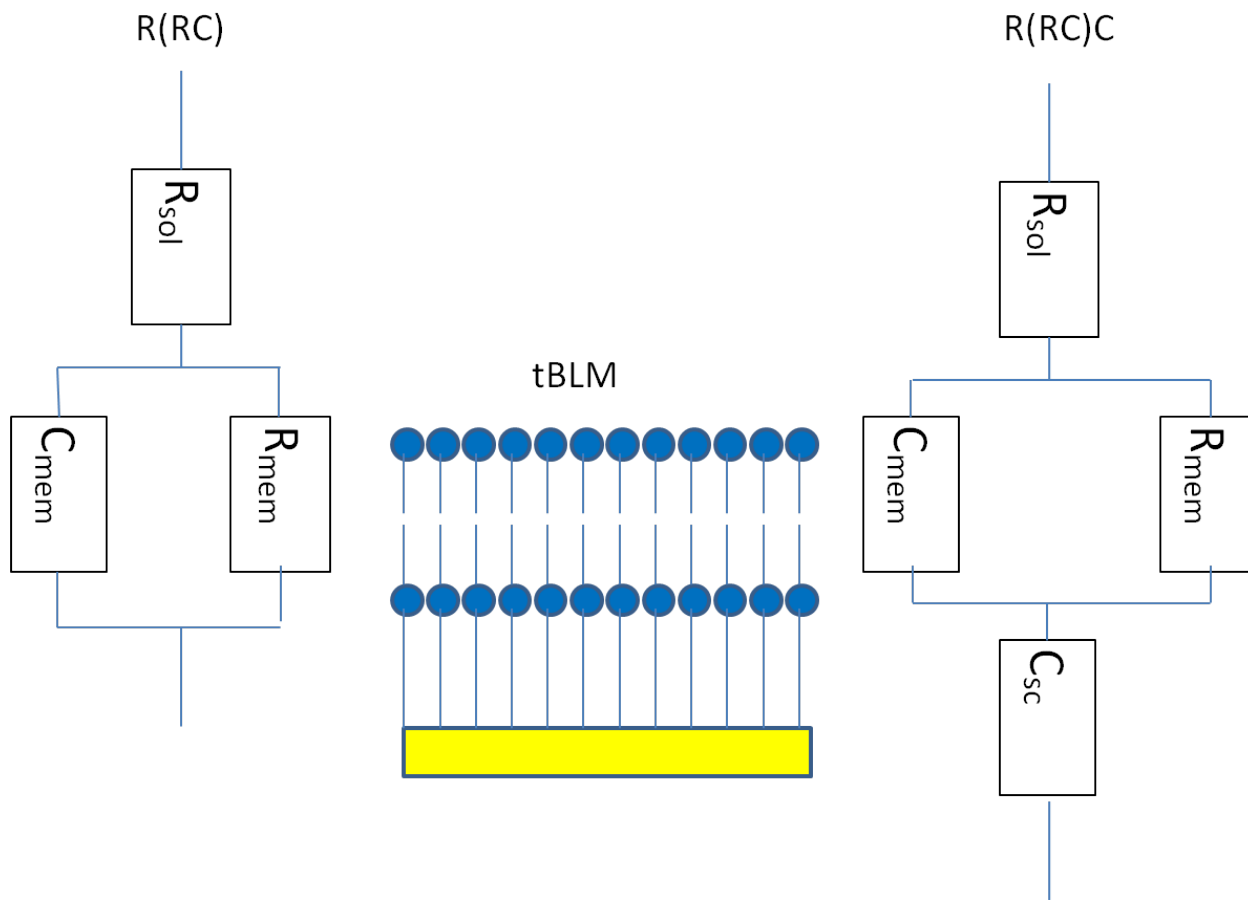


Figure 2.8 Two equivalent circuit models used to model tBLM in this work. The position of the circuit components corresponds to the tBLM components. R_{sol} is the solution resistance. R_{mem} and C_{mem} is the resistance and capacitance of the membrane, while C_{sc} is the space charge capacitance.

In the R(RC) model, the solution resistance R_{sol} is in series with the resistance and capacitance of the lipid mono/bilayer R_{mem} and C_{mem} . The (RC) denotes a resistance in parallel with a capacitance. The rationale is that the lipid mono/bilayer acts as a resistor in tandem with a capacitor. In the R(RC)C model, R_{sol} is in series with R_{mem} and C_{mem} and space charge capacitance C_{sc} . The C_{sc} represents the ionic reservoir in the tether region of a tBLM as well as the gold electrode. The first model can be used for exceptionally good bilayers where the C_{sc} lies far in the low frequency region and not visible in the measurement. The second model is usually used for bilayers which have defects, making the C_{sc} appear in the range of measured frequencies. In cases of membranes that have more defects, the C_{mem} can be replaced by a Constant Phase Element (CPE). The CPE represents a distribution of parallel capacitors with different capacitances. The CPE is characterised by two values, the average value of the capacitors and the value of the distribution or spread of the capacitances.

The R(RC)C model has been used to model tBLM [25]. The R(RC) model, also called the Randles cell, has been used to model many systems [44]. Valincius et al [45] argued that for tBLM with defects, a more correct approximation is to derive the model circuit from mathematical considerations and not from ECM. Nevertheless, the ECMs proposed here are simple enough to describe the data and at this stage, a more complicated model is not needed.

To get a precise value of the equivalent circuits, a fitting program, in this case, ZView, is used. A good starting estimate for R_{sol} is about 100 Ω , while for R_{mem} it is about $10^6 \Omega$, and for C_{mem} and C_{sc} it is about 10^{-6} F and 10^{-5} F respectively. Alternatively, the values can be approximated by looking at the Bode Plot (Figure 2.7). The complex impedance is the sum of solution resistance, membrane resistance and capacitance and possibly also space charge resistance. For the R(RC) model, also called the Randles cell the total complex impedance is given by

$$Z = R_{sol} + \frac{R_{mem}}{1 + (\omega R_{mem} C_{mem})^2} + j \frac{-\omega R_{mem}^2 C_{mem}}{1 + (\omega R_{mem} C_{mem})^2}$$

[44]. With the addition of space charge resistance in R(RC)C model the equation becomes

$$Z = R_{sol} + \frac{R_{mem}}{1 + (\omega R_{mem} C_{mem})^2} + j \left(\frac{-\omega R_{mem}^2 C_{mem}}{1 + (\omega R_{mem} C_{mem})^2} + \frac{-1}{\omega C_{sc}} \right) (*)$$

remembering that the impedance of a capacitor is given by $Z_c = \frac{-j}{\omega C}$. Although the expression looks complicated at very high and very low frequencies the expression becomes simpler. When the frequency is very high the denominator in the second and third term approaches $(\omega R_{mem} C_{mem})^2$. This transforms the equation to

$$Z = R_{sol} + \frac{1}{R_{mem} (\omega C_{mem})^2} + j \left(\frac{-1}{\omega C_{mem}} + \frac{-1}{\omega C_{sc}} \right)$$

As the value of ω becomes very large the last three terms becomes vanishingly small leaving the first term. This means that the impedance purely comes from the solution resistance. So, the R_{sol} can be estimated by looking at the constant resistance part in the high frequency region and reading the impedance values. At high frequency the solution resistance dominates the circuit impedance and this impedance is independent of frequency as shown by the equation and the flat line in the figure. In this region the phase difference between the potential and the current is small. As the frequency decreases the impedance and the phase difference increases until the intermediate frequency region where the

phase difference is high, nearing 90° and the impedance slope becomes -1. The impedance in this region is dominated by capacitance as indicated by the high phase difference. The capacitance comes from the membrane because the space charge capacitance is ideally constant.[25] The space charge capacitance becomes dominant in very low frequency region. The value of the capacitance can be calculated by reading the value of impedance at $\omega=1$. At this point, the value of C_{mem} becomes $C_{mem} = \frac{1}{|Z|}$. The value of the frequency displayed on the Bode plot axis, f is related to the angular frequency ω by $\omega=2\pi f$. In the low frequency region, the impedance still has a slope but the phase difference has decreased. Referring back to equation (*), ω tends to zero so the third term vanishes and the second term becomes just R_{mem} but the fourth term becomes very large. So the total impedance is

$$Z = R_{sol} + R_{mem} + j \frac{-1}{\omega C_{sc}}$$

With the addition of C_{sc} , the slope of the impedance becomes non-zero as in the case of very high frequency. This in fact is what is observed in Figure 2.7. This means that the impedance of this region is the total contribution of membrane and solution resistances as well as space charge capacitance. In addition to that, the phase difference is still quite high although it is lower than in the intermediate frequency region. This also indicates that the impedance in this region is a combination of resistance and capacitance. If the membrane is perfect, then the Bode plot can be fitted with the R(RC) model. At low frequency, the phase difference will decrease to near zero and because the space charge capacitance does not play a part, the impedance will consist of membrane and solution resistances only. These resistances are independent of frequency and will show on the plot as a flat line like in the very high frequency region. Since the EIS can measure the membrane's electrical resistance, this technique can investigate the electrical sealing properties of the membrane. A good membrane with no defects will have high impedance, more than $1 \text{ M}\Omega$, and large (about 90°) phase difference while a not so good membrane with many defects will have low impedance, about $100 \text{ k}\Omega$, and lower phase difference (less than 80°).

EIS can also monitor drug-membrane interaction via the changes of membrane resistance and capacitance as it interacts with the drug. A drug's interaction with the tBLM will affect the structure of the membrane in some way. Usually the interaction will introduce defects in the membrane that will decrease the membrane resistance and increase the membrane capacitance. This change will appear in

the Bode plot as a decrease in the impedance part. If the interaction is reversible, then after the drug is washed away, the impedance will return to its previous value.

Some practical issues that need to be considered in doing EIS experiments are the contact between the gold and the working electrode clip. To improve the contact area, a thin aluminium foil can be slipped between the gold and the clip. The second consideration is on how to put the prism after a bit of the index matching oil had been smeared on the back side of the slide. To prevent any air bubble coming between the prism and the slide, a sure way is by carefully sliding the prism on the slide while it is placed on top of the flow cell. This has the effect of decreasing the quality of the monolayer because the fragile monolayer is rubbed against the O-ring, however. It is possible to carefully put the prism on top of the index matching oil so as to not move the prism or the slide at all but it is difficult. An easier way is to slide the prism on top of the index matching oil while holding the slide above the flow cell. Only after the prism is on top of the slide then both the slide and the prism are lowered on to the flow cell.

2.3 Ultraviolet-visible spectroscopy

Ultraviolet-Visible spectroscopy (UV-Vis) uses light from the ultraviolet and visible spectrum to identify and measure the concentration of chemical species. Different chemical species or atoms absorb light at different wavelengths. The concentration of a chemical species is proportional to the absorbance of the light and can be determined from a calibration curve using Beer-Lambert law. In this work, UV-Vis spectroscopy is used to measure the concentration of the model drug and the concentration of gold nanoparticles. Before a measurement of certain chemicals, the blank, that is the solution with no chemical of interest, must be measured to provide a baseline. The UV-vis instruments used in this work were Cary 50 UV-Vis spectrophotometer and Cary 60 UV-Vis both from Agilent Technologies.

2.4 Dynamic light scattering

Dynamic light scattering (DLS) is a method using monochromatic light scattering and Brownian motion to determine the distribution of particle sizes [46]. As the particles moved around jostled by the solvent molecules, some of the laser light will be scattered by the particles. The scattered light will then form a pattern of constructive and destructive interference called a speckle pattern.[47] Because the particles move around, the speckle pattern or intensity will change with time. Due to the random nature

of the Brownian motion, the pattern at time $t=\infty$ will be completely unrelated to the pattern at time $t=t$. If the time difference between the two patterns being compared is very small, on the order of microseconds, there will be some correlation. The correlation between two compared signals is exponentially decaying with time and the function that describes this decay is called the correlation function. The function decays from 1, meaning perfect correlation to 0 meaning no correlation at all. The instrument uses a correlator to both compare the speckle patterns and create the correlation function. For monodisperse particle the correlation function is given by [47]

$$G(\tau) = A[1 + Be^{-2\Gamma\tau}]$$

where

$$\Gamma = D((4\pi n / \lambda_0) \sin(\theta / 2))^2$$

Where G is the correlation function, τ is the time difference between two compared pattern, D is the translational diffusion coefficient. n is the refractive index of the dispersant, λ_0 is the wavelength of the laser, and θ is the scattering angle. A is the baseline of the correlation function and B is the intercept of the correlation function. When the correlation data is fitted to the correlation function by the DLS program the value of D can be obtained. D is a measure of the diffusion rate or speed of the particles. The faster the diffusion rate of particles, the quicker the loss of correlation, shown as a steeper decline of the correlation function and vice versa. D is related to the particle diameter by Einstein-Stokes equation. [47] The equation is given by $d(H) = \frac{kT}{3\pi\eta D}$, where $d(H)$ is the hydrodynamic diameter, k is the Boltzmann constant, T is the absolute temperature, η is the viscosity of the solvent and D is the translational diffusion coefficient. The final result is the hydrodynamic diameter which is the diameter of a sphere moving with diffusion rate of D. A slower particle will be interpreted by the instrument as having bigger hydrodynamic diameter. This means that the correlation function of particles with a big hydrodynamic size will decline more slowly compared to the correlation function of particles with smaller hydrodynamic size.

Because what is measured is a hydrodynamic sphere, some limitations of this technique are apparent. One limitation of this method is the particles are always modelled as perfect spheres. If the shape of the particles deviates strongly from a sphere then there will be some error in the results. Another limitation of this technique is that the hydrodynamic sphere includes the particle and the electric double layer

around it. The hydrodynamic size is dependent among other things on the ionic strength of the solution. A stronger ionic strength will result in smaller hydrodynamic size, closer to the exact particle size.

There are three modes of particle size measurements, the particle size by intensity, by volume, and by numbers. The particle size by intensity is the raw data, the data that should be reported in papers. However stronger intensity only means stronger scatterers which may or may not reflect the amount of particles in the solution. Size distribution by volume and by numbers is used to make certain the amount of smaller particles which may be hidden by bigger particles in the size distribution by intensity data. The particle sizing instrument used in this work was Malvern Zetasizer Nano ZS from Malvern.

2.5 Contact angle measurement

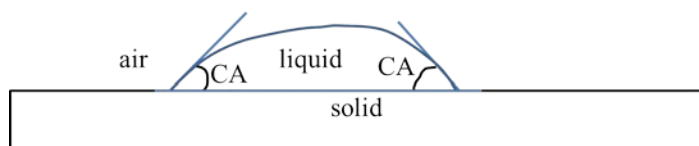


Figure 2.9 Schematic of the contact angle (CA) between liquid and solid phases.

The contact angle (CA) is a method to determine the hydrophobicity of surfaces (Figure 2.9). The contact angle is related to the hydrophobicity of the surface. The higher the contact angle the more hydrophobic the surface. There are several variations of the contact angle analysis, but in this work the sessile drop method is used. This method involves dropping a droplet of water on the surface of the gold coated glass slide. The contact angle where the gold, water and air meet at the left and right side of the droplet is measured with the help of a camera and software. The contact angle determination can be done manually or by automatic fitting. To determine the overall hydrophobicity of the gold surface, the sessile drop method is repeated several times on different spots on the gold coated slide and then the contact angles are averaged. This method was used to determine the coverage of tethered lipid monolayer on the gold coated glass slide in preparation for tBLM formation. The contact angle measuring instrument used in this work was an OCA 15 plus contact angle system from Data Physics.

2.6 Zeta potential measurement

The zeta potential (ZP) is a measure of the surface electrical charge of nanoparticles and also an indication of the nanoparticles' stability. To measure the ZP, a special cell with electrodes is used. This cell has a U shaped column and the electrodes are positioned on the upper end of the U column. When an electric potential is applied between the electrodes, the charges on the surface of the

nanoparticles make them move toward electrodes with opposite charges with a certain speed [46]. This phenomenon is called electrophoresis and the speed is called the electrophoretic mobility. This electrophoretic mobility is related to the ZP of the particles by the Henry Equation, given by [48]

$$U_E = \frac{2\varepsilon z f(\kappa a)}{3\eta}. U_E \text{ is the electrophoretic mobility, } \varepsilon \text{ is the dielectric constant of the solvent, } z \text{ is the}$$

zeta potential, η is the viscosity of the solvent and $f(\kappa a)$ is Henry's function. The value of Henry's function is dependent on the ratio of the thickness of the electrical double layer, given by κ^{-1} and the particle radius given by a . In practice, two cases exist that simplifies the approximation of the value of Henry's constant. The first case is when the size of particles is larger than 200 nm and the solvent is aqueous or polar. In this case the value of the function can be approximated with a value of 1.5 and is called the Smoluchowski approximation. The second case is when the size of particles is smaller than 200 nm and the solvent is non-aqueous or non-polar. In this case the value of the function can be approximated with a value of 1.0 and is called the Huckel approximation.

The electrophoretic mobility is measured by using laser Doppler electrophoresis [46]. This technique combines electrophoresis and the Doppler Effect which is change of frequency caused by the velocity of a wave source. A laser beam is passed through the cell and will be scattered by the particles moving under the applied electric field. The moving particles which scattered the light acts as new "light source" and the frequency of light scattered from these particles will be modified by the velocity of the particles which is the Doppler Effect. Because the scattered light will have a different frequency from the incoming light, there is a frequency difference that is related by the velocity of the particles given by $\Delta f = 2v \sin(\theta/2) / \lambda$, where Δf is the frequency difference, v is the particle velocity, θ is the scattering angle and λ is the wavelength of the laser.[49] To measure the frequency difference, this technique uses a split laser beam, one is the reference beam and the other is the beam that is shone on the particles and then scattered. [50] The scattered and reference beam are then combined, producing a fluctuating intensity signal with frequency beats. To determine the sign as well as the value of the ZP, one of the laser beams is modulated using an oscillating mirror to produce a reference beat frequency. The frequency beat from the sample beam is then compared to the reference frequency. If the detected signal's beat frequency is lower than the reference signal, then the ZP is negative and vice versa. The value of the ZP is proportional to the difference between the beats.[49] The ZPs in this work were measured by Malvern Zetasiser Nano ZS from Malvern.

2.7 Fourier transform infra-red spectroscopy

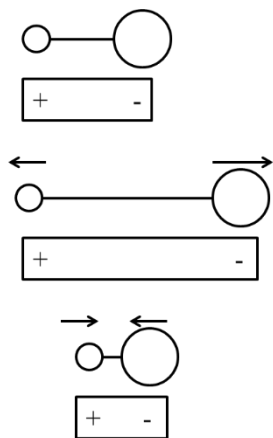


Figure 2.10 An illustration of electrical dipole moment change as a diatomic molecule vibrates.

Fourier transform infra-red spectroscopy (FTIR) is a spectroscopy technique that can determine the chemical species of molecules by absorption of IR radiation at specific frequencies or wave numbers. Absorption of IR by the molecules occurs if two conditions are fulfilled. The first condition is that the difference between vibrational energy levels of the molecule matches the energy of the incoming IR radiation. The second condition is that the molecules are IR active. To be IR active the molecule must undergo an electric dipole moment change as it vibrates (Figure 2.10). An IR source in the spectroscope emits infrared light of varying frequencies that have different energies. Certain frequencies that fulfil the first criteria will be absorbed, and characteristic mode of vibration of the molecule can be identified. This is the fingerprint of the molecule.

The Fourier transform in FTIR refers to a mathematical transformation of the IR signal. The IR radiation was manipulated by an interferometer before going through the sample. The IR was split into two beams, one beam was directed to and reflected by a stationary mirror and the other beam was directed to and reflected by a moving mirror. The two beams were combined and produce constructive and destructive interference pattern due to path length difference between the beam from stationary and the beam from moving mirrors. The combined beams were passed through the sample into a detector (Figure 2.11). The detected signal is then Fourier transformed by the computer to produce IR absorbance or transmittance spectrum. The advantage of FTIR is that it is faster than non-fourier transformed IR spectroscopy [51, 52] The FTIR instrument used in this work was Perkins-Elmer FTIR Frontier Spectrometer from Perkins-Elmer with the universal attenuated total reflectance accessory.

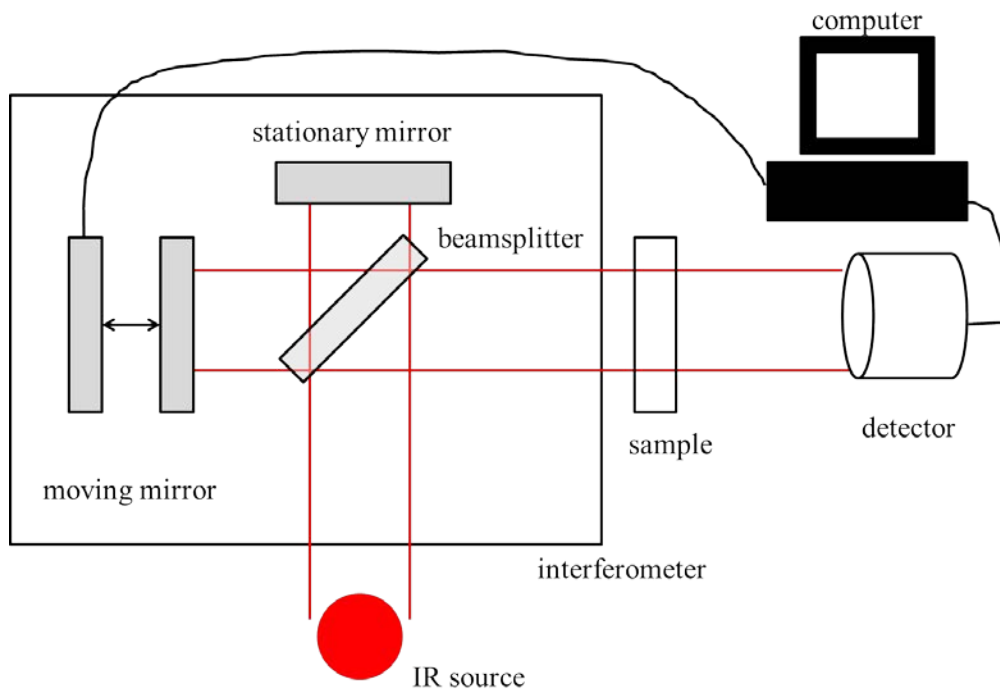


Figure 2.11 Instrument setup of FTIR spectroscopy. The IR radiation was split by the beam splitter then reflected and combined before passing through the sample. The IR is then recorded by a detector and the signal is processed by a computer.

2.8 Transmission electron microscopy

Transmission electron microscopy (TEM) is an electron microscopy technique that uses transmitted electrons from a sample to image it. Electrons from an electron gun are focused on a thin sample using magnetic lenses. The electrons then interact with the sample and are scattered. The scattered electrons that pass through the sample are then magnified by another lens and collected on a detector. The detected signals are then converted into an image by the control computer. The advantage of TEM is that it can reach a resolution of about 1 \AA [53]. This is much smaller than what can be resolved using visible light microscope, owing to the smaller electron wavelength compared to visible light.

One of the considerations in using a TEM is that the sample slice must be thin enough to be transparent to electrons [53]. The thickness depends on the material of the sample, but generally it is around 100 nm. This limitation in thickness is actually an advantage when imaging nanoparticles whose size is actually around 100 nm or smaller. Since nanoparticles are powdery, a TEM grid is used to handle the sample. The TEM used in this work is JEM 1200EX from JEOL.

CHAPTER 3 DRUG-MEMBRANE INTERACTION

3.1 Introduction

Drugs are important for the treatment of many diseases and illnesses. Many drugs have to pass through cell membranes in order to reach their intracellular target [7]. Some drugs have to bind to a specific protein receptor before they can act [54]. Therefore, studying drug-membrane interaction is important for understanding the mechanism of drug action. Previously, mainly the binding interaction between the drug and the receptor on the membrane was deemed important and the rest of the membrane, the phospholipid component, was considered passive background [54]. Recent research has found that the membrane phospholipid can influence drug distribution, efficacy, accumulation, and penetration [7, 11, 54-56]. Not only that, drugs can also influence the membrane structure and protein conformation [54, 56]. In other words, drug-membrane interactions seem to be reciprocal.

Drug-membrane interaction studies can be carried out using cell membranes or model membranes. In the study of drug-membrane interaction, model membranes give several advantages over cell membranes. The first is that the model membranes are simpler than the complex cell membrane. The second is that the model membranes are usually easier to handle than cells. The simplicity of a model membrane over the complexity of the real cell membrane is a major advantage when trying to study it. With a model membrane, a researcher can focus on the few relevant membrane elements in the study which can simplify analysis. This is why many if not most drug-membrane interaction studies are done using model membranes.

Several drug-membrane interaction studies using model membranes have been done before [10, 11, 20, 21, 55, 57]. Usually, the model membranes used were liposomes and supported lipid bilayers. Lipid monolayers and black lipid membranes were also used. The previous research on drug-membrane interaction has been done with various techniques, AFM, SPRS, EIS and a few others. Therefore, a brief review on the studies of drug-membrane interaction will be presented. Then the aim of this research will be stated, followed by the materials and methods, and then results and discussion.

In this first part of the work, the drug membrane interaction is going to be studied by two complementary techniques: SPRS and EIS. SPRS and EIS allow to monitor the optical and electrical properties of the interaction. Combining the techniques should give a more complete understanding on the process of drug-membrane interaction. Since SPRS and EIS are the main techniques in this work,

the reviews are going to be grouped on the analytical techniques used: SPRS, EIS, and other techniques. The reviews presented here are only a few select examples and are not meant to be exhaustive.

3.1.1 Drug-membrane interaction studies by techniques other than SPRS or EIS

Many analytical techniques have been used to study drug membrane interactions. Each of the techniques only focused on small aspects of the drug-membrane interaction. The analytical techniques actually will complement each other in providing a piece of the puzzle in order to build up more complete understanding of drug membrane interaction. Therefore the techniques should not be used in isolation but used together to comprehend the mechanisms of drug-membrane interaction. The examples in this review will show how each technique highlights one aspect of the interaction and how combining several techniques will result in a more complete understanding.

Nunes et al. [55] studied the drug-membrane interaction of NSAIDs (Non Steroidal Anti Inflammatory Drugs) with liposomes, lipid monolayers and supported bilayers at two pH values, 5 and 7.4. They used fluorescence steady state anisotropy, surface pressure-area isotherms, infrared reflection-absorption spectroscopy (IRRAS), and atomic force microscopy (AFM) in their study. The fluorescence steady state anisotropy technique was used to characterise the phase transition temperature of the membrane in the presence and absence of the NSAIDs. The surface pressure-area isotherms enable the researchers to detect drug penetration into the model membrane via the increase of molecular area. The pressure-area isotherm measurement was done simultaneously with the IRRAS measurement. Combining the data from both techniques revealed that the drugs caused increase in the phase transition pressure, which cannot be deduced from surface-area pressure isotherms alone. Finally, the topographical changes of the membrane caused by drug-membrane interaction were shown by AFM. The AFM showed that every drug tested except nimesulide created holes in the bilayer, the number of holes increasing with interaction time. The overall conclusion from the research was that first, pH was an influential parameter in determining drug-membrane interaction as it influenced the structure of the membrane and the ionisation of the drugs. Second, the drugs interacted preferentially with the head group of the lipid at both pH 7.4 and 5.0. However, at acidic pH the drugs could penetrate deeper into the bilayer core. Third, all of the drugs except nimesulide increased fluidity of the membrane and caused holes in the bilayer. This was taken as a proof of concept of the gastric toxicity of the other NSAID drugs and relative non-toxicity of this drug.

Pinheiro et al. [10] studied the rifabutin-membrane interaction using large unilamellar vesicles (LUV) as model membranes. The vesicles were made from two different lipids, one was composed of zwitterionic lipid and the other was of anionic lipid. The zwitterionic lipid vesicles represented human cells and the anionic lipid vesicles represented bacterial cells. They used fluorescence quenching spectroscopy, UV-Vis derivative spectroscopy, dynamic light scattering, and steady state fluorescence anisotropy. The fluorescence quenching showed that the drug's location depends on the type of the membrane. The drug did not have preferred location in the zwitterionic membrane but they preferred the ionic head group of the negatively charged membrane. The UV-Vis derivative spectroscopy is a technique that takes the second and third derivatives of the absorbance spectrum. These derivatives can be related to the partition coefficient and lipid concentration by an equation. Fitting the derivative vs concentration data by this equation at certain wavelengths where light scattering by liposomes is eliminated yields the value of the partition coefficient. The partition coefficient result showed that the drug interacted more strongly to the anionic membrane than the zwitterionic one. The dynamic light scattering technique determined the transition temperature of the model membranes. That technique was used together with the fluorescence anisotropy technique to study membrane fluidity by measuring the transition temperature, cooperativity and lipid order. The effect of the drug on both kinds of membranes was revealed to be the decrease of lipid cooperativity and increase of lipid order. The main conclusion of the study was that the Rifabutin drug showed strong interaction with the negatively charged membrane models compared to the zwitterionic membrane models. This indicated the preference of the drug to bacterial cell membranes compared to human cell membranes, although the experiment showed that it could penetrate both membranes.

Pinheiro with other collaborators also studied rifabutin-liposome interaction using wide angle and small angle X-ray scattering (WAXS and SAXS) [11]. With this technique, they were able to determine the structure of the model membrane and the changes brought about by the interaction of the membrane and the drug [11]. The main results of this study were that first the concentration of the drug, the type of phospholipid headgroup and the hydrocarbon chains influenced the drug-membrane interactions. Second, the drug affected the gel phase of the human model membrane but not the liquid phase which correlated to some side effect of the drug observed *in vivo*. The drug however strongly affected the liquid phase of the bacterial model membrane, and caused disruption in membrane ordering by phase separation and therefore the membrane function. This was a proof of concept for the effectiveness of this drug against bacteria.

Foglia *et al.* investigated the drug-membrane interaction between Amphotericin B (AmB) enveloped in sodium cholesteryl sulphate (SCS) micelles and POPC containing vesicles and monolayers. [58] There were three types of lipids used in this experiment: pure POPC, POPC-cholesterol, and POPC-ergosterol. POPC-cholesterol mixture represents mammalian cell membranes and POPC-ergosterol mixture represents fungal cell membrane. They analysed the drug-membrane interaction with Langmuir surface pressure-area isotherms, small angle neutron scattering (SANS) and neutron reflectivity. The Langmuir surface pressure-area isotherms revealed that free AmB and AmB-SCS caused a change in surface pressure which indicated a change in the structure of the monolayers. The change is greater for POPC-ergosterol than the other two types of lipids. The change was also more significant for AmB-SCS than free AmB. Neutron reflectivity added to the isotherm result in showing that interaction with AmB-SCS and AmB increased thickness and roughness of both the tail and head regions. The SANS studies of drug-vesicle interaction showed that interaction with both formulations of AmB changed the thickness of the bilayer. The change was comparable between all three types of vesicles but the onset of change and the time to complete the change was shortest in the POPC-ergosterol vesicles. The researchers concluded that the AmB only bound to the surface of the pure POPC vesicles by combining the results from surface pressure-area isotherms and SANS. In contrast, both formulations of the drug formed pores in the POPC-sterol model membranes by inserting into the bilayers. This was because the time to complete the change in bilayer was faster than for the corresponding monolayer in case of sterol containing membranes. The overall results were that SCS formulation improved the interaction of AmB with the model membranes and that AmB had stronger affinity to POPC-ergosterol than POPC-cholesterol. This fits with the *in vivo* fact that amphotericin B have a higher affinity to fungal cell membrane compared to mammalian cell membrane.

Neves *et al.* investigated liposome-Resveratrol interaction.[59] The liposomes were made of different compositions of egg phosphatidylcholine (EPC), cholesterol (CHOL) and sphingomyelin (SM). The first membrane consisted only of EPC, the second membrane of EPC-CHOL and the third membrane of EPC-CHOL-SM. Using derivative spectrophotometry they concluded that Resveratrol entered easily into pure EPC membrane compared to the other two. Using fluorescence quenching, they found that Resveratrol located both in the headgroup and hydrophobic core of all types of membranes used in this study. Using fluorescence anisotropy, they concluded that for a fluid EPC membrane, Resveratrol had the effect of making the membrane stiffer. For EPC-CHOL and EPC-CHOL-SM membranes which were stiffer, the Resveratrol had the opposite effect of making them more fluid.

Recently a drug-membrane interaction study using several techniques by Ferreira et al. revealed the possible mechanism of action of Thymol, a biocidal compound (antibacterial, antifungal, antiprotozoan).[60] The techniques employed were pressure-surface area isotherms, polarisation modulation IRRAS (PM-IRRAS), Brewster angle microscopy and molecular simulation. By interacting Thymol with a Langmuir monolayer in air-water interface composed of DPPC it was found that Thymol decreased the order of packing of lipids. The increase of lipid packing disorder was determined by the PM-IRRAS data. PM-IRRAS also confirmed the presence of Thymol in the monolayer by the presence of a peak that signified the aromatic ring vibration. The molecule preferentially bound to the hydrophobic tail of the phospholipid as predicted by molecular dynamics simulation (MDS). The effect became pronounced at concentration of 3% of Thymol. At this concentration, the drug caused the monolayer to expand while at lower concentrations the effect was not as pronounced. This could be seen in the surface pressure-area isotherms where the shift to higher area was not as pronounced for Thymol concentrations of 1% and 2% compared to 3%. The result of Brewster angle microscopy showed that the presence of Thymol destroyed the homogeneity of DPPC monolayer, making areas of bright phase contrast. These areas showed domains of lipid-Thymol aggregates. These areas only appeared after a high enough concentration of Thymol (3%) was added, however.

In 2017, Alves et al. studied the interaction between Daunorubicin, an anticancer drug, and liposomes [61]. The liposomes were varied in their phospholipid compositions and the concentration of the drugs was increased. They used several analytical techniques to study the interaction: derivative UV-Vis spectrophotometry to calculate the drug partition coefficient, ZP measurement to measure the liposome surface charge before and after drug addition, fluorescence spectroscopy to determine the drug's location in the model membrane, and fluorescence anisotropy spectroscopy to determine the fluidity of the membrane. From these studies they found that the drug's permeation of the membrane depended on the composition of the membrane. Membranes that contained phosphatidylethanolamine (PE) were more permeable to the drug. Membranes that contained cholesterol were less permeable to the drug. Zeta potential measurement showed that all the liposomes with different lipid composition have negative ZP, but addition of Daunorubicin caused their ZP to be less negative. This is because the drug has positive charge at pH=6.3 which is the pH used in the experiment. They also found that the drug was located between the polar head group and the nonpolar tails. This is because the drug has both positive charges that can interact electrostatically with the negatively charged head group and a residue that can interact hydrophobically with the tail group. Final finding about the drug was the drug changed

the fluidity of the membrane differently between the polar region and the nonpolar region. The drug made the polar region more fluid while increasing the packing of the nonpolar region.

From all the aforementioned drug-membrane interaction research, some general conclusions can be drawn. First, drugs do enter the membrane. Some of the drug types prefer to stay on the exposed hydrophilic head group of the lipids while other types can penetrate into the hydrophobic core of the membrane. Second, drugs can affect the structure of the lipid membranes. Most of the biocidal drug will increase the disorder of membrane but other compounds can increase the lipid packing order. Third, the binding of the drug is affected by the type of lipid and lipid composition.

Beside experiments, researchers have studied drug-membrane interaction through molecular dynamics simulation (MDS), as was the case with Ferreira et al. [60]. This approach through computer modelling has at least two advantages over studies done by laboratory experiments. First, it can provide insights of the interaction at the atom scale that would be difficult to get through experiments. Second, it can predict properties in the drug-membrane interaction such as partition coefficient and drug permeability. [62] The disadvantage however, is the computational cost make MDS prohibitive for drug screening studies, although this maybe no longer the case, as a group of researchers have used MDS for fragment based drug optimisation [63]. Considering the advantages and disadvantages, MDS can provide information that complements experimental studies and a more complete understanding on drug-membrane interaction. An excellent review of research in this area has been written by Lopes et al. [62].

All the techniques reviewed have shown that they can only study a very limited aspect of the drug membrane interaction. Some studies have made the case that combining two or more techniques will complement the techniques' disadvantages such as the studies by Nunes and Ferreira et al.. Combining two or more techniques also provides a more complete picture of the mechanism and aspects of the interaction. The choice of the combination depends on what aspects of drug-membrane interaction that are going to be studied.

3.1.2 Drug-membrane interaction studies using SPRS technique

Several research groups have used supported lipid bilayers model membrane and SPRS technique to study drug-membrane interaction [20, 21, 57, 64]. Kamimori et al. [57] studied membrane-peptide interaction using supported lipid bilayers which modelled human and bacterial cells and SPRS analysis. The peptide, called Kalata, has the potential to be developed into antimicrobial drug. SPRS enabled the group to study the kinetics of the peptide-membrane interaction. The data was then fitted to a kinetic

model that enabled the researchers to deduce the kinetic rate constants and drug affinity constants. From the affinity constants values, they concluded that the peptide had higher affinity to the bacterial membrane model than human membrane model.

Onishi and Kamimori [64] studied the interaction of antifungal drug AmB with supported lipid bilayer models of human and fungal cell membranes using SPRS technique. Oka and Kamimori [20] studied the interaction of the formulation of the AmB called Fungizone with the same model membranes and technique. Fungizone was a formulation where the AmB was encapsulated in deoxycholate micelles. In both investigations, the researchers used SPRS to study the kinetics of the interaction and then deduce the kinetic rate constants and affinity constants by fitting the data to a kinetic model. Comparing both studies, AmB and Fungizone had higher affinity to fungal membrane model compared to human membrane model. Oka and Kamimori also compared their results with the results of Onishi and Kamimori and found that the affinity of AmB was nine times higher than Fungizone.

Nascimento et al. studied the interaction between the antimicrobial peptide Magainin I (MagI) with a HBM model membrane [65]. The model membrane was made by functionalising a gold electrode with 3-mercaptopropyltrimethoxysilane (MPTS) and then depositing phospholipid liposomes. In one of the experiments the vesicles were coated with Synperonic (Synp), a type of block copolymer and in the other experiment, they were not. They used several analytical techniques such as SPRS, EIS, Scanning Electron Microscopy (SEM), Cyclic Voltammetry, DLS and ZP measurement. The SPRS result showed that the addition of phospholipid layer (PL) without Synp resulted in a higher angle shift than the addition of PL with Synp. After the formation of HBM was completed, the excess liposomes were washed, which resulted in slight decrease of the resonance angle. When MagI was added, the plasmon resonance angle increased again but, after the peptide was washed, the decrease of plasmon resonance angle of the system without Synp was greater than with Synp. This indicated that without Synp, the MagI disrupted the PL and that the MagI along with some of the PL were washed away. With Synp, the PL, Synp and even the MagI were retained even after washing. This pointed to the function of Synp as a sealant that protects the PL from MagI destructive effects. This was further supported by the EIS result.

SPRS has been used as an analytic technique that is able to monitor the kinetics of the drug-membrane interaction. Compared to other techniques that provide kinetic information such as the surface pressure-area isotherms and SANS, SPRS is more direct in detecting and measuring the drug-membrane interaction kinetics. Furthermore, analysis of SPRS data can yield kinetic rate and affinity constants

that tell how fast and how strongly a drug is interacting with the membrane. SPRS is then more suited for kinetic measurements and can complement other techniques.

3.1.3 Drug-membrane interaction studies using EIS technique

Nascimento et al. used EIS technique in conjunction with the SPRS technique to study the interaction between MagI peptide with hybrid bilayer model membrane and the effect of Synperonic. When MagI were introduced to PL without Synp, the membrane resistance decreased. For the PL + Synp system, introduction of MagI increased the membrane resistance. This was also shown in the membrane resistance versus time plot. The plot showed that for the PL only system, the circulation of MagI caused an initial decrease of the membrane resistance followed by an increase after a few minutes. The authors concluded that this behaviour was consistent with the toroidal pore formation model proposed by Chang et al. [66]. The increase of membrane resistance in the PL+Synp system on the other hand indicated that MagI was retained.

A paper by Mallaiya et al. studied the interaction between the drug midazolam hydrochloride (MDZ) and black lipid membranes as the model membrane with EIS as the analytical technique [14]. The researchers measured the resistance and the capacitance of the membrane while increasing the concentration of the drug. They also used two concentrations of NaCl solution (0.1 and 1 M) in their study. The MDZ drug existed in three forms, neutral, protonated, and ion pairs in solution. NaCl concentration had an effect on the MDZ-membrane interaction. At 0.1M NaCl, there was higher excess of negative charges on the membrane surface and a higher proportion of protonated drug compared to neutral drugs compared to 1 M NaCl. The EIS result showed that increasing drug concentration decreased the membrane resistance and increased the membrane capacitance. The decrease of resistance was caused by fluidisation and destabilisation of the membrane while the increase of capacitance was observed to happen in two phases. This was shown in membrane capacitance vs concentration plot. The first phase happened when the protonated form of the drugs interacted with the polar headgroups and decreased the distance between the leaflets of the membrane. The second phase occurred when the neutral and ion pair forms of drug molecules penetrated into the bilayer. The fluidisation and destabilisation of the membrane by MDZ was interpreted by the authors as supporting the neurotoxicity of the drug.

Chang et al. used EIS and polymer supported bilayer membrane to study the pore forming mechanism of two antimicrobial peptides [66]. One of the peptide was FSKRGY, a potent pore former while the

other was AGGKGF, a poor pore former. By fitting the EIS data with an equivalent circuit model, the researchers obtained parameters that represented the membrane's resistance and homogeneity. The change of these parameters before and after the peptide was injected into the model membrane indicated the most likely pore forming mechanism of the peptides. There were four pore forming mechanisms considered: barrel-stave pore, toroidal pore, carpeting, and detergent like membrane disruption. The data of the EIS suggested that the potent pore former peptide used the carpeting or the detergent like disruption mechanisms. The poor pore formers just adhere or intercalate into the membrane without forming pores. From these results the authors concluded that EIS can be used to distinguish between different pore forming mechanisms of peptides. EIS also had the advantage of monitoring the membrane while the pore formation happened. These are only few examples of many peptide-membrane interaction studies with EIS as one of the analytical techniques. The examples of drug-membrane interaction studied by EIS showed that EIS is useful in monitoring the process of membrane pore formation. EIS study then can give insight on the possible pore formation mechanism on the membrane as a result of interaction with the drug.

3.1.4 Previous research on CPZ interaction with membranes

One of the model drugs used in drug-membrane interaction studies was Chlorpromazine hydrochloride (CPZ) (Figure 3.1) [21, 22], the drug also has been used in this thesis.

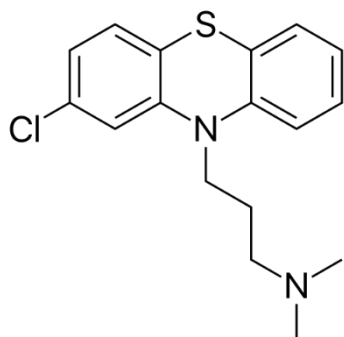


Figure 3.1 The molecular structure of CPZ.

Chlorpromazine is used to treat psychotic disorders and its intended target is the D2 receptor [67] although a research has hypothesised that CPZ has effect on other targets beside D2 receptor [67, 68]. Some studies used CPZ as a model drug, focusing on its cationic amphiphilicity in particular. Other studies focused on the CPZ function as an antipsychotic drug and focusing on its interaction with cell receptors. This work will use CPZ as the model drug in the drug-membrane interaction study.

CPZ had been used by Nussio et al. in drug-membrane interaction studies for investigating the effect of cationic amphiphilic drugs (CADs) on the membrane [21] and the fluidisation effect of the CPZ on the model membrane [22]. The first study used captured liposomes on the Biacore sensor chip as the model membranes and Biacore SPRS as the analytical technique.[21] The second study used SLB formed by liposome fusion on mica as the model membrane and AFM to investigate fluidisation of the membrane caused by CPZ [22].

In the first study, they focused on the interaction between CPZ and two other CADs and captured liposomes made from three different types of phospholipids [21]. Using SPRS, they determined the kinetics of the drug-membrane binding interaction. They identified from the kinetic data which drug had the greatest uptake by model membranes and which model membrane had the greatest interaction with the drugs. They were also able to conclude from the data, combined with the results from other experiments, that the drugs may be able to change the fluidity of the membranes. They also concluded that the drugs did not dissociate completely from the membranes because the SPRS baseline level before the introduction of the drug could not be recovered except for very low concentrations (Figure 3.2) [21]. This showed the accumulation of the drugs in the model membrane.

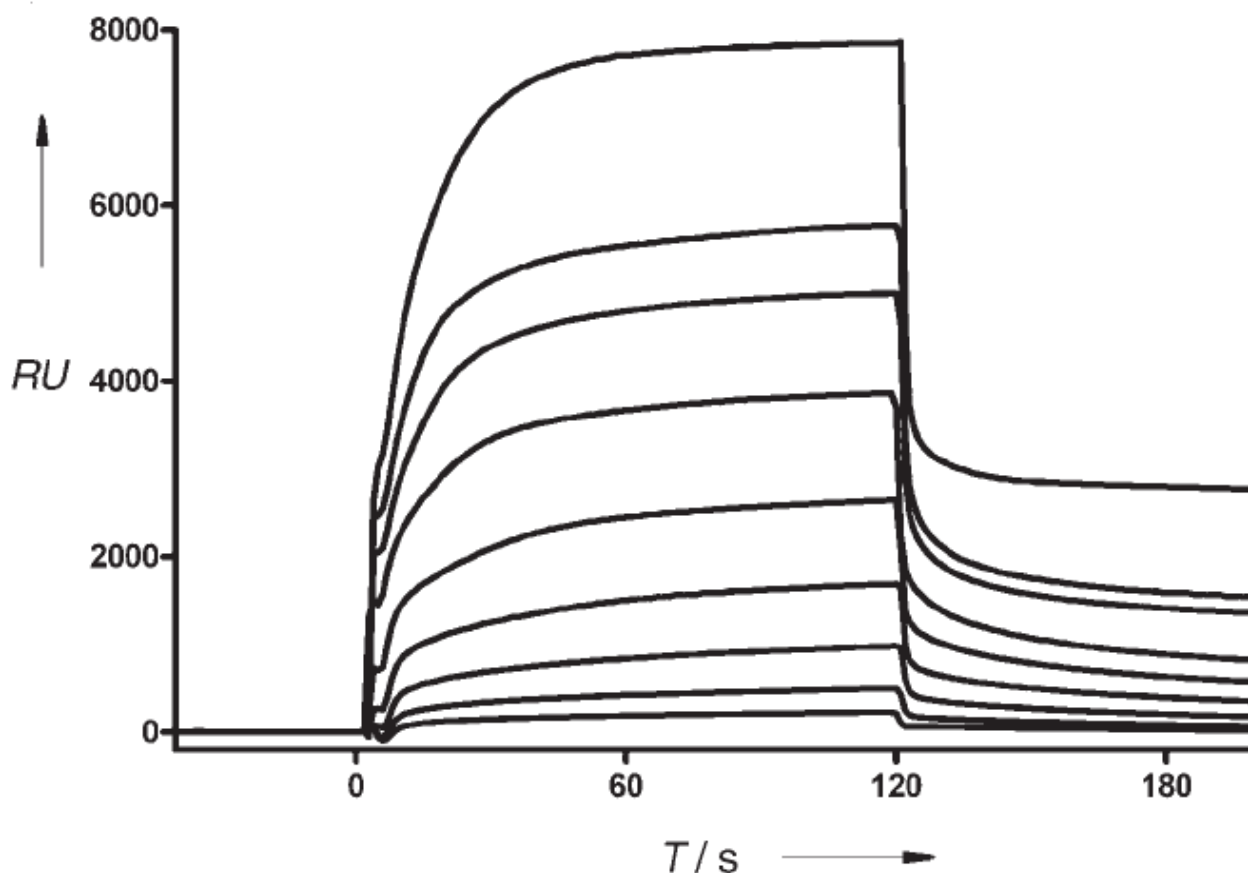


Figure 3.2 The SPR graph of response units versus time (in seconds) from a CPZ-DOPC bilayer interaction. The graph showed binding curves of CPZ with increasing concentration from 15.625 to 1500 μM . Reused from [21] with permission of John Wiley and Sons.

By plotting the maximum response unit versus drug concentration and fitting it with a kinetic model that included nonsaturable and saturable binding sites, Nussio et al. also concluded that two binding mechanisms occurred depending on the concentration. Below 500 μM the kinetics followed a saturable model while above it the kinetics followed a non-saturable model, as seen by the straight line fitting for these concentrations (Figure 3.3). The second drug-membrane interaction study by this group was about the fluidisation of the model membrane by CPZ. Their investigation revealed that the CPZ introduced to the model membrane created defects in the membrane by making the membrane transition temperature change and they were also able to determine that the kinetics of the drug-membrane interaction was first order.

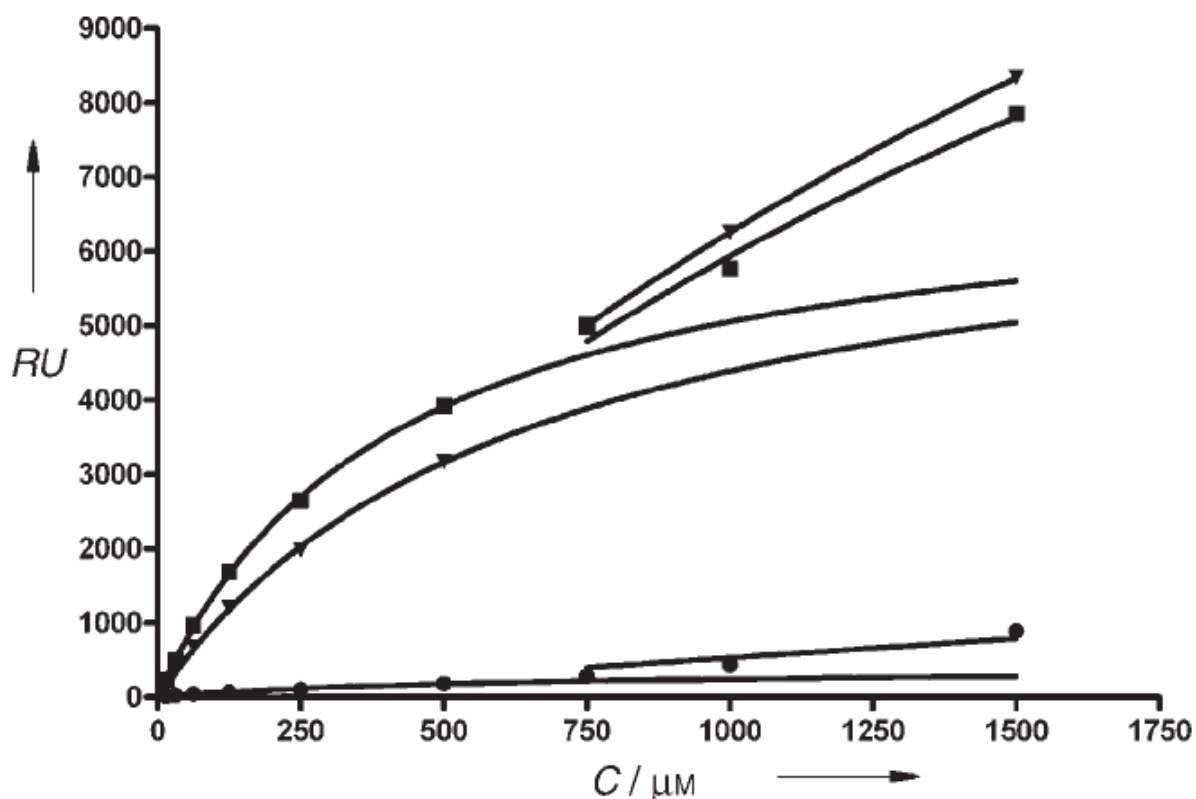


Figure 3.3 The SPR maximum response units versus CPZ concentration. For CPZ concentration below 500 μM , the drug-membrane interaction kinetics followed a saturable model as seen from the fitted line. Above 500 μM , the fitting follow straight line which indicated a nonsaturable kinetics. (\blacksquare), (\blacktriangledown), and (\bullet) are for DOPC, DMPC, and DSPC bilayers respectively. Reused from [21] with permission of John Wiley and Sons.

There were also some studies on the CPZ-cell membrane interaction using the patch clamp technique with whole cells. Sahlholm et al. studied the rate of dissociation of typical and atypical antipsychotics from the D2 receptor expressed on oocyte cells from the current-voltage (I-V) data [69]. They used 17 different compounds but the main study was comparing the dissociation rate of typical antipsychotic CPZ with three atypical antipsychotics amisulpride, clozapine and quetiapine. They did this by measuring the current before the drug bound, when the drug bound and when the drug was removed. When the antagonist substances bound to the receptors, the current/response units decreased. After the antagonists dissociated from the receptor, the response units return to the level before binding. The main result of the article was that the dissociation rates of typical and atypical antipsychotic drugs did not significantly differ.

Another group of researchers also used the patch clamp technique to study the proton current reduction by CPZ and haloperidol in glial cells [67]. Shin and Song studied the effect of antipsychotic drugs on voltage gated proton channels expressed in microglial cells. They measured proton currents during the addition of drugs and the removal of the drugs. The result indicated that the current decreased when the

drugs were added and recovered when they were washed. The proton current was reduced further with increasing concentration of the drugs. The authors hypothesised that proton current reduction played a role in inhibiting neuroinflammation which was one cause of schizophrenia. Since CPZ and haloperidol's main function was to block the dopamine receptor D2, the authors carried out an experiment where dopamine was added to the cell culture and no effect on the current was observed. Then they measured the current reduction by the drugs in the presence and absence of dopamine. The result showed that there was no significant difference in the measured current whether dopamine was present or not. The conclusion was that the reduction of proton current was not related to the D2 receptor binding by these drugs.

Another group of researchers found that CPZ also interacted with and activated ion channels called BK_{Ca} , not only with D2 receptors [68]. The effect of CPZ on the channel was protection against brain ischemia. Li et al. measured the I-V of the channels using patch clamp method and calculated the open channel probability as well the infarct size of the brain tissue of mice treated and not treated with CPZ. The I-V curve indicated that with CPZ, generally the measured current was higher than the control. The infarct caused by ischemia was found to be smaller with treatment of CPZ compared to non-treated infarct. As a further control, the researchers also combined CPZ with a hydrophilic or a hydrophobic drug that blocked the BK_{Ca} channels. The presence of these drugs rendered the CPZ ineffective in protecting against ischemia as shown by the larger infarct size in the presence of these blockers compared to no blockers. As these blockers worked by different mechanisms, this could be interpreted as meaning that the non-protection of the brain tissue was caused by the prevention of CPZ from activating the BK_{Ca} channels.

In addition to experimental studies, theoretical modeling of antipsychotic drugs and D2 receptor study has also been carried out. Pratap et al. did a computational modelling study of drug-ligand or receptor binding simulation and calculated the binding energies of several drugs to the simulated D2 receptor protein [70]. They used 8 kinds of antipsychotics: CPZ, thioridazine, promazine, prochlorperazine, perfenazine, triflupromazine, haloperidol, and trifluperidol. On comparing the calculated binding energies of the drugs to D2 receptor, prochlorperazine had the highest magnitude among the drugs. The conclusion was prochlorperazine was the most potent antipsychotic drug.

A summary of the research reviewed in sections 3.1.1-3.1.4 is given in **Table 3.1**.

Table 3.1 Summary of the drug-membrane interaction research reviewed, focusing on the information gained from the analytical techniques used.

Research group	Model membrane	Drugs	Techniques	Information from measurement
Nunes et al. [55]	Liposomes Lipid monolayers Supported lipid bilayers	Indomethacin Piroxicam Nimesulide Meloxicam	Fluorescence steady state anisotropy Surface area-pressure isotherms IRRAS AFM	It measured phase temperature change because of the interaction with the drug. It measured change of surface area when drugs insert into the monolayer. Combined with the surface area - pressure isotherms, it measured the pressure change caused by the interaction with the drugs. It showed that the drugs except nimesulide caused holes to appear on the supported lipid bilayers.
Pinheiro et al. [10]	Large unilamellar vesicles	N'-acetyl-rifabutin (RFB2)	Fluorescence quenching spectroscopy UV-Vis derivative spectroscopy Dynamic light scattering Fluorescence steady	It showed the drug's location in the membrane. It can be used to calculate the membrane drug partition coefficient. It can be used to measure the transition temperature of the membrane. It measured the cooperativity of the

			state anisotropy	membrane; combined with DLS it measured the membrane fluidity and the effects of drug on the membrane fluidity.
Pinheiro et al. [11]	Liposomes	N'-acetyl-rifabutin (RFB2)	WAXS SAXS	By combining the results from both WAXS and SAXS, researchers can determine the structure of the membrane and the change to that structure because of drug membrane interaction.
Foglia et al. [58]	Vesicles Monolayers	Amphotericin B (AmB) AmB - SCS	surface area-pressure isotherms SANS Neutron reflectivity	It measured the change in pressure caused by the interaction with drugs. This indicates a change in monolayer structure. It measured the change of thickness of the membrane caused by interaction of the drugs with the model membrane. Combination of this method and surface area-pressure isotherms indicated that interaction with both drugs increases the thickness and roughness of the model membranes.
Neves et al. [59]	Liposomes	Resveratrol	UV-Vis derivative spectrophotometry	It showed that Resveratrol entered more easily into liposomes made of pure EPC

			<p>Fluorescence quenching</p> <p>Fluorescence anisotropy</p>	<p>compared to ones made of mixed lipids.</p> <p>It showed that after interaction, Resveratrol was found in both the head group and tail group of the lipids.</p> <p>It showed that the interaction of EPC liposome with Resveratrol makes the membrane stiffer. On the other hand for mixture membranes EPC-CHOL and EPC-CHOL-SM, which was already stiff, Resveratrol decreased their stiffness.</p>
Ferreira et al. [60]	Monolayer	Thymol	<p>surface area-pressure isotherms</p> <p>PM-IRRAS</p> <p>Brewster angle microscopy</p>	<p>It showed that at Thymol concentration of 3% the drug caused the monolayer to expand, which was not occurring for lower concentrations.</p> <p>It showed a decrease of the order of lipid packing in the monolayer after interaction with Thymol.</p> <p>It showed bright phase contrast which indicated that Thymol destroyed parts of the monolayer.</p>

			molecular dynamics simulation	It predicted that Thymol preferentially bound to the hydrophobic tail region.
Alves et al. [61]	Liposomes	Daunorubicin	UV-Vis derivative spectrophotometry Fluorescence spectroscopy Fluorescence anisotropy ZP measurement	The data from this technique showed that membrane permeability to the drug is affected by the membrane's composition. It showed that the drug was located between the polar head group and non-polar tail. It showed that the drug changed the fluidity of the head groups differently than the tails. It showed that the interaction of liposomes with drugs caused the zeta potential of liposomes to be less negative.
Kamimori et al. [57]	Captured vesicles	Kalata	SPRS	It showed that Kalata has higher affinity to model membranes that represent bacterial cell than ones that represent human cell.
Onishi and Kamimori [64]	Captured vesicles	AmB	SPRS	Combining and comparing the results of AmB and Fungizone experiments showed that AmB's affinity to fungal cell membrane model was 9x higher than the Fungizone
Oka and	Captured vesicles	Fungizone	SPRS	

Kamimori [20]				<p>formulation.</p> <p>The results from both experiments also showed that both AmB and Fungizone have higher affinity to fungal cell membrane model than human cell membrane model.</p>
Nascimento et al. [65]	Hybrid bilayer membrane	MagaininI (MagI)	<p>SPRS</p> <p>EIS</p> <p>Cyclic Voltammetry</p> <p>DLS</p> <p>ZP measurement</p> <p>SEM</p>	<p>This technique showed that without Synperonic polymer MagaininI destroyed the HBM and parts of the lipid gets washed away with the peptide. With Synperonic, both peptide and HBM were retained after washing.</p> <p>EIS showed that for HBM only system, membrane resistance initially decreased when MagI was added. The resistance increased again after a few minutes. With HBM+Synp membrane resistance increased after addition of MagI.</p>

Mallaiya et al. [14]	black lipid membrane	Midazolam (MDZ)	EIS	The technique showed that membrane resistance decreased when drug was added. This is interpreted as the drug destabilised the membrane. EIS also showed that membrane capacitance increased in two phases. In the first phase the drug was interacting with the polar head group and decreasing the distance between upper and lower leaflet. In the second phase, the drug penetrated the model membrane.
Chang et al. [66]	polymer supported bilayer	FSKRGY AGGKGF	EIS	EIS could determine that the FSKRGY peptide used either carpeting or detergent like membrane disruption from the change in membrane resistance and homogeneity. Meanwhile EIS also showed that the AGGKGF peptide did not form pores and likely only adhere or intercalate to the membrane.
Nussio et al. [21]	Captured vesicles	Chlorpromazine (CPZ)	SPRS	SPRS had determined that there were two binding phases of the drugs; this depended on the concentration. Up until 500 μ M the drugs

		Amitriptyline Propranolol		bind according to saturable model. Above this concentration the drugs bind according to non-saturable model.
Nussio et al. [22]	Supported lipid bilayer	CPZ	AFM	AFM showed the defects on the bilayer membrane caused by interaction with CPZ and it also measured the kinetics of the interaction.
Sahlholm et al [69]	D2 receptor expressed on oocyte cells	CPZ Amisulpride Clozapine Quetiapine Other drugs ¹	Patch clamp	This technique showed that when the drugs bind the current decreased, when the drug were released/dissociate, the current returned to previous level. Measurement using this technique showed that that dissociation rates between typical and atypical antipsychotics did not differ.
Shin and Song [67]	Microglial cells	CPZ Haloperidol	Patch clamp	It detected proton current reduction when the drug bind to voltage gate receptor. CPZ and haloperidol were also designed to block the D2 receptor but whether this receptor is blocked or not does not impact the current at

¹ Haloperidol, Asenapine, N-desmethylozapine, Olanzapine, Paliperidone, Remoxipride, Risperidone, (-)-Sulpiride, Preclamol((-)-3PPP), Pridopidine(ACR16), (-)-OSU6162, NS30678, JNJ-37822681.

				all. This meant that the current reduction was not because D2 receptor binding.
Li et al. [68]	Brain cells	CPZ	Patch clamp Photo of brain cell samples	The technique showed an increase in current when CPZ bind to the BK _{Ca} channel and activated it compared to when no binding occurred The photos showed that the brain cells where CPZ activated the channels have smaller area with ischemia compared to cells who did not have CPZ activating the channels.
Pratap et al. [70]	simulated D2 receptor	CPZ Prochlorperazine Other drugs ²	molecular dynamic simulation	Binding energy calculation showed that Prochlorperazine has the highest binding energy. This meant that this drug was the most potent antipsychotic.

² Perfenazine, Triflupromazine, Haloperidol, Trifluoperidol, Thioridazine, Promazine.

3.1.5 Research aims and objectives

The literature reviewed in sections 3.1.1 and 3.1.3 showed that environmental factors such as temperature, ionic strength and pH had an effect on drug membrane interaction in influencing the membrane phase, ionisation state of the drug and membrane surface charge. An ionised drug will interact more strongly to the polar region of the membrane while neutral drug will interact more favourably with the nonpolar part. The surface charge of the membrane had been shown to have an effect on drug selectivity. Membrane phase (gel or liquid crystal) had been shown to interact with the drugs differently. The literature has shown how a membrane could affect drug bioavailability and conversely how a drug affected the structure and properties of the membrane. Several studies also pointed to the location of the drugs in the membrane. There also have been several studies on the effect of drugs that could cause defects or destabilise the model membrane which was related to the toxicity to the intended target or to the host patient. Drugs could also affect the transition temperature of the membrane. Several studies also have shown that drugs, including peptides could have an effect to another target on the membrane instead of intended receptor. Yet another studies revealed that some drugs were selective in their interaction with the model membranes. Membranes made from lipids that represent bacterial cell membranes were preferentially targeted by antibacterial drugs, while membrane made from lipids that model fungal cell membranes were targeted by antifungal drugs. All these studies are made possible by different techniques, which can complement one another. For example SPRS could give information on drug association and dissociation rate to the membrane while EIS can give information on how the drug-membrane interaction influenced the electrical properties of the membrane. These studies point to the necessity of studying drug-membrane interaction with various complementary techniques.

The reviewed literature showed that most studies using model membranes usually used liposomes, and a few used supported lipid bilayer. Most studies on ion channel and receptor interaction used whole cells with patch clamp technique. Using whole cells for drug-membrane interaction make it difficult to disentangle the various factors influencing the CPZ-receptor interaction. The tBLMs make possible the study of drug-receptor or drug-ion channel interaction using model membranes but there is a lack of drug-membrane interaction study using tBLMs. One possible research using tBLMs then is to study the proportion of drugs that bind to the receptor or ion channel to the proportion of drug that bind to the lipid polar region and the drugs that penetrate into the bilayer core.

Previous studies of CPZ-membrane interaction characterised the effect of the drug on the model membrane, which is changing the fluidity and generating defects on the model membrane. By comparing the CPZ-membrane interaction studies and studies made with other drugs, studies about the effect of ionic strength and pH on CPZ-membrane interaction can be carried out. It is possible as well to study the effect of CPZ on membranes made of lipids that represent bacterial and fungal membrane instead of human or mammalian membrane. There is also need for research on additional target for CPZ. So a research using tBLMs incorporating voltage gated proton channel proteins is also relevant to further the previous research.

In drug-membrane studies where ion or proton transport was involved, EIS and patch clamp techniques was usually employed. The patch clamp is harder to perform than EIS and it used live cell which need to be maintained under strict conditions to maintain viability. In addition the patch clamp measures the current-voltage relationship only while the EIS can measure the resistance and capacitance of the membrane. EIS can provide information such as membrane tightening (increasing capacitance) which patch clamp technique cannot. So EIS-tBLM experiments can complement the previous patch clamp-cell experiments. Sahlholm et al hinted that penetration of CPZ into the cytoplasm may have important consequences *in vivo*. Of course this study can be done with whole cell but maybe the cytoplasm can be modelled by the water in the tether region of tBLMs.

Previous research using SPRS technique usually studied the binding kinetics of drugs to the membrane. From the kinetic data, the selectivity or affinity and accumulation of the drug in the membrane can be determined. This information, combined with the techniques that can pinpoint the location of the drug in the membrane and can analyse the structural changes of the membrane will provide a more complete picture of the CPZ-membrane interaction. SPRS is an essential part of the techniques to understand drug-membrane interaction.

In this work, a different way to study drug accumulation on membranes is studied. The aim of this research is to study the drug-membrane binding to answer the question: Is the amount of drugs that can bind to the lipid bilayer limited by the binding sites of the membrane or by the concentration of drugs in solution? The answer will contribute to the understanding of drug accumulation.

Studying drug membrane interaction is very important to determine how membranes can influence the effectiveness of a particular drug. Research on drug membrane interaction will allow us to understand the toxicity or negative side effects of drugs. Finally, understanding how drug membrane interaction

influence drug action can lead to the discovery and development of new drugs and new drug delivery systems.

3.2 Experimental

3.2.1 Materials

The glass slides used in all experiments were LaFSN9 with refractive index (n_D) of 1.8449 from Hellma. The gold nuggets for coating the slides were supplied from Peter W. Beck Australia. The chromium sputter coater target was supplied by Quorum Technologies. 2,3-di-O-phytanoyl-glycerol-1-tetraethylene glycol-D,L-lipoic acid ester lipid (DPhyTL) was synthesised in the lab. 1,2-di-O-phytanoyl-*sn*-glycero-3-phosphocholine (DPhyPC) was supplied by Avanti. Dimethyl sulfoxide (DMSO) was supplied by Sigma-Aldrich, 4-(2-hydroxyethyl)-1-piperazineethanesulfonic acid (HEPES) was supplied by Sigma. Sodium chloride (NaCl) was supplied by Chem-Supply. CPZ was supplied by Fluka. Sodium hydroxide for pH adjustment was supplied by Chem-Supply.

Ethanol (EtOH) was supplied by Chem-Supply, High Performance Liquid Chromatography (HPLC) EtOH were supplied by Scharlau, Ultrapure water (resistance $>18M\Omega$ cm, MilliQ) was obtained from the Labconco water purifier. Hellmanex cleaning solution was obtained from Hellma, Germany. The cleaning solution used to wash the glassware in all experiments was made by mixing 50 ml of Hellmanex with 1 L of MilliQ.

3.2.2 Gold coated slides preparation and functionalisation

LaFSN9 glass slides were first washed by sonication in the cleaning solution for 5 minutes followed by sonication in MilliQ then EtOH for the same duration. After cleaning, the slides were dried by blowing nitrogen over them. The dried slides were then coated by a thin layer of chromium (~ 2 nm) using Q300T-D dual target sputter coater from Quorum Technologies. The sputtering current was 100 mA and the layer thickness was set to 3 nm. After the chromium layer was deposited, gold layer was deposited on top by electrothermal evaporation process. The evaporation was carried out by COVAP II evaporator from Angstrom Engineering which is a part of the Australian National Fabrication Facility (ANFF). The thickness of the gold film was set at 50 nm and the deposition rate at 1 Å/s.

The prepared slides were then dipped in 10 ml of 0.2 mg/ml DPhyTL in HPLC EtOH solution overnight. The DPhyTL molecules would self-assemble on the gold surface. After the self-assembly

was complete, the slides were taken out of the solution then washed thoroughly with EtOH and dried under nitrogen stream.

3.2.3 Formation of tBLM

The functionalised gold coated slide was then placed on the SPRS flow cell, gold side facing inward. The glass side was then wetted with index matching oil from Cargille Labs $n_D=1.72$ and a prism was placed on top. The assembly was placed in a sample holder and put in the SPRS instrument.

The vesicle solution was prepared by making 2 mg/ml DPhyPC solution in MilliQ. Then the solution was vortexed for 1 minute and heated in 40 °C water bath for 1 hour to improve the mixing of lipid and water. After heating, the solution was vortexed again for a while and then extruded 25 times through a 50 nm pore diameter membrane filter (Millipore). 200 μ l of the resulting clear solution were then mixed with 5 ml of 0.1 M NaCl solution before being cycled through the flow cell at 0.5 ml/min flow rate. The tBLM was formed by vesicle fusion in 0.1 M NaCl solution overnight and the kinetics of vesicle fusion was observed by SPRS. If a good upper layer is obtained, the thickness usually will be 6-10 nm. Good upper layer formation also showed as the increase of impedance and decrease of capacitance in the EIS Bode plot. Fitting with a RRCPE model should give impedance of about 1 M Ω and a capacitance of 1 μ F.

3.2.4 Drug-membrane interaction

After the tBLM was completed, it was used as the platform to study drug-membrane interaction. The chlorpromazine drug was dissolved in a buffer containing 150 mM NaCl, 10 mM HEPES and 1% DMSO pH5.5. Three different kinds of experiments were carried out. First, single concentrations of drugs were cycled through the flow cell. 250, 500 and 1000 μ M CPZ in buffer were cycled through the flow cell with the rate of 0.1 ml/min. Each concentration used a different tBLM. The kinetics of adsorption and desorption were observed with SPRS fixed angle mode. Fitting the kinetics to Langmuir adsorption kinetics was attempted. Second, different concentrations of drugs were cycled sequentially using the same tBLM. Third, three different batches of the same concentration were cycled sequentially using the same tBLM. For the second and third sets of experiment the concentrations used were: 62.5, 125, 250, 500, and 1000 μ M CPZ. For the multiple drug circulation experiments, the kinetics were not fitted because the desorption rate cannot be resolved for each concentration; and so the adsorption rate also cannot be fitted for each concentration.

Figure 3.4 gives the flowchart of the experimental steps.

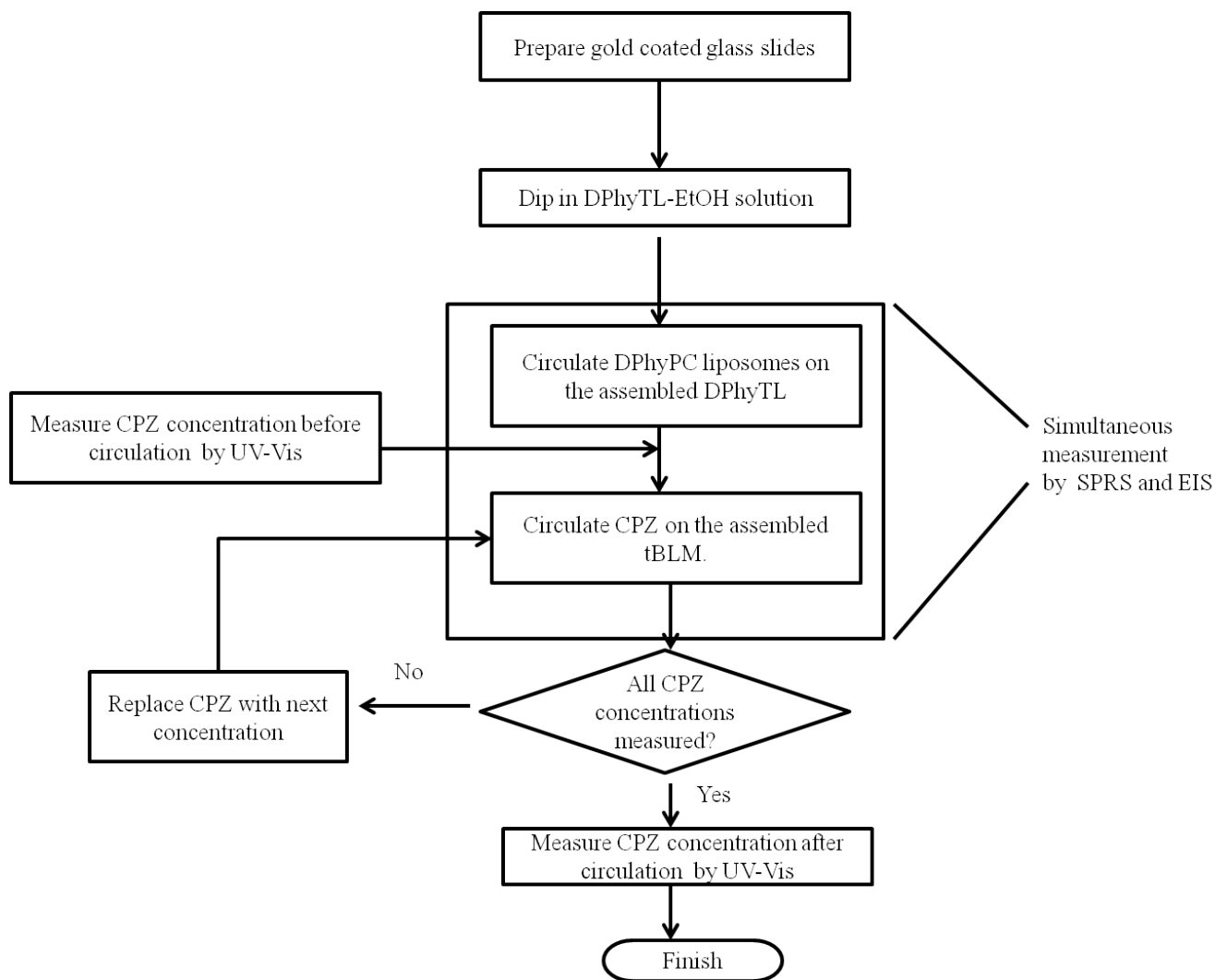


Figure 3.4 Flowchart of drug-membrane interaction experiment.

3.3 Results and Discussion

3.3.1 Monolayer self-assembly and bilayer formation

The tBLM in this work was made of DPhyTL as the lower leaflet and DPhyPC as the upper leaflet. DPhyPC was chosen because this phospholipid is a good representation of the main phospholipid component in human cell membranes. DPhyTL was chosen because the lipid component of the thiolipid is the same as DPhyPC. Additionally DPhyTL has an excellent membrane resistance [25] which is good for a tBLM experiment. Tethered lipid self-assembly was usually completed overnight, but depending on the solution and slide it can also take several days to finish. A reasonably good monolayer is achieved when the optical thickness of the layer in air is about 3 nm. (Figure 3.5)

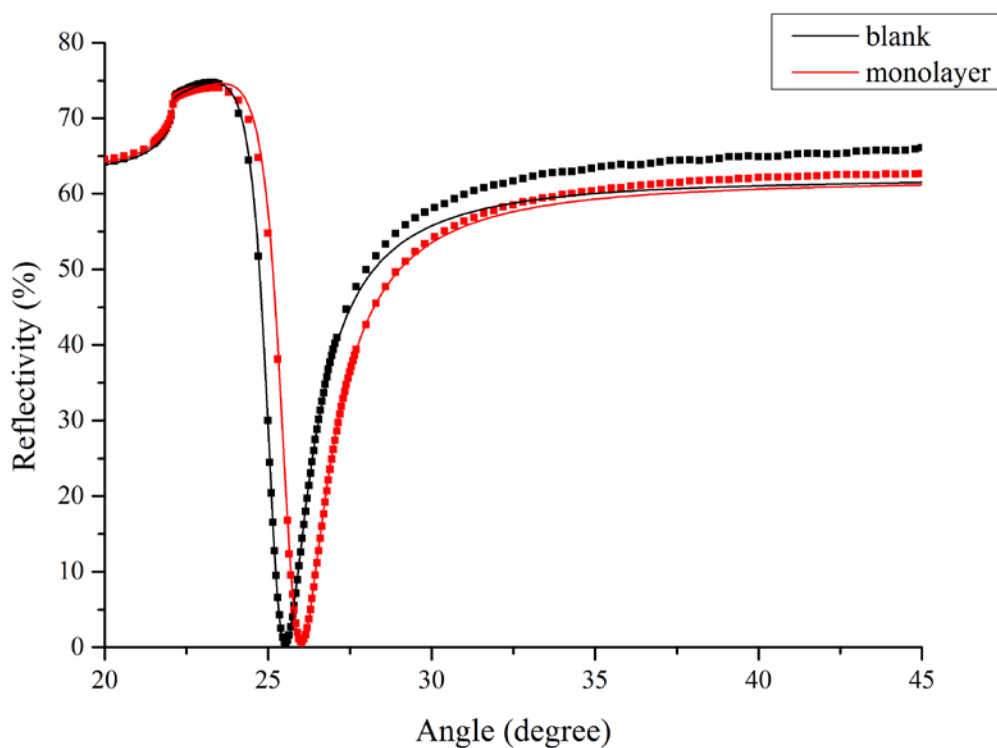


Figure 3.5 Angle scan and fitting for a blank sample (substrate without the monolayer) and the sample with self-assembled DPhyTL in air. The fitting parameters of the monolayer curve give optical thickness of 3 nm. The squares are the data points from the measurement while the lines are the fitting of the curve.

Contact angle experiments showed that just deposited gold had contact angles of about 40° while gold with good coverage of DPhyTL monolayer had contact angles of approximately 100° - 110° . Gold with slightly poor coverage of DPhyTL had contact angles of around 90° . The CA experiments also showed that gold exposed to ambient air had contact angles of approximately 84° . It could be concluded that a slide covered with DPhyTL had a high degree of hydrophobicity, while slides exposed to ambient air become less hydrophobic due to contaminants adsorbing onto the surface.

Bilayer formation typically completed after 12-20 hours (Figure 3.6). The angle shift caused by the addition of the upper layer differed from sample to sample. Most of the upper leaflets were about 5 nm thick, but some samples showed 8 or even 10 nm thickness. Although the theoretical length of the DPhyPC is 3.5 nm, several experiments showed that upper layer optical thickness of 3-4 nm often resulted in unexplainable CPZ kinetics. This thickness value indicated that the formed bilayer was not complete and cannot be used for further experiments. Meanwhile upper layer with optical thickness of more than 6 nm often showed an initial increase in kinetic response when CPZ was bound followed by continuous decrease until it flattened out at a certain value. This was interpreted as CPZ destroying the additional lipids on top of the formed bilayer. Therefore the optical thickness of more than 6 nm was

deemed too much and was assumed to be caused by adsorption of still unfused vesicles on the bilayer. EtOH-water mixture with concentration of 10% or 25% (v/v) was used to wash these excess lipids. Once the final top layer thickness was determined to be around 5-6 nm, then it was used for drug-membrane interaction (Figure 3.7).

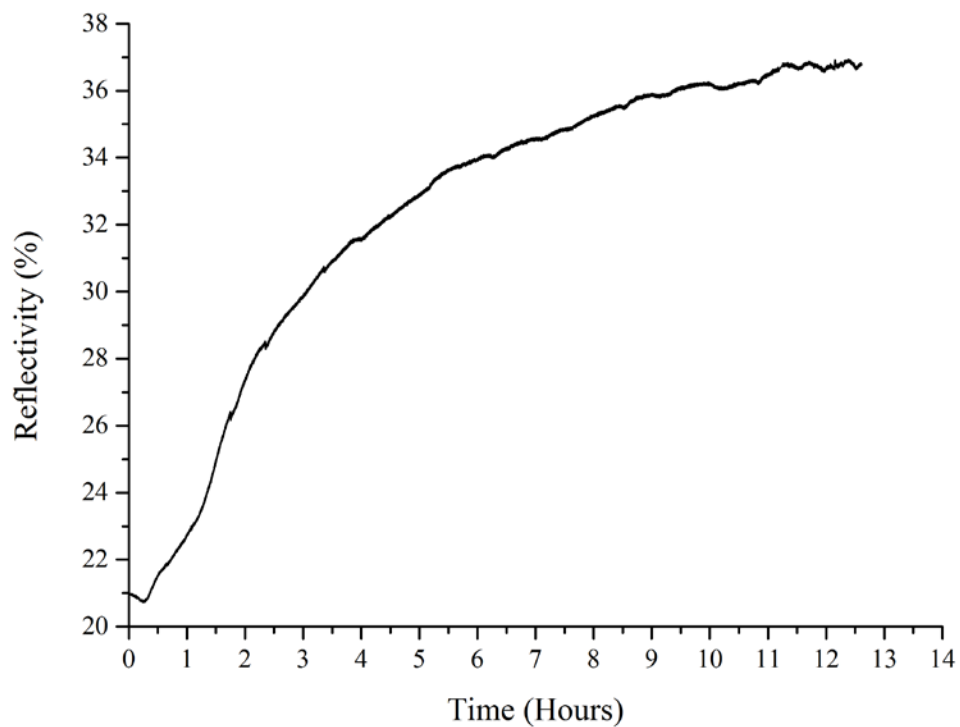


Figure 3.6 Bilayer formation kinetics in flow cell with 1 ml volume.

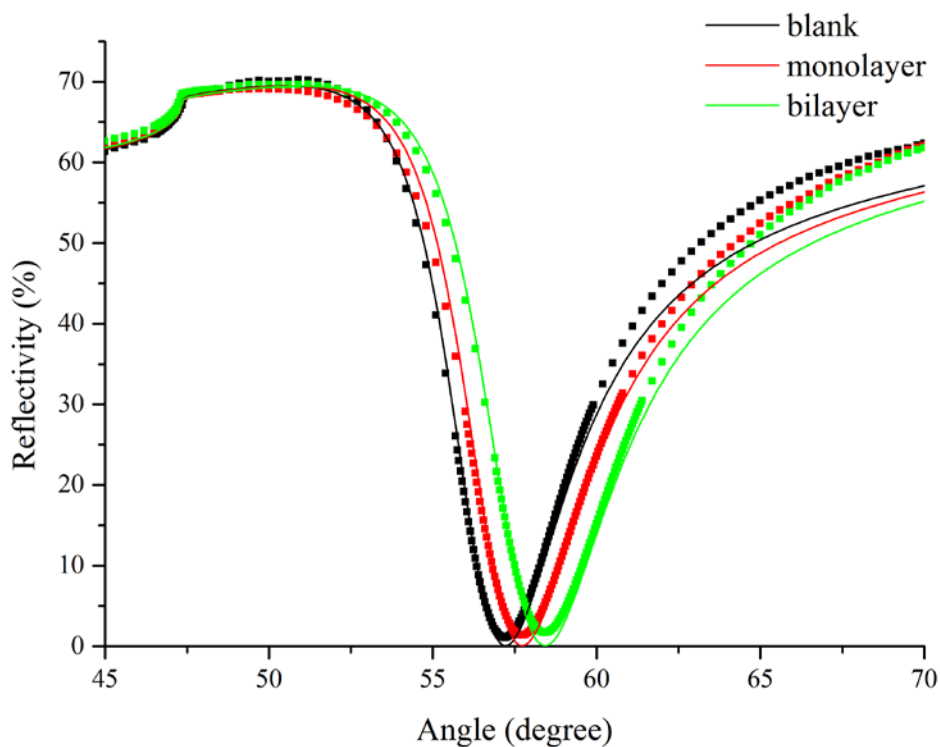


Figure 3.7 Angle scan of a blank sample (sample not coated with thiol molecules), the sample with self-assembled DPhyTL monolayer, and the sample with complete bilayer in sodium chloride solution. The fitting parameter for the upper layer gives an optical thickness of 5 nm. The squares are the data points from the measurement while the lines are the fitting of the curve.

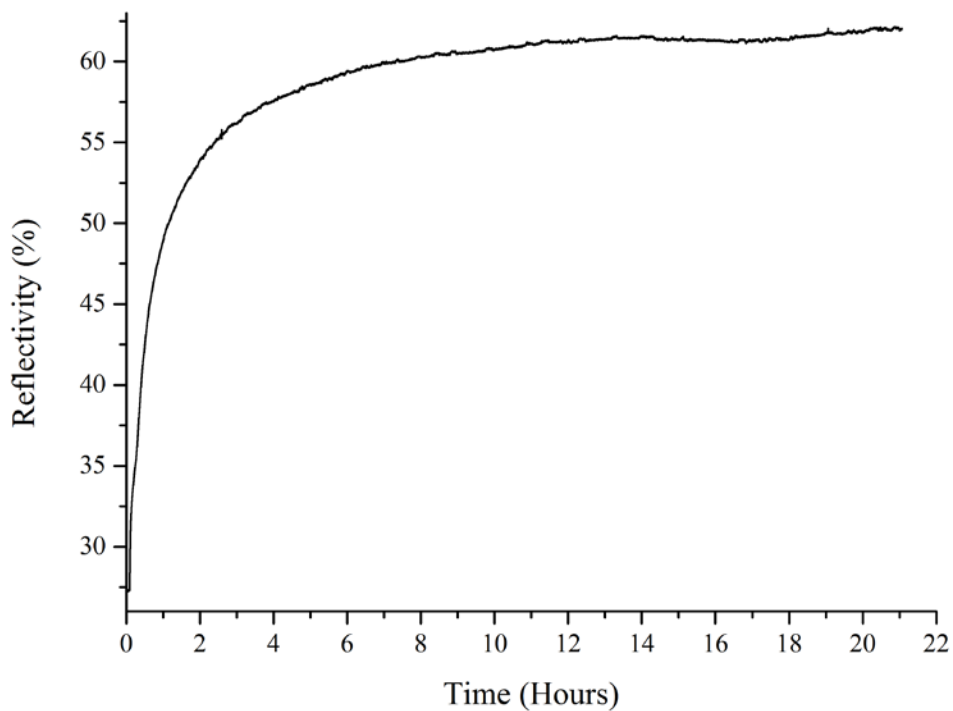


Figure 3.8 Bilayer formation kinetics in flow cell with 100 µl volume.

The size of the flow cell used apparently affected how quickly the bilayer was formed. The microfluidic flow cell with a volume of about 100 μl showed faster bilayer completion than the standard flow cell with 1 ml volume. With the microfluidic flow cell, the bilayer was complete around 6 hours (Figure 3.8).

3.3.2 CPZ-tBLM interaction

After successful bilayer formation, titration like drug-membrane interaction SPRS experiments using sets of three different CPZ concentrations were carried out. The concentrations used were 62.5, 125, 250, 500, and 1000 μM . The experiment using 62.5 - 250 μM CPZ showed that the addition of higher concentration of drugs increased the reflectivity to a stable new level (Figure 3.9). The rate of drug association for each concentration was also different, with the first circulation the fastest to reach stable equilibrium.

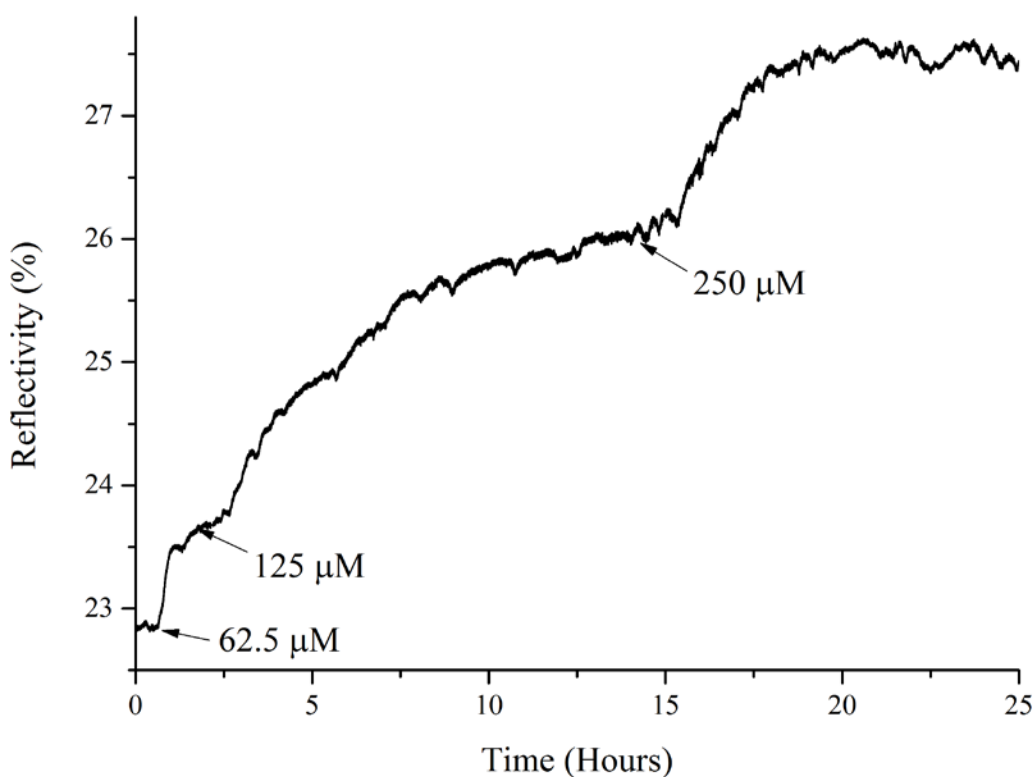


Figure 3.9 kinetics of 62.5 - 250 μM CPZ recirculated sequentially.

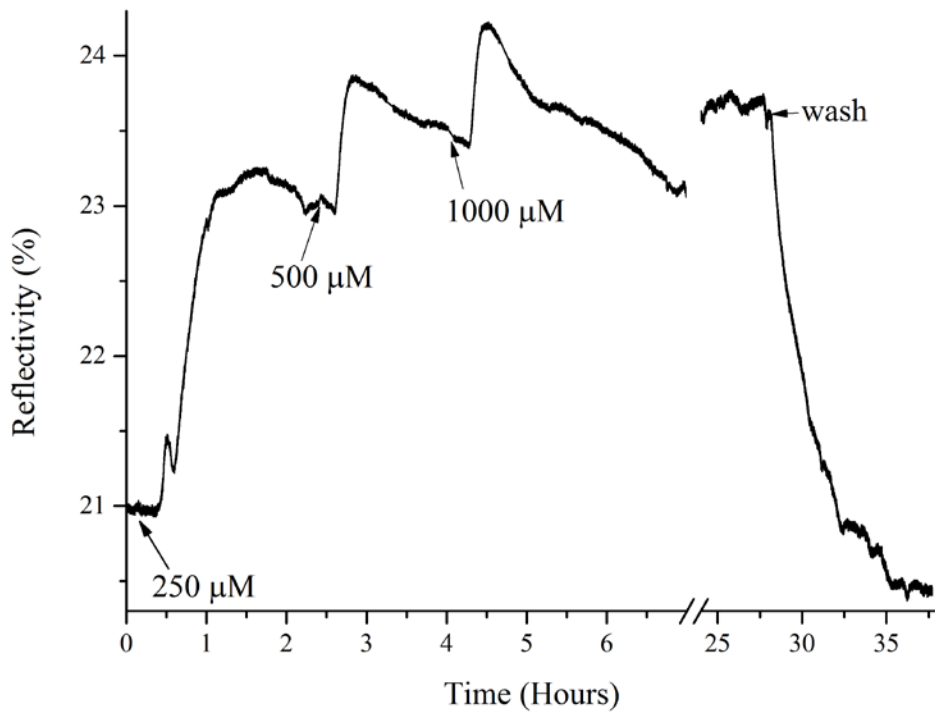


Figure 3.10 multiple drug concentration recirculation 250, 500, and 100 μM CPZ.

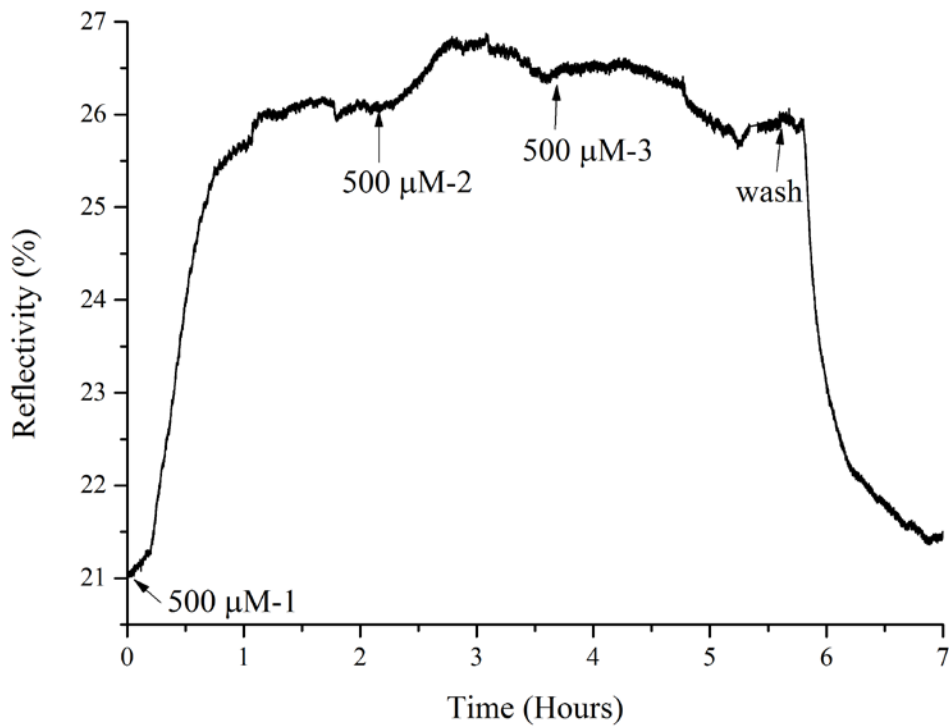


Figure 3.11 Kinetics of 3 batches of 500 μM CPZ recirculated sequentially.

When the triple concentration drug-membrane interaction experiment was done with 250, 500, and 1000 μM however, overshoots in the kinetic happened with the addition of the last two concentrations

(Figure 3.10). When 500 and 1000 μM concentrations were added, there was a quick initial increase, followed by slower decrease and this was called an overshoot. It can be seen in the figure that after a long time, around 20 hours, the decrease was reversed and the reflectivity increased slowly until equilibrium was reached. It seemed as if the drug tried to bind to the membrane as soon as there was a concentration difference between free drug and bound drug, but then the binding spot was not available and the bound drug was released again into solution. This overshoot phenomenon has been observed before in the literature [71, 72].

In [71], a drug called PSA was stored in a donor layer, separated from an acceptor layer by a permeable membrane. An overshoot was observed in the acceptor layer and attributed to the supersaturation of the drug in the donor layer. The slow decrease after initial quick increase was interpreted as caused by some drugs in the acceptor layer permeate back into the donor layer. In [72] a drug was injected into the bloodstream of mice and then collected in the brain extracellular fluid after the drug passed through the blood-brain barrier (BBB). The overshoot was attributed to the possibility that the drugs eventually replacing the protons that was used by the BBB transporter. Because the transport is two-way between blood and brain, some of the drugs may have been transported back to the bloodstream. This caused the initial quick increase followed by slower decrease. From these two articles, it can be concluded that an overshoot is an indication that a solute or analyte slowly reverses its diffusion.

The experiments described in two articles detected the drugs as they moved into the second compartment. In this work, the SPRS detected the binding of the drug to the model membrane. Although the reasons for the overshoot in the two articles could not be applied here, the fact that an overshoot happened was an indication that the drugs that first were accumulated on the membrane were slowly being released back into solution. Since this overshoot did not happen with lower concentration of drugs, a plausible explanation for the cause of the overshoot was that finally the membrane binding sites were saturated and could not accommodate more drugs.

To test whether the binding of drug to the membrane was affected by the availability of binding sites or by the concentration of free drugs, the same concentration of drug was injected three times into the flow cell. This experiment was done for each concentration used, with the representative result shown in Figure 3.11 for CPZ 500 μM . A single concentration of drug was split into three equal batches and then measured with UV-Vis spectroscopy to get the absorbance before and after the drug membrane interaction experiments. Then each batch was injected into the flow cell containing the tBLM in a

certain interval. The kinetic result indicated that the reflectivity increased only a little during the second addition, and by the third addition, no significant increase was observed. Furthermore UV-Vis measurement after the interaction with the membrane revealed that all three batches lost some of the free drug; the first one lost the most and the second and third circulations lost the least amount of drug (Figure 3.12). This indicated that the drug binding was driven by the concentration difference of bound and free drugs and that the membrane tried to accommodate as many drugs as it could. This was also supported by the general trend shown in the figure for different CPZ initial concentrations. The larger the initial concentration, the larger the concentration decrease. This was additional support to the notion that the higher the free concentration, the more drug bound to the membrane. These values of CPZ concentration were calculated using several calibration curves from absorbance vs concentration data (Figure 3.13). The error bar was calculated from the error in the proportionality constant using error propagation formula. The error bars for all concentrations except 125 μM in Figure 3.12 were derived from the proportionality constant error of the first calibration curve. The error bars for 125 μM CPZ was derived from the from the proportionality constant error of the fourth calibration curve. The result in Figure 3.12 was not corrected for the dilution and mixing effect. Because of the way the experiment was conducted, when the first batch was injected, there was CPZ buffer already running in the system and the CPZ buffer diluted the concentration of the first batch. The second and third batch was injected with the previous CPZ batch still remaining, which resulted in mixing of previous batch with the new one. The result was also not corrected for nonspecific adsorption of CPZ to other surfaces than the tBLM. This was because correcting the results for these sources of errors resulted in nonsensical data (negative decrease).

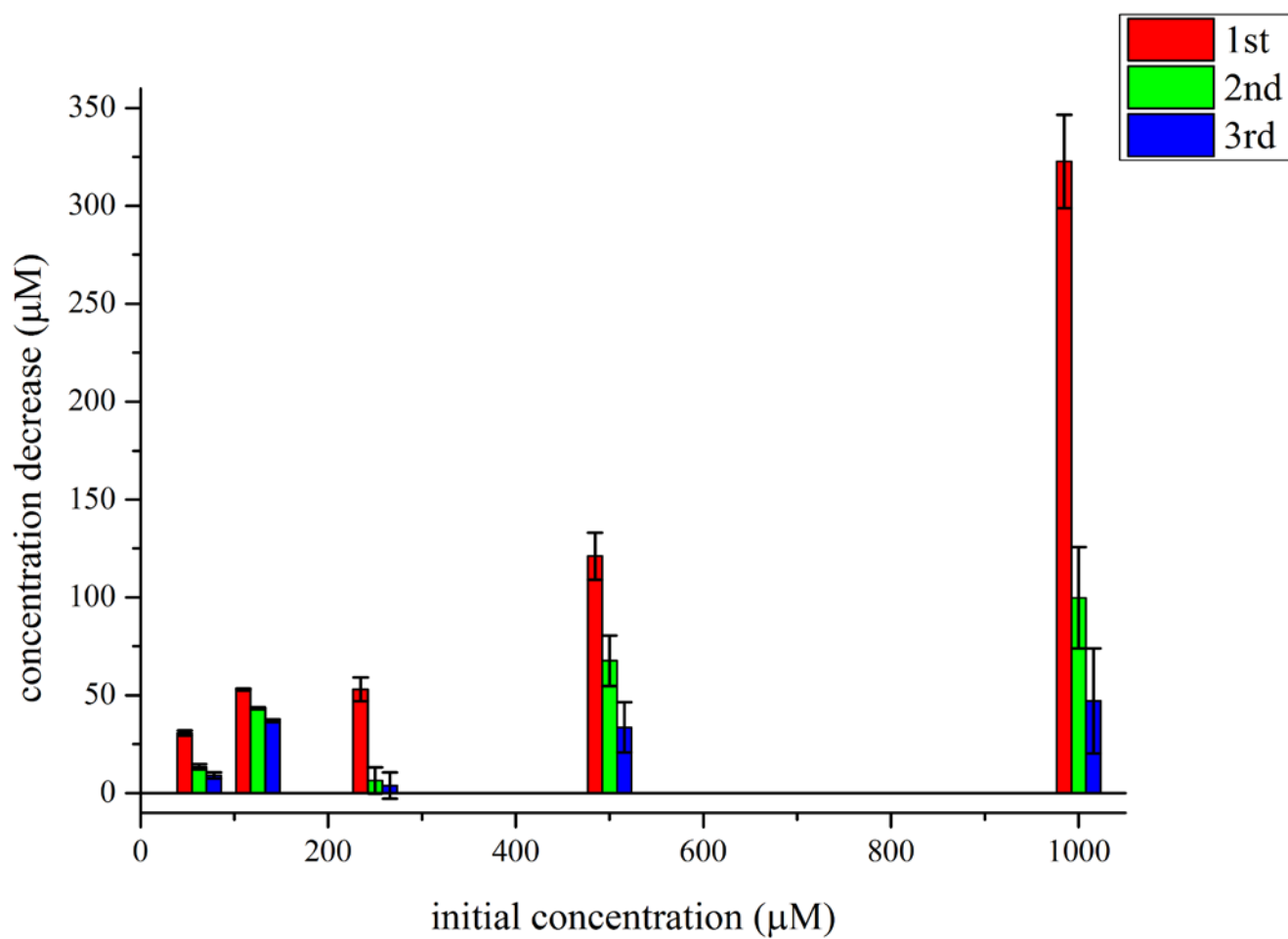


Figure 3.12 Concentration decrease resulted from CPZ binding as measured by UV-Vis from the triple same concentration kinetic experiment. The values at the middle of each column triplet indicate the initial concentration. Red, green, and blue columns represent the first, second, and third batch. See text for the explanation of the error bars.

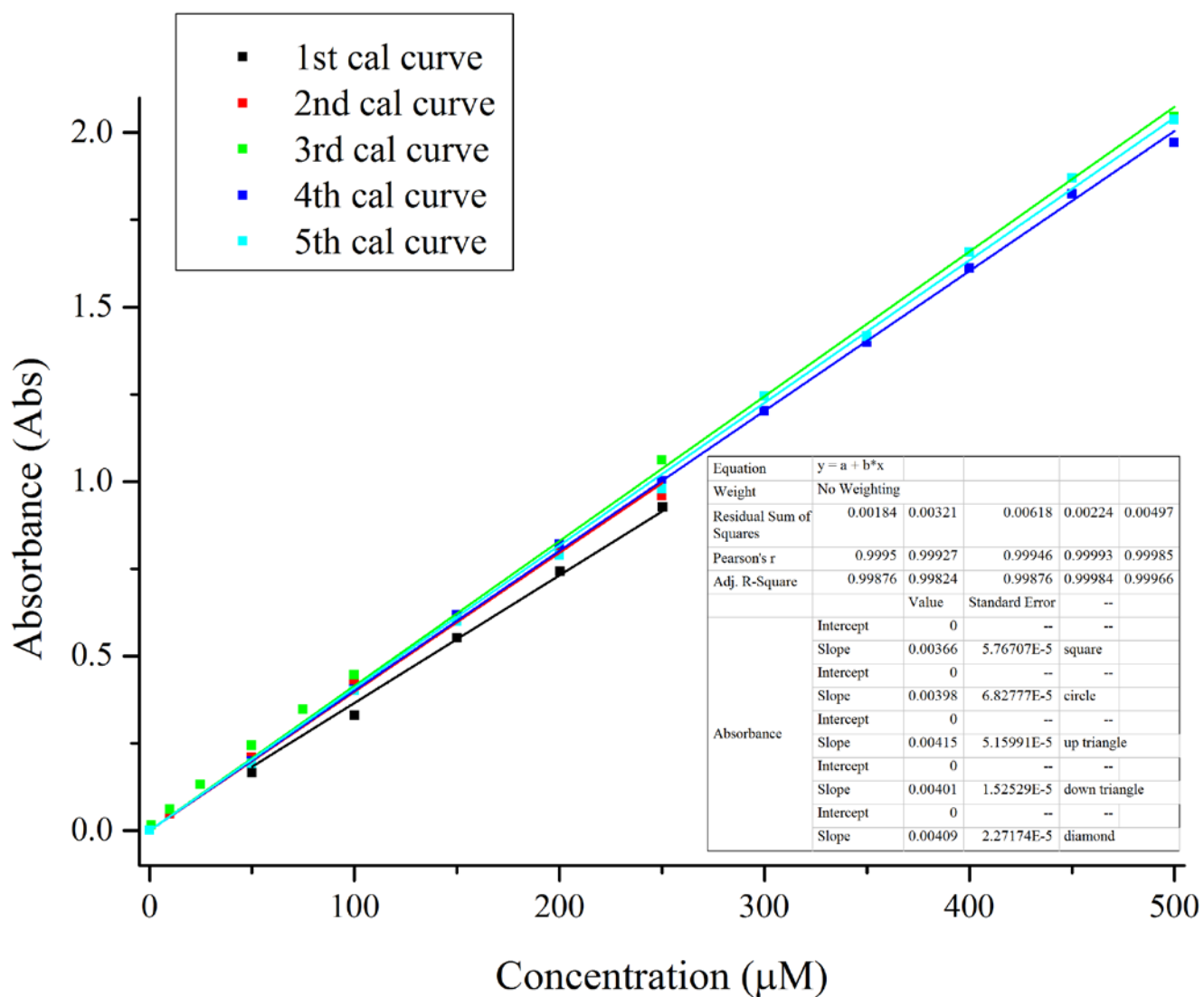


Figure 3.13 All calibration curves used in this work with their linear fits. The concentrations and corresponding errors in the previous figure were derived using the first and the fourth calibration data.

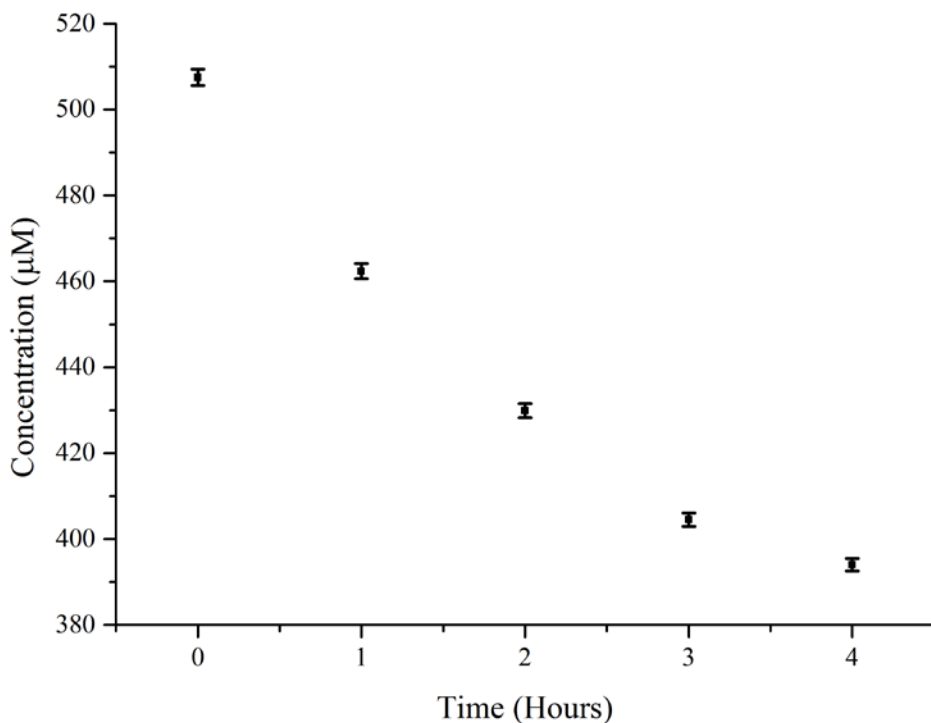


Figure 3.14 500 μM CPZ concentration decrease because of nonspecific adsorption as measured by UV-Vis.

It is interesting to note that although the third circulation of the same concentration did not increase the reflectivity response, the UV-Vis measurement still detected loss of drugs. Control experiments using uncoated glass slides and flow cell revealed nonspecific drug adsorption to the cell, glass and tubings (Figure 3.14). This figure shows that as the circulation times neared infinity, the amount of free drug slowly decreased toward an asymptotic limit. From the measurement of nonspecific adsorption of other drug concentrations, it can be concluded that after a long time the free drug decreased to around 70-80% of the initial concentration. This meant that the nonspecific adsorbed drugs reached a saturation level of 20-30% from the initial concentration.

These previous kinetic experiments were done in less than 24 hours. It might be possible that longer circulation times would show an increase of reflectivity. To test this possibility an experiment with longer circulation times, around 50 hours and three times 125 μM CPZ circulations had been done (Figure 3.15). The first circulation with more than 15 hours circulation time showed that once stable saturation level was reached, the reflectivity did not increase. The second circulation also did not increase the reflectivity response just like the previous experiment with shorter circulation times. The third circulation seemed to increase the reflectivity, but because the circulation times was more than 50 hours, the membrane maybe changed so much that the increase in reflectivity cannot be attributed

purely to CPZ binding. Most likely it is caused by signal drift, because the increase is not as significant as the first batch. Therefore, the kinetic behaviour was not affected by circulation times.

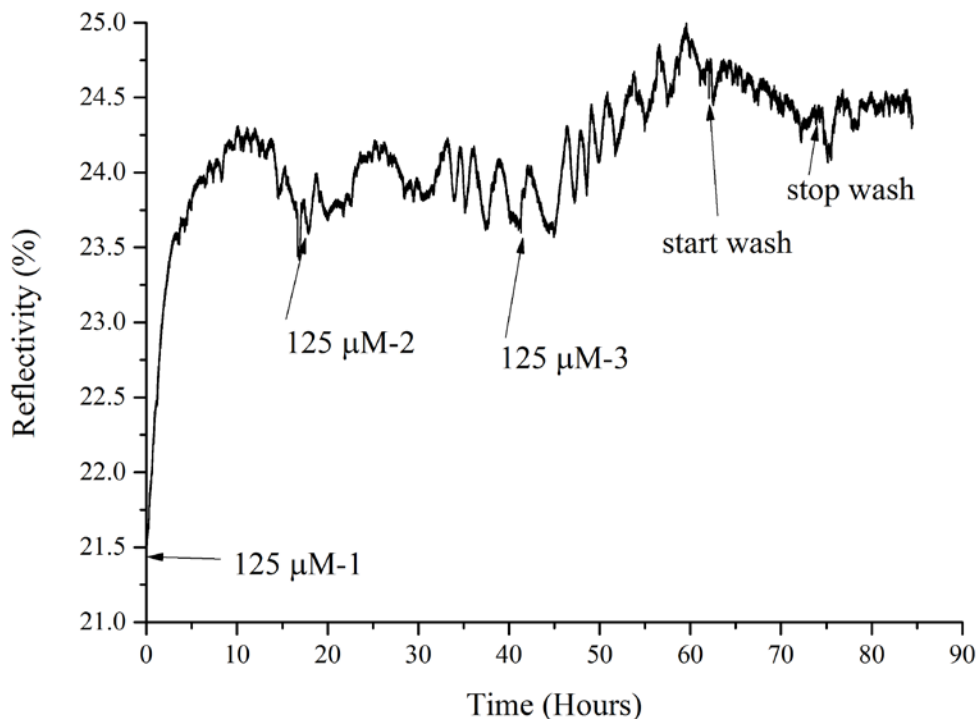


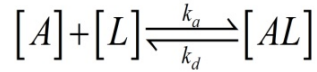
Figure 3.15 Kinetics of 3 batches of 125 μM CPZ recirculated sequentially over 50 hours.

There were several conclusions from the different and same concentration kinetic experiments, as well as the UV-Vis free drug concentration measurement. First, the adsorption depended on the concentration of the free drug instead of the available binding sites. If there was only a little amount for binding, the increase was not much, but when there was a lot to bind, the concentration increases a lot. Second, there was a saturation limit of the membrane in which the membrane would not bind more drugs as seen from the 250-1000 μM experiments. There was a possibility as well that the binding of the drug was not a monolayer but multilayer. Attempts to fit single concentration drug-membrane interaction kinetics to the Langmuir or 1 to 1 layer showed (Figure 3.16) that the model did not fit the kinetics.

The Langmuir model of adsorption or Langmuir isotherm is based on several simplifying assumptions. First assumption is that the binding sites are all identical. Second assumption is that bound molecules do not interact with each other, only with the binding sites. Third assumption is the adsorption only forms a monolayer. [73] The Langmuir model is the simplest of adsorption models and often is the first model to go to fit adsorption and desorption kinetics. From the fit, the desorption and the adsorption

rate constants can be derived. The Langmuir model was first developed to explain the adsorption of gases to planar surfaces.[74] Since then, it has been adapted for binding of analyte molecules to binding sites in SPRS kinetic experiment. The Langmuir model had been used in similar approaches as the drug-membrane interaction experiments done here, therefore this model was the model used for kinetic fitting.

The equation of Langmuir adsorption is



Where [L] is the concentration of ligand or binding sites, [A] is the concentration of analyte molecules, in this case CPZ. [AL] is the analyte-ligand complex formed when a drug binds to a site. The symbols k_a and k_d are adsorption and desorption rate constants respectively. The half left and right arrows represent the dynamic equilibrium of drug associating and dissociating from the binding site.

From that equation, the kinetic rate equation for the binding process can be derived

$$\frac{d[AL]}{dt} = k_a [A][L] - k_d [AL]$$

Where $\frac{d[AL]}{dt}$ is the binding rate. By using the relation of $l_0 \propto R_{\max}$ where l_0 is the concentration of bound analytes and R_{\max} is the maximum reflectivity at steady state, the rate equation can be converted to SPRS signal equivalent

$$\frac{dR}{dt} = k_a C (R_{\max} - R) - k_d R$$

R is the reflectivity at time t , and C is the total concentration of analyte. If this equation is integrated an expression to obtain the kinetic curve fit for adsorption is obtained

$$R_a(t) = (R_{\max} - R_i) \left(1 - e^{-(k_a C + k_d)(t - t_i)}\right) + R_i$$

$R_a(t)$ is the reflectivity during adsorption or binding phase as a function of time t while R_i and t_i are the initial reflectivity at baseline and the starting time of analyte adsorption, respectively. To fit the

desorption phase, the rate equation must be integrated after setting the first term to zero which resulted in

$$R_d(t) = (R_{\max} - R_f) e^{(-k_d(t_f - t))}$$

$R_d(t)$ is the reflectivity during desorption or release phase as a function of time t while R_f and t_f are the final reflectivity at the new baseline and the finishing time of analyte desorption, respectively. This derivation of the Langmuir adsorption model for SPR analysis was slightly modified from <https://www.sprpages.nl/kinetics/association> and <https://www.sprpages.nl/kinetics/dissociation>. As can be seen from the integrated adsorption equation, the desorption phase needs to be fitted first to obtain k_d before the adsorption phase can be fitted. Therefore, if the desorption phase cannot be fitted, the adsorption phase cannot be fitted as well.

The desorption of the drug from the membrane clearly showed at least two stages, where only the first stage can be roughly fitted with the Langmuir adsorption model shown by the blue line. The adsorption stage too, cannot be fitted entirely by the Langmuir model and showed multiple stages. Although the kinetics did not follow Langmuir adsorption model, these attempts showed that the kinetics of CPZ-membrane interaction was very complex. It was possible that the different stages of dissociation pointed to multilayer adsorption, where drug can also bind to another drug below it and not only to the membrane.

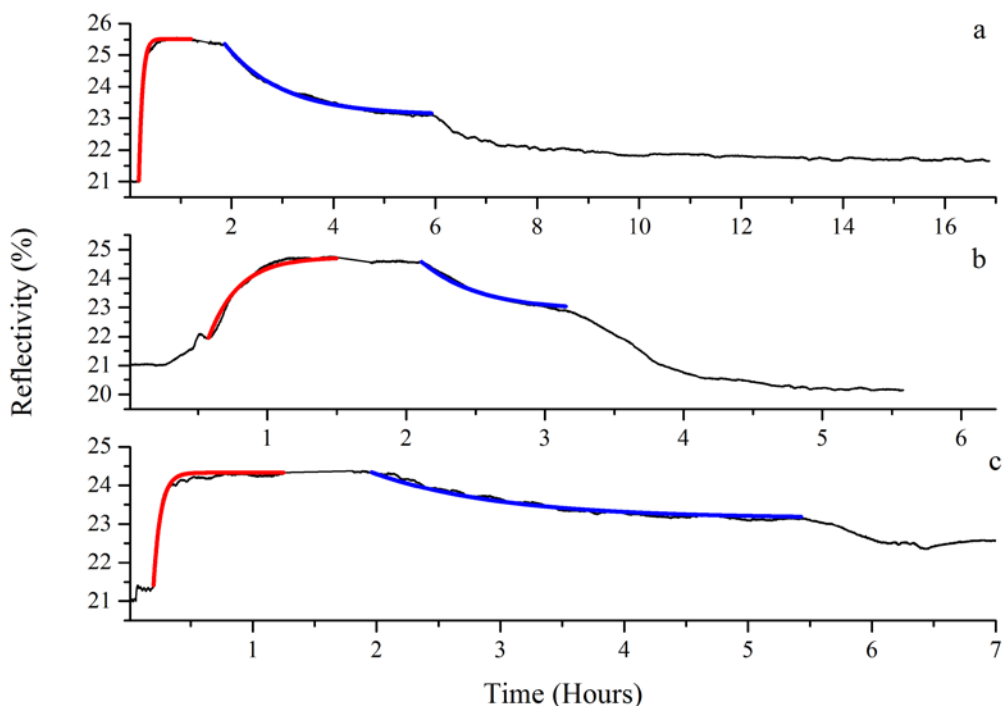


Figure 3.16 Attempt to fit the drug-membrane interaction kinetics with the Langmuir adsorption model. a is 250 μM CPZ, b is 500 μM CPZ, and c is 1000 μM CPZ. Red line is the attempted fitting at association phase and blue line is the attempted fitting at dissociation stage.

Since the Langmuir model did not apply to the drug-membrane interaction for all concentrations used in this experiment some other model must be used to explain the kinetic behaviour. It was even possible that two different non-Langmuir kinetics apply to the different concentration ranges, one from 62.5-250 μM and the other from 250-1000 μM . This was because in the first range the membrane did not reach saturation while in the second range the membrane reached saturation.

This result was quite different from that of Nussio et al. [21]. Their result indicated that CPZ drugs can bind to the model membrane from 15 μM -1500 μM without ever reaching saturation of the membrane. Below 500 μM , the drug concentration vs response unit plot looked like the binding would reach saturation, but above that concentration, instead of saturation the plot followed a linear trend, which meant the binding would not reach saturation. This difference may be caused by the actual difference of the model membranes. It was possible that the liposome capture process by the Biacore SPRS sensor chip preserves the liposome form [75], while the angular shift in the SPRS instrument used in this work indicated that the vesicles fused to form a bilayer membrane.

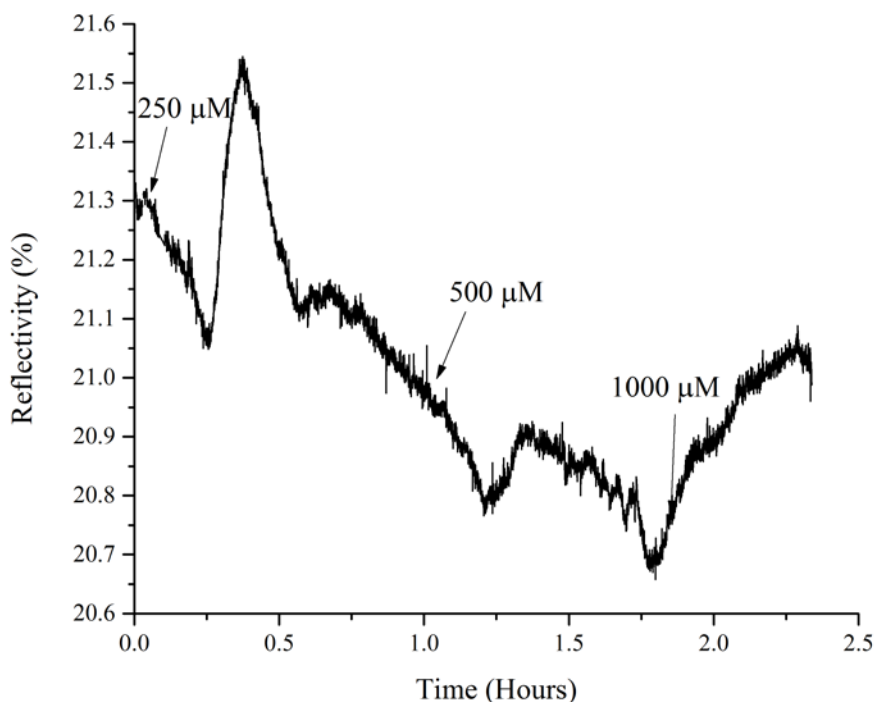


Figure 3.17 CPZ interaction with a monolayer made of DPhyTL with concentrations 250 μM , 500 μM , 1000 μM sequentially recirculated. The model membrane used here is not a DPhyTL-DPhyPC bilayer as in previous figures. The binding is within the noise level. This indicated that there is no binding between the drug and the monolayer.

As a control, a drug binding experiment with a DPhyTL monolayer was also attempted with 250, 500, and 1000 μM CPZ. (Figure 3.17). The kinetics showed that although the drug initially seemed bound to the monolayer, the drug was quickly released into solution. Further addition of drugs decreased the kinetic signal even lower below baseline. The decrease and later increase is still within the noise level of the instrument. This showed that drugs could not bind to the monolayer where the hydrophobic tail was exposed to the solution. Therefore, a successful binding event needed the lipid upper layer where the hydrophilic head was exposed to the solution. From all the above results, it can be concluded that the CPZ-tBLM interaction did not follow the Langmuir adsorption kinetics and was dependent on the free drug concentration, up to a certain point.

3.3.3 EIS results

The formation of a bilayer as seen by EIS showed that the capacitance decreased while the mono/bilayer resistance increased. The values of the resistance and capacitance from fitting with R(RCPE) model can be seen in Table 3.2. As can be seen from the table, the membrane resistance of the bilayer was higher than the monolayer by approximately 10 $\text{M}\Omega$. The capacitance of the bilayer however, was slightly lower than the monolayer by 0.03 μF . This increase of resistance and decrease of

capacitance was expected for a good quality bilayer. [25, 26] The interaction with CPZ showed a slight change in bilayer resistance in spite of the same concentration of CPZ used (Figure 3.18 and Table 3.2). The first, second, and third circulation of 125 μM CPZ decreased the bilayer resistance. This was an indication that bound CPZ caused slight disruption to the bilayer's ordered structure. However the bilayer resistance values from the fitting did not change very much from the first to the second circulation. This was corroborated by Figure 3.15 where the second addition of CPZ batch did not cause the reflectivity to increase. Figure 3.18 also shows only very slight difference between the resistance values of the tBLM at the first and second circulation. The third circulation of the 125 μM CPZ caused the resistance to drop by 10 $\text{M}\Omega$ as shown in the table. Figure 3.18 also shows more significant decrease of the membrane resistance compared to the second circulation. This could be connected to the fact that the reflectivity increased a little when the third batch was added. This was possibly showing that the drugs decreased the order of the bilayer even more, although not to the point of destroying the membrane or forming pores. When the CPZ was washed from the bilayer, the resistance recovered although not to the original level. This showed that the CPZ effect was somewhat reversible and that the order in the bilayer was not completely restored. This may be caused by the CPZ that cannot be washed, as shown by the kinetic results.

Table 3.2 EIS fitting parameter from the R(RCPE) equivalent circuit model for the data in Figure 3.18.

Name	Resistance ($\text{M}\Omega$)	Capacitance (μF)
Monolayer in NaCl	35.90 \pm 1.61	0.58 \pm 0.007
Bilayer in NaCl	43.30 \pm 2.75	0.55 \pm 0.008
Bilayer in CPZ Buffer	46.39 \pm 6.81	0.52 \pm 0.009
First 125 μM CPZ addition	19.95 \pm 1.00	0.56 \pm 0.01
Second 125 μM CPZ addition	24.47 \pm 1.59	0.59 \pm 0.02
Third 125 μM CPZ addition	13.95 \pm 0.72	0.62 \pm 0.02
Washing CPZ with the buffer	32.43 \pm 1.72	0.60 \pm 0.01

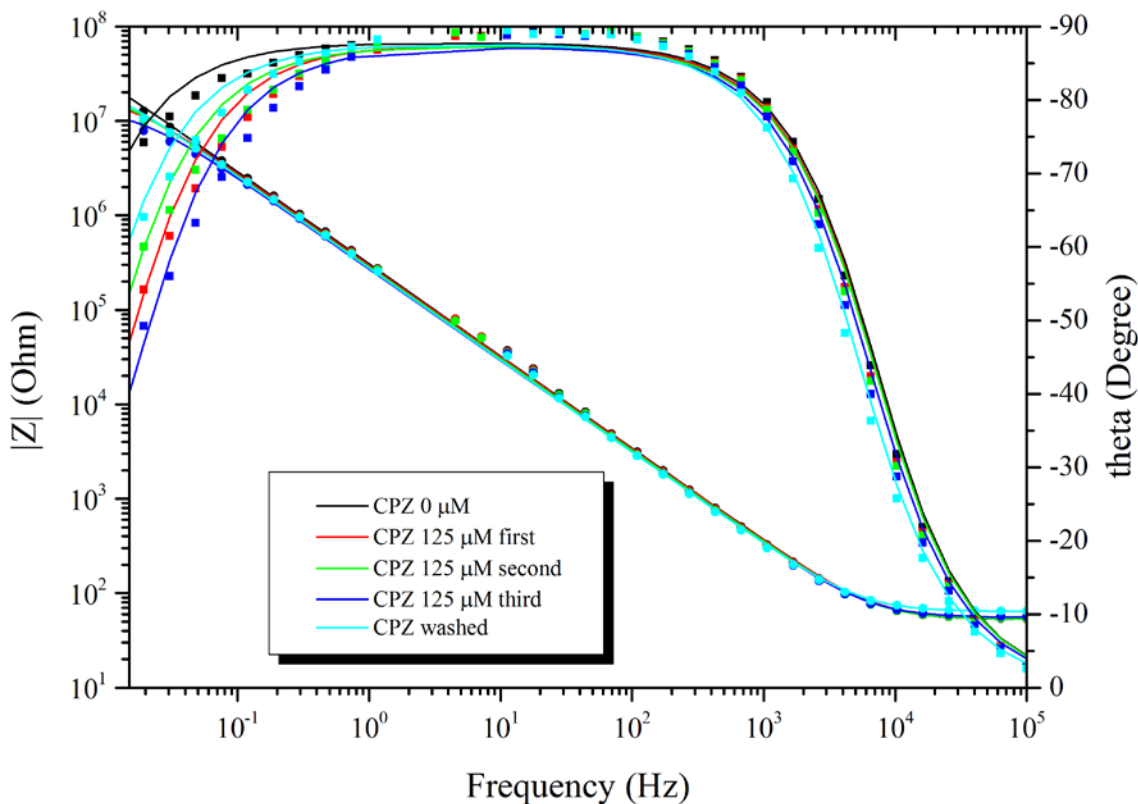


Figure 3.18 Bode plot of CPZ-tBLM interaction with 125 μM CPZ injected three times.

3.4 Conclusion and outlook

The tBLM has been successfully made and used as a platform for drug-membrane interaction investigation. Kinetic studies using SPRs and electrical impedance measurement using EIS showed that CPZ-membrane interaction was very complex. The drug binding depended on the concentration of the drugs. Below a certain concentration, drugs can bind to the membrane as long as there was a significant difference between the concentration of bound drugs and free drugs. Above this concentration limit, addition of more drugs caused the saturation of the binding sites. At this stage, drug binding was limited by the availability of free sites on the membrane. This answered the question of what controls drug binding posed as the aim of this research. Additionally, it is found that, CPZ binding to the membrane did not follow the Langmuir adsorption model, possibly formed multilayers, and slightly reversible. It also did not disrupt the membrane packing order very much, not to the point of forming pores or destroying the membranes. Future prospect of drug-membrane interaction research can include finding a kinetic model that can represent the interaction more accurately and investigating CPZ interaction with membranes made of different lipids.

CHAPTER 4 TETHERED LIPOSOME COATED GOLD NANOPARTICLES

4.1 Introduction

The development of new model membranes will certainly benefit the investigations of the cell membrane, membrane processes, and drug-membrane interaction. In this chapter, a new model membrane is proposed. This model membrane consists of a gold nanoparticle core surrounded with liposome shell that is also tethered to the membrane. This model membrane combines two model membranes discussed in chapter 1: liposomes and tBLMs. By combining both model membranes, the advantages of each model membranes can be combined. The advantages of liposomes are that they are easy to make and their three dimensional nature. The advantages of tBLMs are that they are exceptionally stable model membrane and that they have a reservoir between the membrane and the support. This reservoir can be thought as representing the inner part of the cell membrane. The reservoir also enables incorporation of membrane proteins without the risk of losing the natural conformation and activity. The tethered liposome coated gold nanoparticles, also called tethered liposome-AuNP hybrid should have the stability of tBLM and the three dimensionality of liposomes. It also will be relatively easy to make and it enables incorporation of proteins and mimicking the inner and outer environment of a cell. The disadvantage of a liposome is that it is not very stable. Liposomes have several issues regarding their stability. From the chemical side, there are degradation processes like oxidation and hydrolysis of the fatty acid chain. From the physical side, there are aggregation and fusion processes [76, 77]. The disadvantage of tBLMs is that the formation depends on uncontrollable fusion process between vesicles and the assembled thiolipids. This means that it is difficult to reproduce tBLM with the same quality. In addition to that the fusion process is dependent on temperature and can last for a few hours to tens of hours. If the temperature is too low, the vesicles will not fuse. So tBLMs are more difficult to make compared to liposomes. But by combining both, they covered each other's disadvantages by their advantages. The hybrid system will be more stable than liposomes while easier to make compared to tBLMs.

The basic structure for a tBLM like “particle” should mirror the stationary tBLM itself. Gold nanoparticles (AuNP) functionalised by tethered lipids with actual lipids for the outer leaflet. The analogue for the gold surface on glass slides is the AuNP, the tethered lipid analogue is the same tethered lipid and the outer lipid analogue is the same lipid.

Another rationale for the design of the AuNP coated with tethered liposome is to make a more robust drug carrier. Hu et al. has argued that with nanoparticle core providing constraints to the size of the liposome, a narrower size distribution would result [78]. This, in turn can increase the probability for uptake of the drug carriers into the targeted cells [78]. Previously there was already an attempt of make a AuNP-liposome hybrid without tether molecules connecting the nanoparticle core and the liposome shell for drug delivery in cancer therapy. [79] This new hybrid of liposomes tethered to the AuNP should be more stable than the untethered liposome hybrid.

The design of AuNP – tethered liposome hybrid for a new model membrane is based on a theoretical modelling done by Hu et al..[78] Although they have argued for the application of drug delivery, this construct can also be developed to study plasma membranes using model systems. The tethered liposome hybrid was first modelled using computer modelling (Figure 4.1).

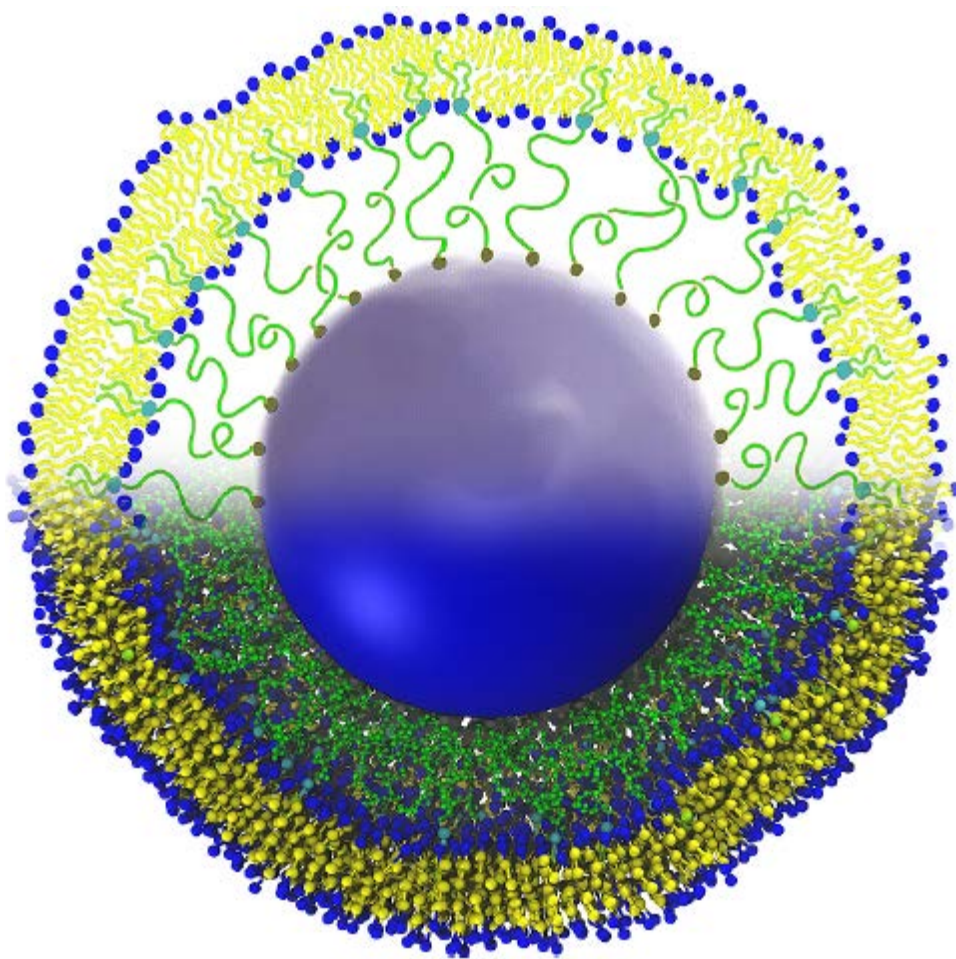


Figure 4.1 Computer modelling of tethered liposome-AuNP hybrid. The blue sphere represents the AuNP, the green lines represent the tether molecules, and the blue balls with yellow tails represent the phospholipids. Reused from [78] with permission of the American Chemical Society.

In their paper, Hu et al. discussed the constraints on the parameters of this construct, particularly the radius of the liposomes. The radius of the core and the length of the tether molecules in relaxed condition impose a limitation for the minimum and maximum radius of the liposomes. If the liposome radius is less than the minimum, the pressure from the tethers will cause the liposome to burst. If the vesicle radius is larger than the maximum limit, the tether molecule can be pulled out of the liposomes (Figure 4.2). However, simulation has shown that it is possible for the liposome to shed lipids to accommodate for the shorter tether length.[78]

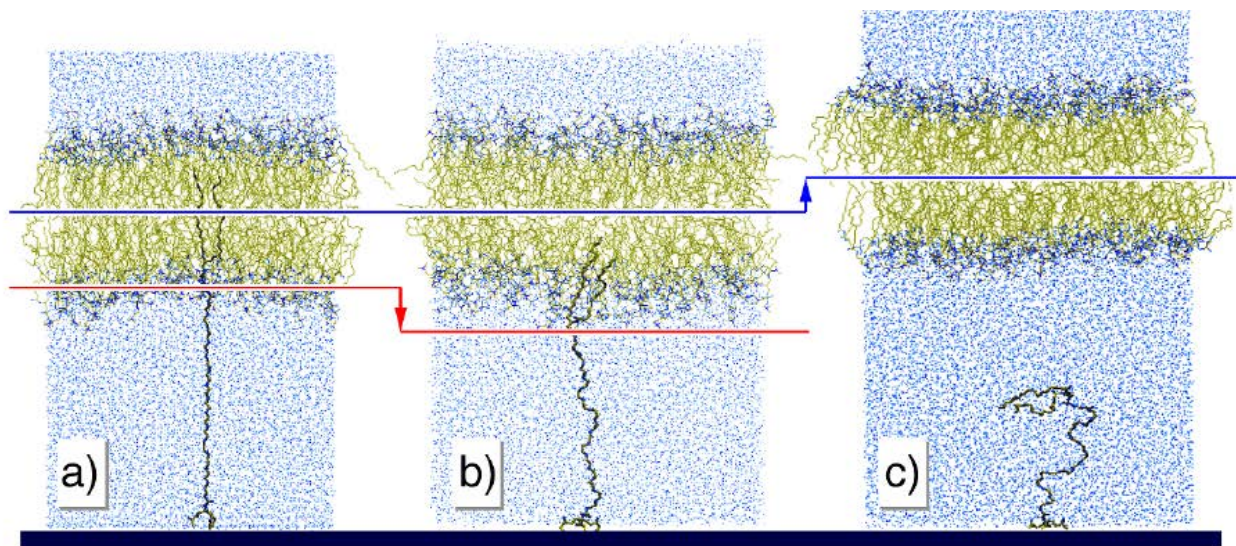


Figure 4.2 Illustration on how a tether molecule can be pulled out of the lipid. a) The starting condition. b) The tether is slightly pulled out of the lipid bilayer after 100 ns. c) The tether is completely pulled out if the lipid is moved farther away as indicated by the blue arrow between panels b) and c). Reused from [78] with permission of the American Chemical Society.

In this work the considerations are a bit different, instead from starting from the core size and tether length, the size of the smallest stable liposome and the tether molecules determine the core size. Since the smallest liposome diameter that is stable is about 50 nm and the tether molecules are about 5 nm then the particle diameter should be around 30-40 nm.

4.1.1 Research aims and objectives

The aim of this work is to synthesise the gold-tethered liposome hybrid as a nanoparticle analogue of a tBLM. This is achieved by first synthesising gold nanoparticles followed by functionalisation with thiolipid molecules (DPhyTL). The functionalised gold nanoparticles will then be coated with liposomes (DPhyPC) by either sonication or extrusion.

4.2 Experimental

4.2.1 Materials

1,2-di-O-phytanoyl-*sn*-glycero-3-phosphocholine (DPhyPC) was supplied by Avanti. Sodium borohydride (NaBH_4) was supplied by Sigma-Aldrich, sodium citrate dihydrate ($\text{HOC}(\text{COONa})(\text{CH}_2\text{COONa})_2 \cdot 2\text{H}_2\text{O}$) by Sigma-Aldrich, chloroauric acid (HAuCl_4) from Sigma-Aldrich. Triton X-100 (TX-100) was supplied by Sigma-Aldrich. Ascorbic acid was supplied by Sigma. Dichloromethane (DCM) was supplied by VWR. Ethanol (EtOH) and Chloroform were supplied by Chem-Supply. Ultrapure water (resistance $>18\text{M}\Omega$ cm, MilliQ) was obtained from the Labconco water purifier. Hellmanex cleaning solution was from Hellma, Germany. The Hellmanex cleaning solution used to wash the glassware in all experiments was made by mixing 50 ml of Hellmanex with 1 l of MilliQ. 36% hydrochloric acid (HCl) and 70% Nitric acid (HNO_3) were supplied by RCI Labscan. Octadecylamine (ODA) was supplied by Aldrich. 1-dodecanethiol (DDTh) was supplied by Aldrich and 3,3,4,4,5,5,6,6,7,7,8,8,9,9,10,10,10-Heptadecafluoro-1-decanethiol (HDFDTh) was supplied by Aldrich.

4.2.2 AuNP synthesis and functionalisation

Two methods were used to synthesise AuNPs for the liposome coated AuNPs. The first method was the Turkevich method [80, 81], where 2.4×10^{-4} M chloroauric acid was mixed with 1.7×10^{-2} M sodium citrate; then continually stirred at 100°C until the solution became deep red. This AuNP suspension was capped and stabilised with the citrate and was stable in water. The particles capped with citrate were then grown using the method of Sau et al. [82] The nanoparticle suspension were first centrifuged at 12000 rpm for 30 mins twice (Allegra X-22 from Beckman Coulter). After the first time the supernatant was taken out and MilliQ was added. After the second centrifugation the supernatant was also taken out. Then 10^{-2} M TX-100 in MilliQ was added to the nanoparticles, followed by 5.7×10^{-4} M chloroauric acid, and 6×10^{-4} M ascorbic acid. The growth process was very quick, only a couple of minutes. After the growth was complete, the solution turned to darker red. Finally, the grown AuNP were mixed with EtOH containing 2 mg/ml DPhyTL such that the EtOH made 10% of the total volume. After mixing with DPhyTL, 2.5×10^{-2} M TX-100 was added into the suspension to stabilise the nanoparticles.

The second method was the modified Brust-Schiffrin method first used by Selvakannan et al. [83] and so will be called the Selvakannan method. Before synthesising the AuNPs using this method, glassware

that would be used in the synthesis were washed with aqua regia made from a mixture of 36% HCl and 70% HNO₃ in 3:1 proportion. After washing with aqua regia, those glassware were then washed with water once to remove the residual acid. Then Hellmanex was added to the glassware and those glassware were sonicated for 5 minutes. After sonication, the glassware were then washed three times with reverse osmosis water, once with MilliQ, and once with EtOH. The glassware were then dried. The AuNP synthesis according to Selvakannan method was as follows: First, 2.5×10^{-3} M chloroauric acid was continually stirred at room temperature. Then 2.5×10^{-2} M sodium citrate was added followed immediately by 0.1 M sodium borohydride. The solution would turn from yellowish to brown or dark brown. After one hour of stirring, 10^{-3} M of ODA in DCM was mixed with the nanoparticle suspension. This caused the nanoparticles to transfer to DCM and the colour of the suspension in DCM was changed to deep dark red. The transfer rate depended on the stirring speed. After the transfer was complete, the phases were separated. The stable AuNP suspension in DCM was stabilised and capped with ODA.

The ODA molecules that capped the AuNPs synthesised in the second method had to be exchanged with HDFDTh or DDTh molecules. This exchange was carried according to several different protocols. The first protocol was to evaporate the DCM that suspended the ODA capped nanoparticles by rotary evaporator (rotavap) and then resuspend the particles in fresh DCM containing 2 mg/ml HDFDTh. The suspension was then constantly stirred by magnetic stirrer at room temperature until most of the nanoparticles settled. The time for complete precipitation varies from batch to batch. Then the particles were centrifuged at 3200 rpm for 30 mins, the supernatant was taken out, and fresh DCM was added. The particles were then resuspended in DCM by sonication. This process was repeated once. Then the suspension was analysed with ATR FTIR. Another batch of the ODA capped AuNPs suspended in DCM was mixed with DCM containing 1 mg/ml DDTh to make the final concentration 0.1 mg/ml DDTh. After several days of continuous stirring at room temperature, the DCM was rotavapped and fresh DCM was added, then the nanoparticles were resuspended in DCM by sonication. Finally this suspension was also analysed by ATR FTIR.

After the characterisation of the AuNPs by FTIR, the protocol for ODA-thiol exchange was modified. This modification was carried out to simplify the exchange process. 5 ml or 10 ml of the AuNP suspension was added into an empty vial instead of evaporating the DCM of the AuNP suspension and thiols (2mg/ml) were added directly to the nanoparticle suspension. The suspension was then incubated for several days at room temperature with constant stirring. If after one day the nanoparticles had not

settled, 2 mg/ml HDFDTh was added every day until the majority of the particles settled down. For the DDTh, similar addition was attempted, but the nanoparticles never become heavy enough or aggregated enough to settle out of solution, so for ODA-DDTh exchange it was deemed complete after continuous stirring for five days. After the exchange was complete, the HDFDTh capped nanoparticles suspension was centrifuged for 30 min at 3200 rpm (Orbital 325 from Clements Centrifuge), rotavapped, and then desiccated overnight. Both thiols were dissolved in DCM, an aggressive solvent that was not compatible with plastic centrifuge tubes. Therefore glass centrifuge tubes had to be used and this limited the centrifugation speed to 3200 rpm. This speed was not enough to separate DDTh capped nanoparticles from the solvent. Since the DDTh capped nanoparticles could not settle down by centrifugation at 3200 rpm, the suspension was just rotavapped and desiccated overnight.

4.2.3 Coating AuNPs with DPhyPC

The coating of nanoparticles with DPhyPC used two methods: extrusion and sonication. The extrusion was tried first because it provided more control of the size of the liposome than sonication. However it seemed that only the liposomes passed the filter of the extruder while the nanoparticles themselves did not. Because of this, the sonication method was used. The sonication method provided less control over the size of the liposomes but it ensured that the nanoparticles were coated at least partially by liposomes. Two types of sonication were used: ultrasonic bath and ultrasonic probe. The ultrasonic bath was tried first as a pilot study of the feasibility of the ultrasonication method. There were some indications of success with this method, so the ultrasonication method was tried again with ultrasonic probe sonicator which delivered more power than the ultrasonic bath cleaner.

4.2.3.1 Coating AuNPs by extrusion

Dried HDFDTh functionalised AuNPs were mixed with 2 mg DPhyPC in MilliQ. The mixture was vortexed for a minute, heated in 60 °C water bath for an hour, and vortexed again briefly. Then, half the solution was extruded through 50 nm Millipore pore filter 25 times while the rest was extruded through 800 nm pore filter also 25 times. The resulting solution from the 50 nm and 800 nm filter was then characterised by DLS and UV-Vis.

To improve mixing between lipids and nanoparticles, another batch of HDFDTh functionalised nanoparticles was mixed with 2 mg DPHyPC in EtOH in a flask then dried overnight by desiccation. 1 ml of MilliQ was then added to the mixture. The suspension was then sonicated with the ultrasonic cleaner for 30 minutes, vortexed for 1 minute and then heated in a 60 °C water bath for 1 hour and

vortexed again. Half of the suspension was then extruded through 50 nm pore filter and the other half was extruded through 800 nm pore filter. Both extrusions were carried out 25 times.

4.2.3.2 Coating AuNPs by ultrasonication

Two types of sonicators were used, ultrasonic cleaner from Unisonics and VibraCell VCX 750 ultrasonic probe from Sonics. For the sonication method using ultrasonic cleaner, citrate capped AuNPs were used. 2 mg of DPhyPC was weighed then dissolved in Chloroform. The solution was then rotavapped and desiccated overnight. Then the AuNP suspension in water was added to the dried lipids and then the solution was heated for 1 hour with intermittent shaking before sonicated in the ultrasonic cleaner for 1 hour. The size and ZP of the nanoparticles before sonication and of the nanoparticles-DPhyPC mixture after sonication was measured by Malvern Zetasizer.

The ultrasonic probe was used to coat citrate capped AuNPs, DDTh functionalised AuNPs, and HDFDTh functionalised AuNPs with DPhyPC liposomes. To coat the citrate capped AuNPs, 2 mg of DPhyPC lipid was dissolved in Chloroform then rotavapped at 60 °C and desiccated overnight. The dried lipid was mixed with AuNP suspension in water and sonicated several minutes with ultrasonic cleaner to get the lipid into the suspension. Then the mixture was heated in a water bath for one hour and sonicated briefly again. Then the water volume was topped to 25 ml. The mixture then was ultrasonicated twice with the probe sonicator 750 W 20 kHz at 30% amplitude for 2 minutes. Before the probe sonication and after, the mixture was characterised for size and ZP.

HDFDTh functionalised nanoparticles were coated with the same protocol as the citrate capped nanoparticles, but there were some differences at certain stages. The differences were that the nanoparticles and the lipid were mixed in Chloroform before evaporation by rotavap and before sonication with probe sonicator, MilliQ was added to make 15 ml total volume. For DDTh functionalised particles, EtOH was used to mix DPhyPC lipid and nanoparticles together before exchange with MilliQ and probe sonication.

The flowcharts of the whole experiment are shown in Figure 4.3-Figure 4.5.

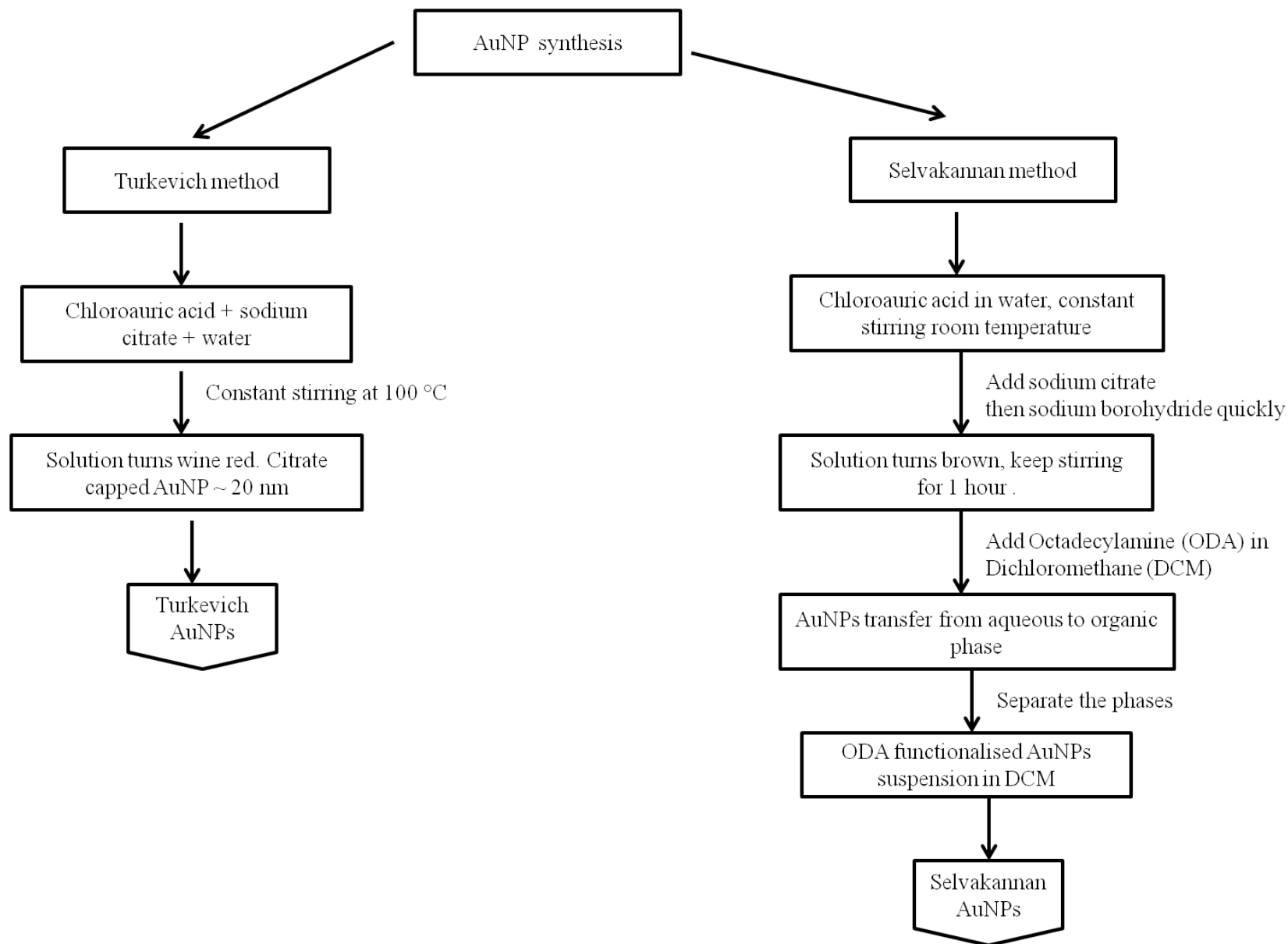


Figure 4.3 A flowchart showing the two AuNP synthesis methods.

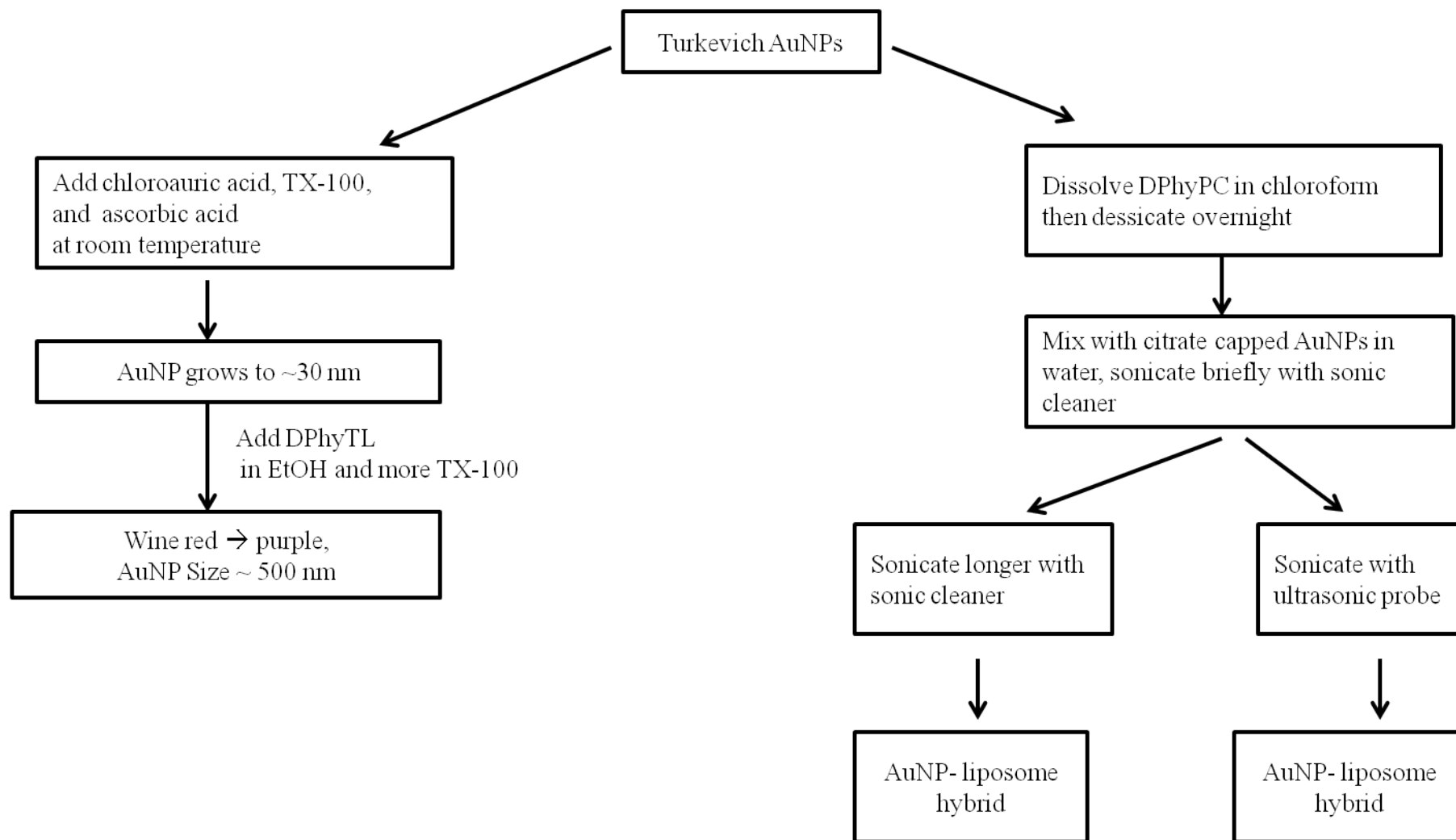


Figure 4.4 A flowchart showing the next experimental steps using AuNP synthesised according to the Turkevich method.

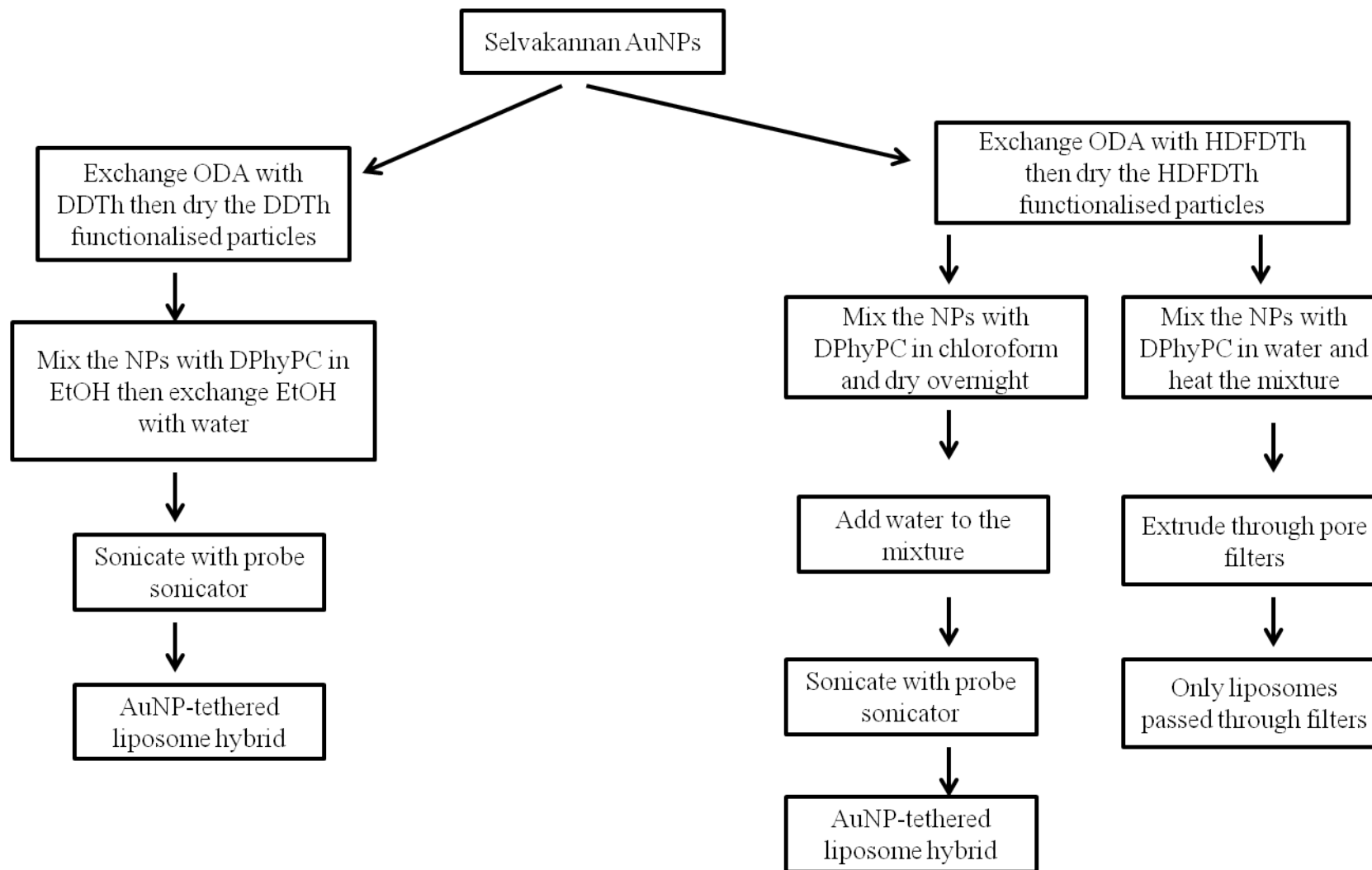


Figure 4.5 A flowchart showing the next experimental steps using AuNPs synthesised according to the Selvakannan method.

4.3 Results and discussion

4.3.1 AuNP synthesis and functionalisation

The first synthesis method tried was the Turkevich method. DLS measurement of the nanoparticles gave hydrodynamic diameter size of ~20 nm (Figure 4.6a). Since the smallest pore size of the extruder filter was 50 nm, the smallest liposome diameter that can be produced by extrusion was also around 50 nm. With the tether molecule length around 5 nm, nanoparticle core of 20 nm was too small to make a stable tethered liposome. As stated in the introduction, a core with diameter 30 – 40 nm was needed. So, the nanoparticles had to be grown and this had been achieved using the method of Sau et al [82] detailed in the materials and methods section. The DLS result showed that the nanoparticles grow from 20 nm to 30 nm (Figure 4.6b).

After growing the nanoparticles, the next step was the functionalisation of nanoparticles with the thiolipids dissolved in EtOH. Mixing suspended nanoparticles in water with DPhyTL in EtOH resulted in aggregation of the nanoparticles. In one of the experiments, after the nanoparticle suspension was washed and EtOH was added, the nanoparticles aggregated to become microparticles and settled out of the solvent overnight. If TX-100 was added to the EtOH then although the nanoparticles aggregated, they did not settle down. Therefore, immediately after the AuNPs were mixed with DPhyTL in EtOH, 10^{-2} M TX-100 was added, to increase the stability of nanoparticles in suspension. These nanoparticles were approximately 500 nm in diameter (Figure 4.6c).

The original aim to functionalise the AuNPs with thiolipids presupposed the AuNPs stability in EtOH. If the nanoparticles were stable, it would be relatively straightforward to functionalise them with the thiolipids by mixing the nanoparticles with thiolipids and incubating them overnight. The nanoparticles could then be separated from unreacted thiolipids by centrifugation. The coating of functionalised nanoparticles with lipids would be assumed to be simple as well. The functionalised nanoparticles would be mixed with DPhyPC lipids in EtOH and then dried overnight. The mixture would then be rehydrated and then either ultrasonicated or extruded through pore filters to make the tethered lipid-AuNP hybrid.

Since the nanoparticles were not stable in EtOH, another method of synthesising nanoparticles in nonpolar solvent was carried out. This Selvakannan method produced a mixture of nanoparticle sizes. Each batch had a fraction of the nanoparticles in the range of 6-10 nm, and another fraction in the range of 100-160 nm as measured by DLS. The proportion of small size to large size nanoparticles was not

consistent for every batch. Some of the batches had larger portion of the small size nanoparticles and some others had larger portion of the larger size nanoparticles (Figure 4.7). The size distribution of nanoparticles synthesised by this method was less consistent from batch to batch unlike the Turkevich method. The advantage was that nanoparticles transferred to the nonpolar solvent are very stable up for months and they could be mixed with thiolipids or thiols without causing immediate aggregation.

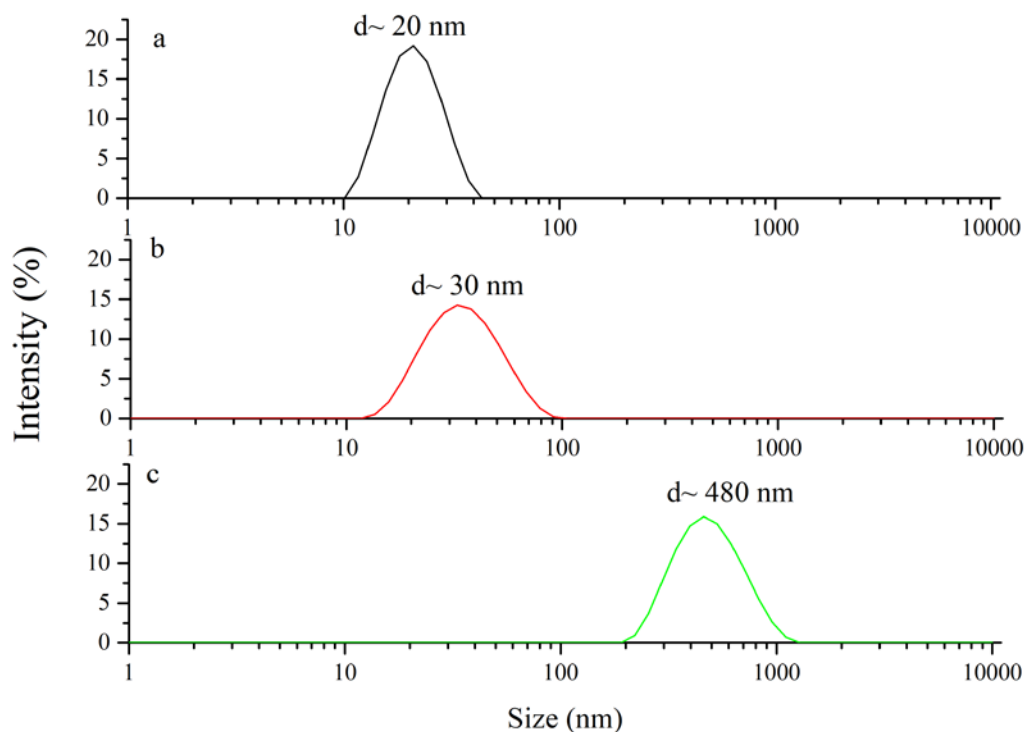


Figure 4.6 DLS results of AuNP synthesis using the Turkevich method. a is the size of just synthesised AuNPs using Turkevich method. b is the size of nanoparticles after being grown and c is the size of the nanoparticles after grown and mixed with DPhyTL in EtOH.

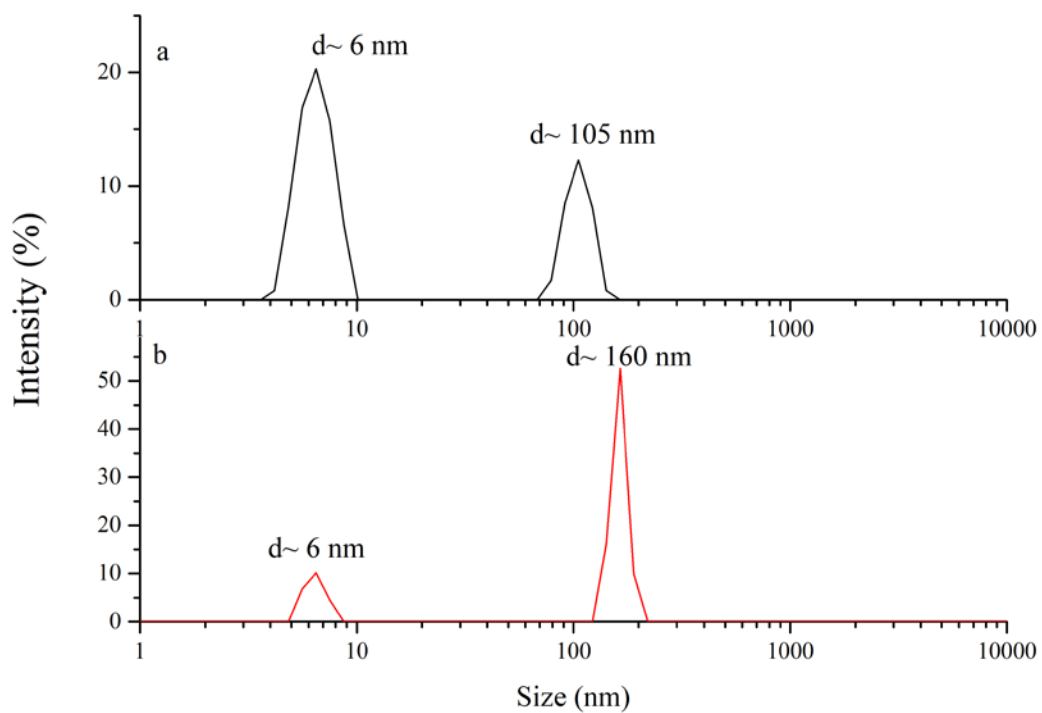


Figure 4.7 DLS results of AuNPs synthesised according to the Selvakannan method. Panels a and b showed particle sizes from different batches.

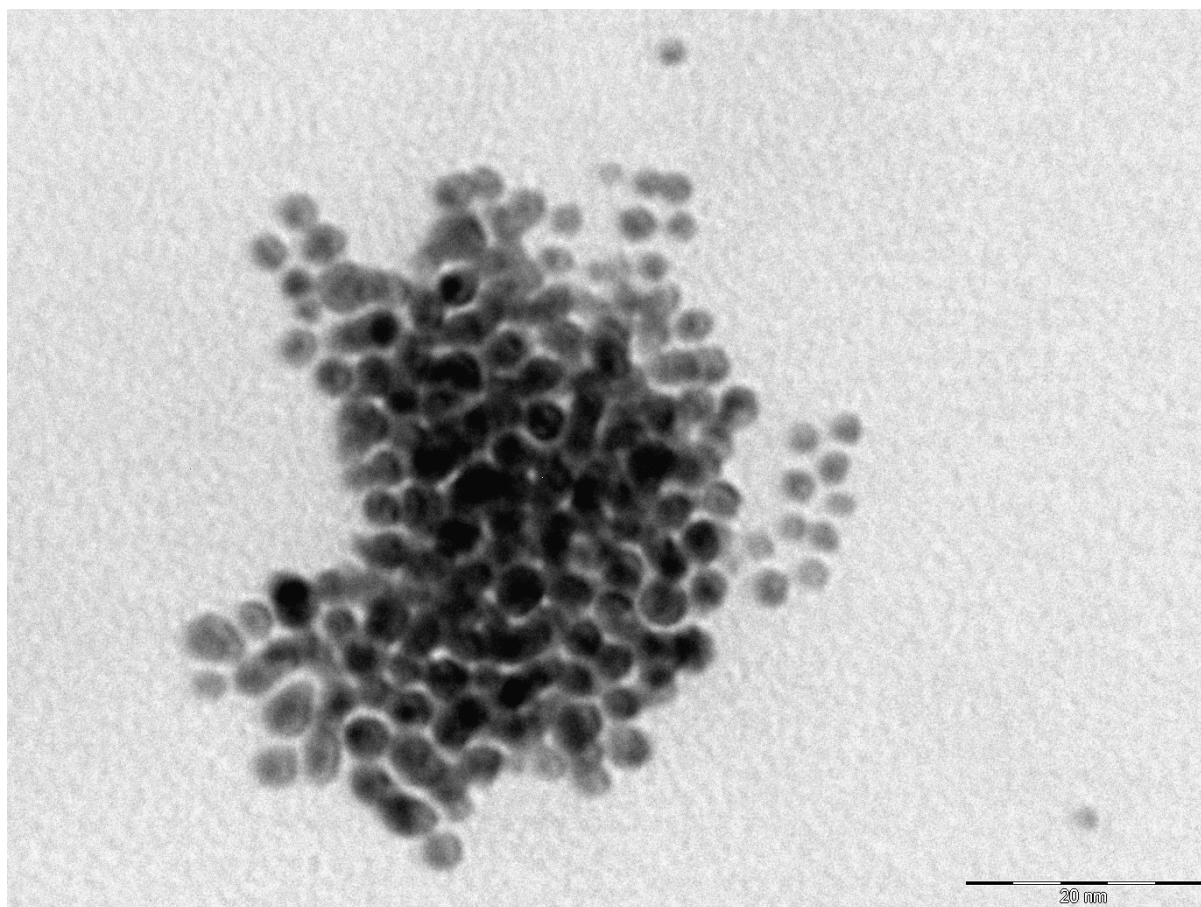


Figure 4.8 TEM image of AuNPs dried from DCM suspension. These nanoparticles were synthesised according to Selvakannan method. The diameter of the nanoparticles is about 3 nm.

A Transmission Electron Microscopy (TEM) image of the particles that were suspended in DCM shows that the particles are actually around 3 nm in diameter but they aggregate (Figure 4.8). The stabilising agent in the phase transfer process, ODA, was not covalently bound to the AuNPs, rather through electrostatic interaction between the amine functional group and AuCl_4^- ion present on the surface of AuNPs [83]. This meant that the ODA can be exchanged with thiol molecules that will bind more strongly to the gold via gold-thiol interaction. In the original aim the thiolipid molecule DPhyTL was to be used. However, considering the limited amount of DPhyTL and the difficulty of synthesising it in the laboratory, commercially available thiol molecules with comparable length were used as substitutes. These thiol molecules were DDTh and HDFDTh. They were used to substitute ODA on the surface of the nanoparticles. Infrared characterisation of the nanoparticles after exchange of functional molecules showed that the exchange process succeeded (Figure 4.9 and Figure 4.10).

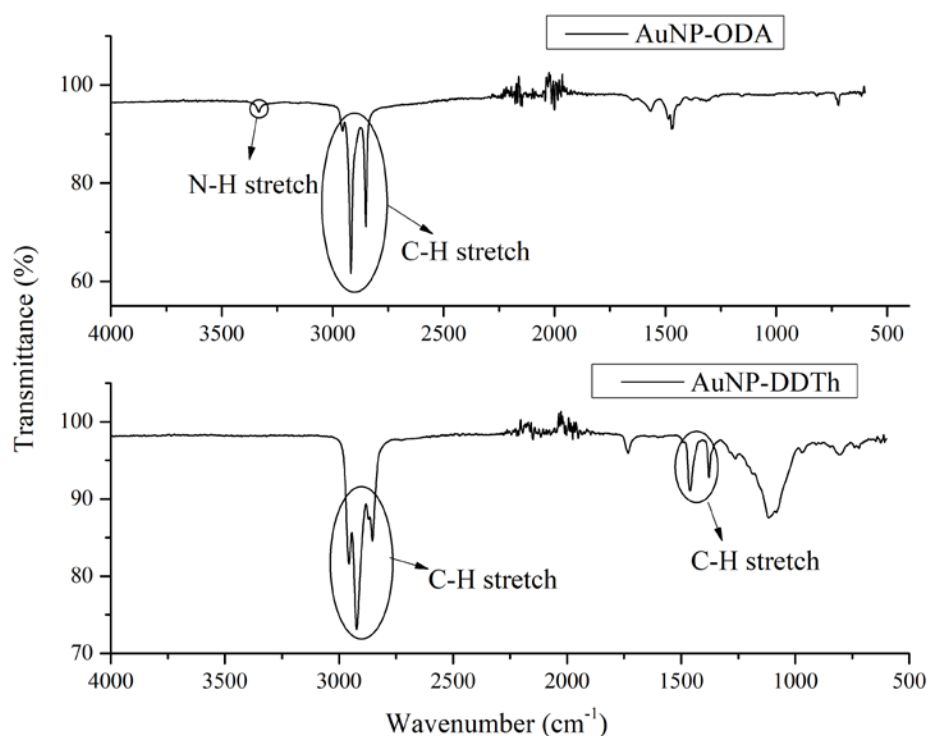


Figure 4.9 FTIR transmittance spectra before and after DDTh exchange. The top panel is FTIR of as synthesised AuNPs. The bottom panel is FTIR of AuNPs that has been functionalised with DDTh. Peaks of interest are 3300 cm⁻¹ for N-H stretch, 2900 and 1300 cm⁻¹ for C-H stretch.

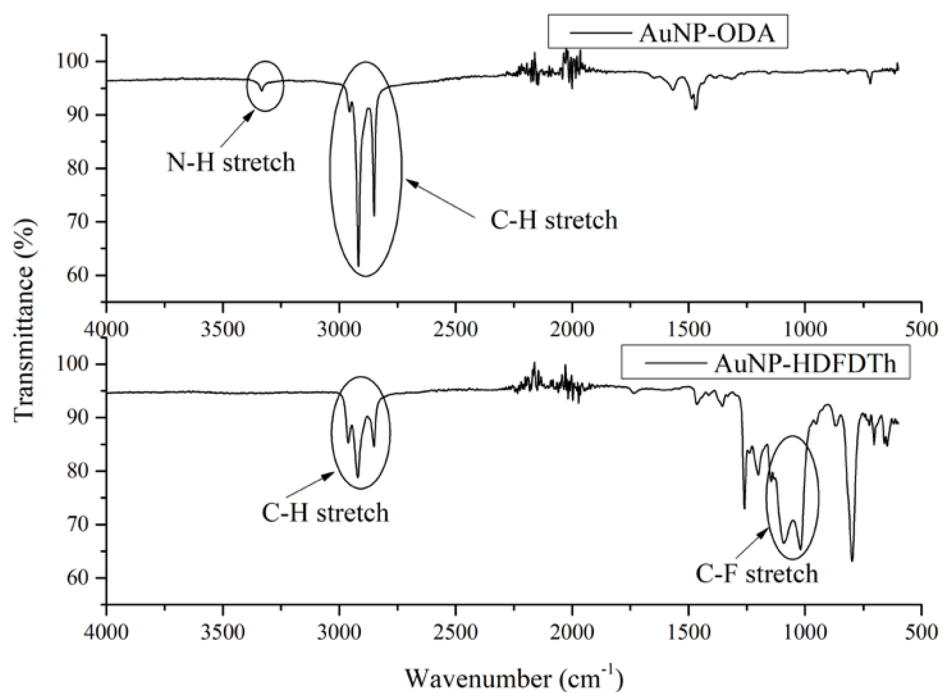


Figure 4.10 FTIR transmittance spectra before and after HDFDTh exchange. The top panel is FTIR of as synthesised AuNPs. The bottom panel is FTIR of AuNPs that has been functionalised with HDFDTh. Peaks of interest are 3300 cm⁻¹ for N-H stretch, 2900 cm⁻¹ for C-H stretch, and 1100 cm⁻¹ for C-F stretch.

The ODA had a small amine peak near 3300 cm^{-1} that disappeared when DDTh replaced them. However, the amine peak was too weak. To get a more definitive proof of the success of the exchange, the HDFDTh was used instead. HDFDTh has few carbon atoms compared to fluor atoms and the carbon-fluor bond gave a strong peak signature in IR. After exchange, the IR peaks of C-H stretch near 2900 cm^{-1} was reduced and different peaks of C-F stretch near 1100 cm^{-1} appeared. This showed that most of the ODA had been exchanged with HDFDTh. However, the HDFDTh-coated particles aggregated, while DDTh-coated particles remained in solution and even after centrifugation only a few particles precipitated.

4.3.2 Liposome coating of functionalised AuNPs

To coat functionalised AuNPs with DPhyPC lipid, two methods, sonication and extrusion had been tried, which was in accordance with the original aim. The first attempt to extrude nanoparticles-DPhyPC mixture through 50 nm pore filter yielded a clear solution. Before the extrusion, the suspension was light pink in colour. Because the solution was clear, most of the nanoparticles were not able to pass through the filter. Although the solution that came out from the extrusion was clear, the solution was subjected to UV-Vis and DLS measurements. The UV-Vis measurement after extrusion did not show any peaks (Figure 4.11). In contrast, just synthesised AuNPs according to the Selvakannan method showed a peak around 520 nm (Figure 4.12). This supported the fact that the nanoparticles were not able to pass 50 nm filter along with the lipids. The DLS measurement showed that there were particles sized 98.49 nm which most likely were the liposomes without the nanoparticles. Some nanoparticle-lipid mixture from the same batch was extruded through 800 nm filter and it still showed a slight pink colour; this solution was characterised with UV-Vis and DLS. Measurement with DLS showed that the size was 604.4 ± 53.6 nm. The UV-Vis result did not show AuNP peak around 520 nm although it was clear that it was different from the baseline MilliQ as well (Figure 4.11). Therefore, some kind of particles, most likely liposomes, passed through the filter but no or insignificant amount of nanoparticles passed through.

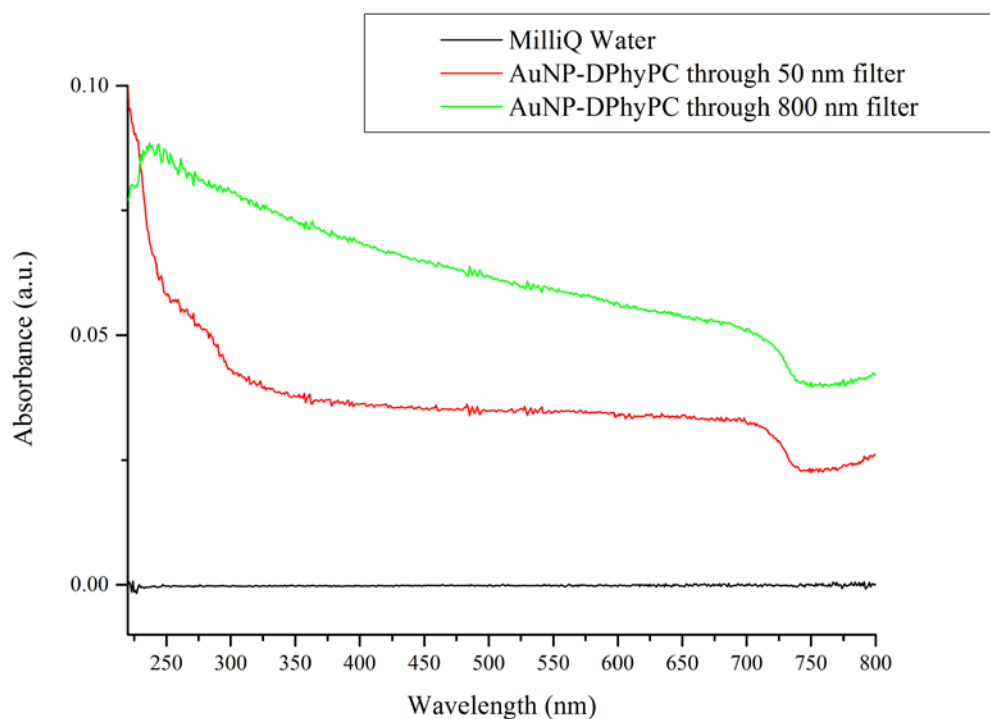


Figure 4.11 UV-Vis absorbance spectra of AuNP functionalised with HDFDTh in MilliQ after extrusion through 50 nm (red) and 800 nm (green) pore filter compared with MilliQ baseline (black).

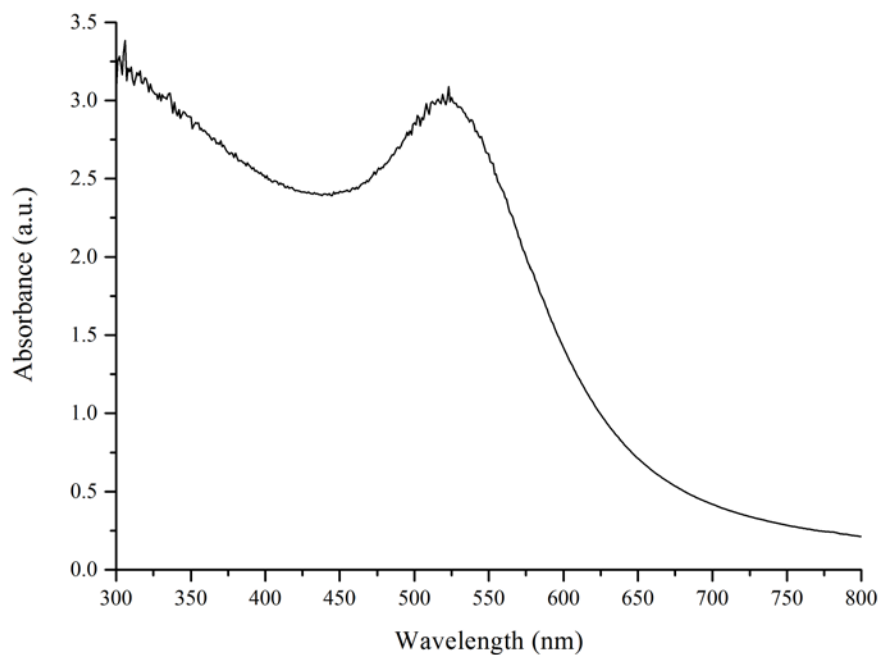


Figure 4.12 UV-Vis absorbance spectrum of ODA functionalised AuNP synthesised according to the Selvakannan method in DCM. A peak is apparent around 520 nm.

In the second attempt, another batch of the nanoparticles was dried, resuspended in EtOH and mixed with DPhyPC, then dried overnight. Later the dried mixture was rehydrated with MilliQ and extruded again through 50 nm and 800 nm filter. The UV-Vis again did not show any gold peak just like Figure 4.11 and the DLS shows 106.5 ± 1.1 nm for the solution that was extruded through 50 nm filter and 514.2 ± 228.7 nm for the one extruded through 800 nm filter.

DLS measurement of the Turkevich method synthesised nanoparticles before and after sonication with ultrasonic bath showed significant changes in size and ZP. Before sonication the size of the nanoparticles was about 30 nm and after mixing with DPhyPC and sonication the size was about 700 nm. Sonication of DPhyPC solution only however shows that the liposomes/lipid globules were still 1-2 μ m. ZP of the nanoparticle only suspension showed approx. -45 mV, after sonication with DPhyPC mixed in -21 mV and vesicle only suspension approximately -15 mV. These results indicated that the sonication changed the AuNP/liposome mixture. The size after sonication showed that maybe the nanoparticles were covered by large multilamellar vesicles. UV-Vis spectra taken before and after sonication showed a gold peak with practically no change in peak position (Figure 4.13).

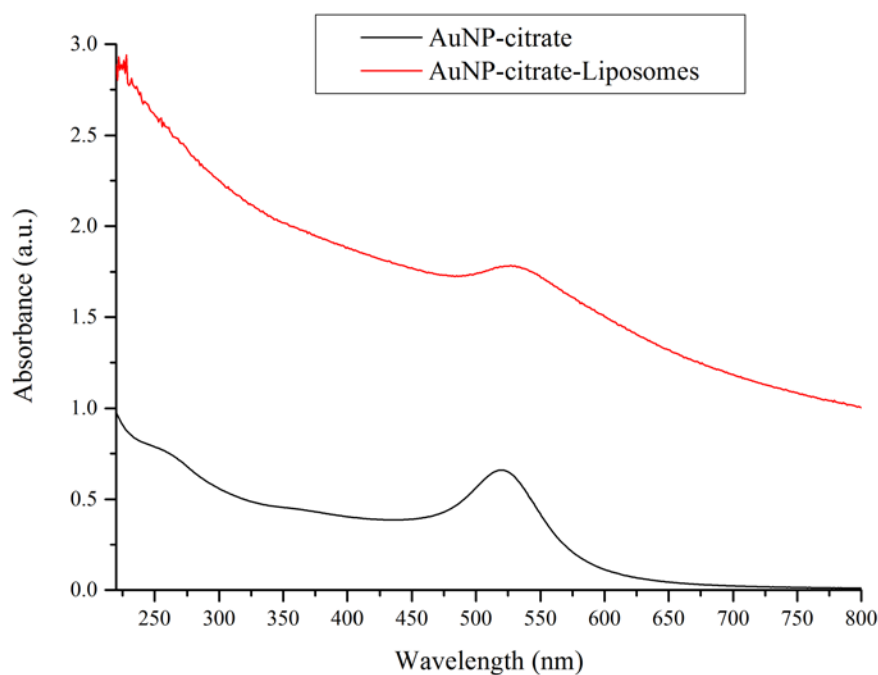


Figure 4.13 UV-Vis absorbance spectra of AuNP capped with citrate (black) and citrate capped AuNP coated with liposomes (red) after sonication with unisonics ultrasonic cleaner for 1 hour.

The DLS size measurement and ZP results of the sonication with probe sonicator can be seen in Table 4.1 below.

Table 4.1 DLS size and ZP measurement of AuNP and DPhyPC mixture before and after sonication with probe sonicator

Nanoparticles	Size before sonication (nm)	Size after sonication (nm)	ZP before sonication (mV)	ZP after sonication (mV)
Turkevich AuNP-liposomes	90	145	-35	-50
AuNP-DDTh-liposomes	370	180	45	46
AuNP-HDFDTh-liposomes	350	200	20	5
DPhyPC liposomes	400	200	-20	-15

Compared to the particles sonicated by ultrasonic cleaner, the size of particles after sonication was smaller, in the order of 100 nm. This was because the probe sonicator was more powerful than the cleaner. Furthermore, sonication with the probe sonicator resulted in transparent suspension while the ultrasonic cleaner still give turbid suspension. In addition, the ZP showed the right trend of summing up the ZP of nanoparticle and liposomes like the results of Kang and Ko [79] except for the DDTh functionalised nanoparticles. Comparing the result of nonfunctionalised Turkevich method nanoparticles to the thiolated nanoparticles showed that the thiolated nanoparticles became smaller after coated with liposomes while the nonfunctionalised ones became bigger. This may be explained by the fact that the thiolated nanoparticles actually aggregated and sonication with liposomes exfoliate the aggregation while the nonfunctionalised nanoparticles were simply being covered by the liposomes.

Table 4.1 does not show the size and ZP of AuNPs functionalised with HDFDTh. This is because the nanoparticles became hydrophobic and did not redisperse in polar solvents; they instead stuck to the walls of the container. To measure size and ZP of particles in nonpolar solvents, a special dip cell kit accessory must be used but because the cost is very high this measurement was not carried out.

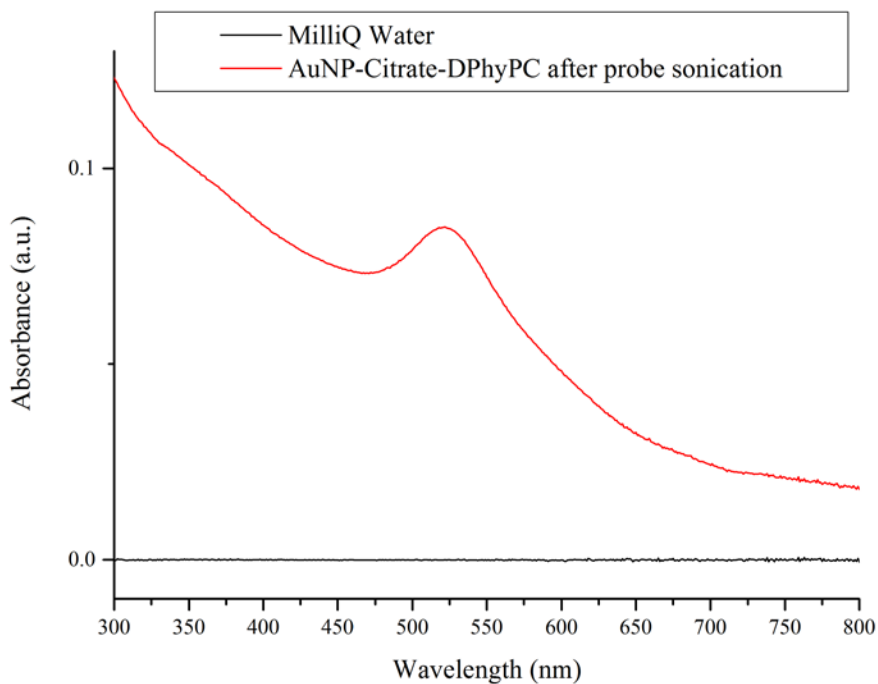


Figure 4.14 UV-Vis absorbance spectrum of citrate capped AuNP after probe sonication (red) compared to the MilliQ baseline (black).

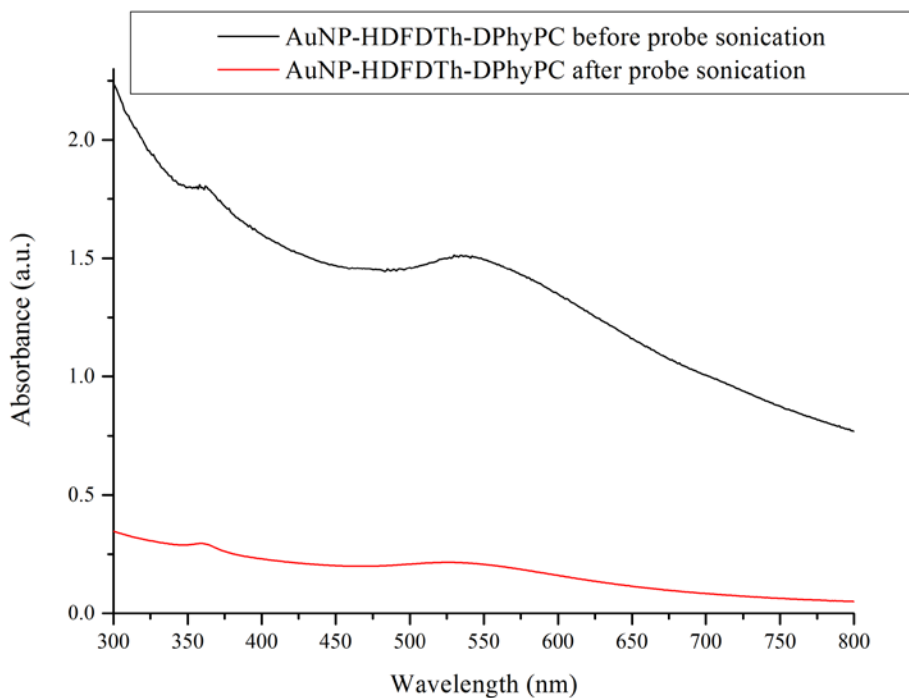


Figure 4.15 UV-Vis of HDFDTh functionalised AuNP before and after mixing with DPhyPC and sonicated.

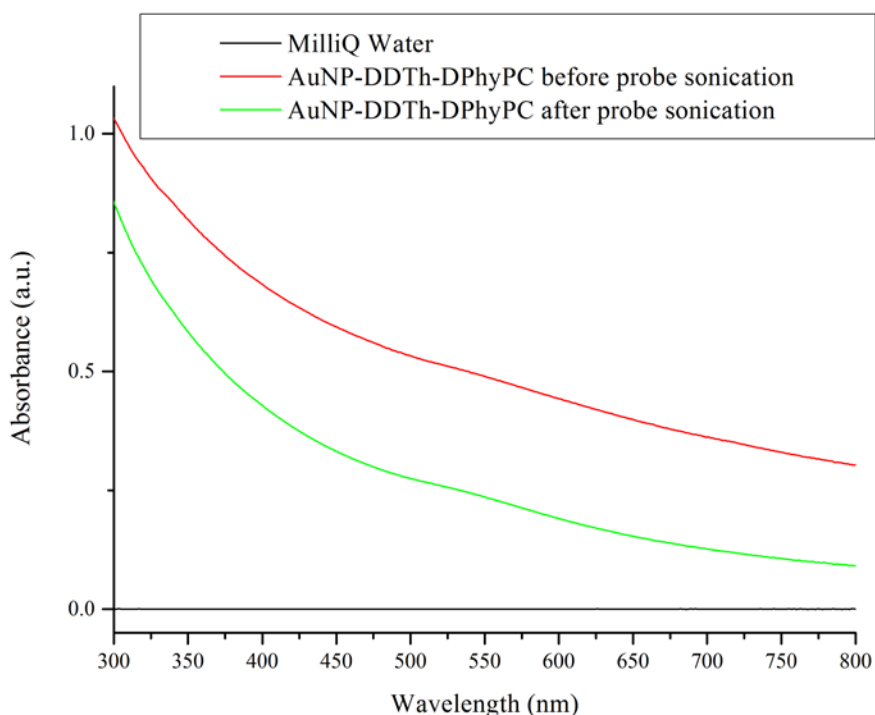


Figure 4.16 UV-Vis absorbance spectra of DDTh functionalised AuNP mixed with DPhyPC before (red) and after (green) probe sonication compared with the MilliQ baseline (black).

The UV-Vis of the citrate capped, DDTh functionalised, and HDFDTh functionalised AuNPs are shown by Figure 4.14 – Figure 4.15 respectively. For citrate capped and HDFDTh functionalised nanoparticles, the gold peak was still visible after probe sonication (Figure 4.14 and Figure 4.15). For HDFDTh coated nanoparticles, the peak maximum was shifted only a little bit to shorter wavelength (Figure 4.15). However, the DDTh functionalised nanoparticle did not show gold peak before and after probe sonication (Figure 4.16). This means that the citrate capped and HDFDTh coated nanoparticles were still present after the sonication. Combined with the ZP data, these particles were most likely partially covered with the lipids. The DDTh coated particles UV-Vis and ZP results were inconclusive and further experiments are necessary.

The best result achieved with the HDFDTh functionalised particles should resemble Figure 4.17 with some lipid molecules missing instead of Figure 4.1. Figure 4.17 resembled HBM (hybrid bilayer membrane) more than tBLMs.

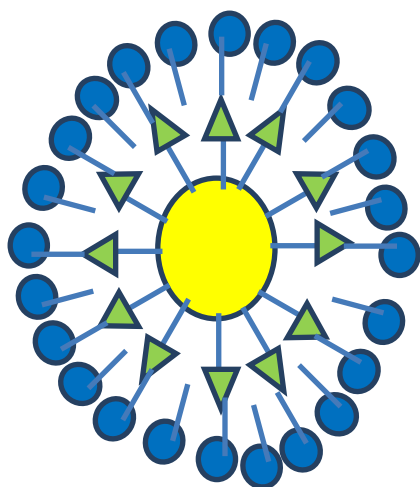


Figure 4.17 The lipid-AuNP hybrid. The yellow circle represents AuNP, the green triangle with lines represent the thiol molecules and the blue circle with protruding lines represent the lipid molecule.

4.4 Conclusion and outlook

The original aim of this work was to produce a three-dimensional analogue of the tBLM by functionalising AuNPs with thiolipids and then coating them with lipids by extrusion or sonication. The nanoparticles were first synthesised according to the Turkevich method. The Turkevich method produced nanoparticles with reproducible sizes from batch to batch but the nanoparticles were not very stable in non-water solvent. Therefore, this method at the present could not be used to form nanoparticle-tethered liposome hybrid. The second synthesis method was the Selvakannan method which produced nanoparticles with sizes that varied from batch to batch but the nanoparticles were very stable in non-aqueous solvent. Nanoparticles produced by this method were used for making AuNP-tethered liposome hybrid. Before the nanoparticles can be coated with lipids, the amine molecules have to be exchanged with thiol molecules. Although originally the thiolipid DPhyTL were to be used for this step, practical consideration led to the substitution of this molecule by HDFDTh and DDTh. HDFDTh was showing more definite proof of being able to substitute ODA than DDTh as shown by the FTIR data. The final step was the coating of the nanoparticles with lipids to form liposomes and three different methods were used to achieve this. Probe sonication was more successful to coat the AuNPs with lipids compared to extrusion or ultrasonication with an ultrasonic cleaner. Comparing the ZPs of citrate capped, DDTh functionalised and HDFDTh functionalised nanoparticles, the HDFDTh functionalised nanoparticles showed the strongest indication that the liposome at least partially cover the nanoparticles.

From the stated aim, only the aim of coating the functionalised particles with sonication or extrusion was achieved. The aim to make a nanoparticle analogue of tBLM cannot be achieved. Instead what was achieved was a good indication of the synthesis of the nanoparticle analogue of HBM.

Further work still needs to be done, mainly to get a ZP on HDFDTh functionalised nanoparticles in nonaqueous solvent, to produce covered nanoparticles with ZP close to small unilamellar vesicles namely -15 mV, and to make sure that each liposome covered not more than a single nanoparticle. If it can be proven strongly that HBM-like nanoparticles have been made, the work can be aimed back towards the original goal of making tBLM-like tethered liposome-AuNP hybrid. This work has highlighted the importance of synthesising gold nanoparticles that can be stable in non-water solvent. This work also indicated that sonication with a powerful sonicator is a possible way to coat the functionalised nanoparticles with liposomes. So the first goal in a future work is to synthesise AuNPs that are stable in EtOH or other non-water solvent such as DCM or Chloroform. If the AuNPs are functionalised with amine molecules as stabilisers, then these molecules need to be exchanged with thiolipids. A better way would be to use the thiolipids as a capping or stabilising agent in the synthesis of the nanoparticles. If this goal can be achieved, the next step would be to coat the thiolipid functionalised AuNPs with lipids. Because the thiolipid functionalised nanoparticles will dissolve in the same solvent as the lipids, mixing and then drying them should be easy. Finally, the mixed nanoparticles and lipids can be rehydrated and then extruded or sonicated with a powerful sonicator to make the tethered liposome-AuNP hybrids.

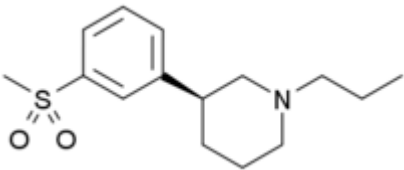
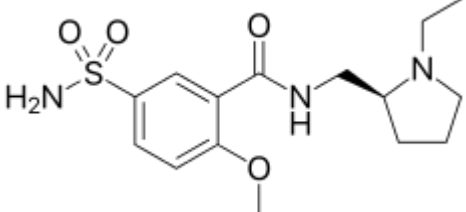
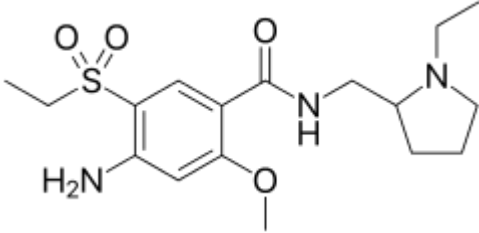
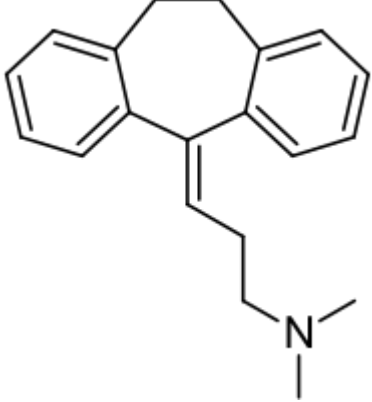
CHAPTER 5 SUMMARY AND OUTLOOK

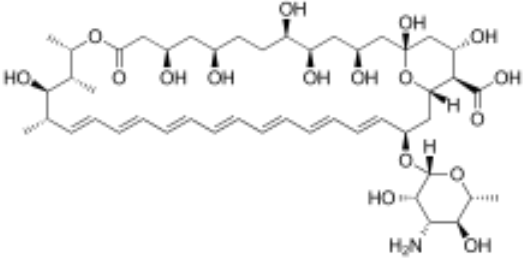
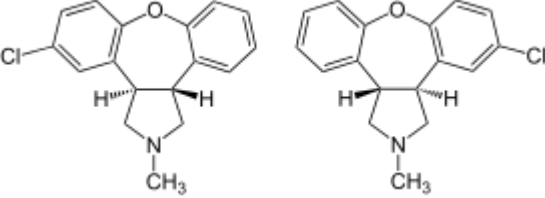
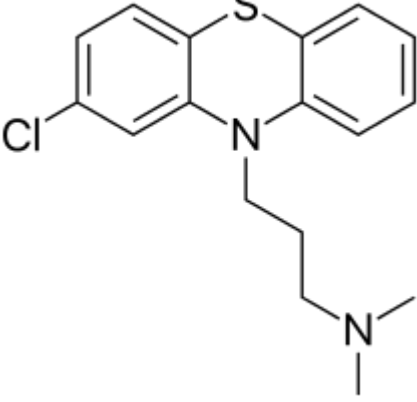
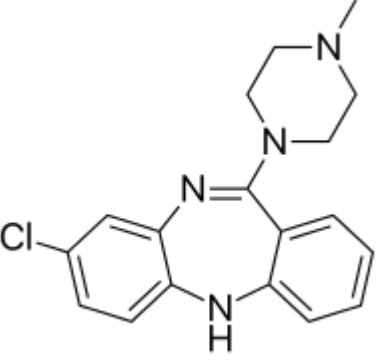
Two different projects have been carried out and described in this thesis. The first project was studying drug membrane interaction using CPZ as the model drug and tBLM as the model membrane. The aim of this project was to investigate if drug binding is controlled by the available binding sites on the membrane or the free drug concentration in solution. This aim has been reached; the answer depended on the concentration of the drug. Below a certain concentration, as long as the difference between the free drug and the bound drug was significant (free drug concentration equals 2x bound drug concentration) drugs will continually bind to the membrane as the result from multiple concentration circulation experiment showed. If the concentration of the free drug equalled the bound drug, the binding did not happen, although some binding sites were available. This was shown by the result of multiple circulation experiments using batches with the same concentration. This meant that the drug binding was controlled by concentration difference between free and bound drug. Above this concentration however, adding more drugs caused the membrane to become saturated and it cannot bind more drugs as shown by overshoots in the kinetic measurement. This meant that at this point drug binding was limited by the availability of binding sites. This study also revealed additional aspects of drug-membrane interaction. One was that the binding and release of the drug to the membrane followed a kinetic model more complex than the simple Langmuir adsorption model. The drug's binding to the membrane was also partially reversible, with a part of the drug remained bound to the membrane even after washing. Finally, the binding of the drug to the membrane disturbed the order of the lipids in the membrane but did not form pores or destroyed the membrane as shown by the EIS measurement. EIS shown that the addition of more CPZ only slightly decreased the membrane impedance without changes in the phase difference curve. This work has contributed the understanding that drug-membrane interaction was very complex as shown by the complex kinetic binding kinetics. This study also contributed to the understanding of the possibility of two different binding mechanism of drugs that depended on the drug concentration. Future direction of this research is studying CPZ interaction with tBLM made from different lipids, either single lipids or mixture of lipids. Studying drug interaction with tBLM using model drugs other than CPZ is also possible. Yet another possible continuation of this project is to incorporate membrane proteins into the tBLM and then studying the difference of drug-protein and drug-lipid interaction kinetics.

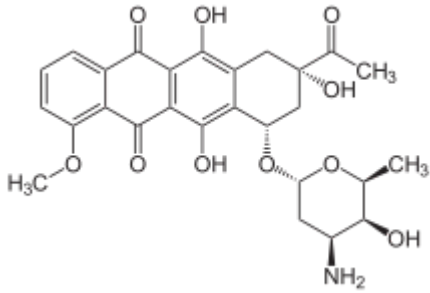
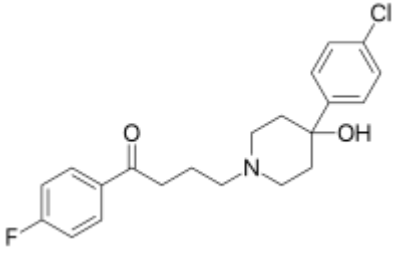
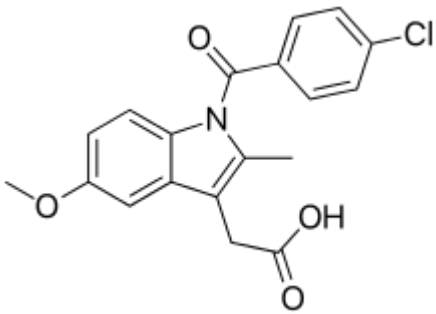
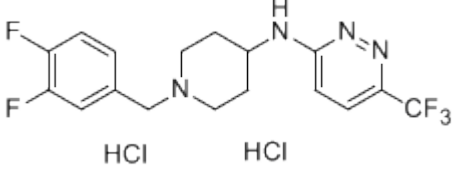
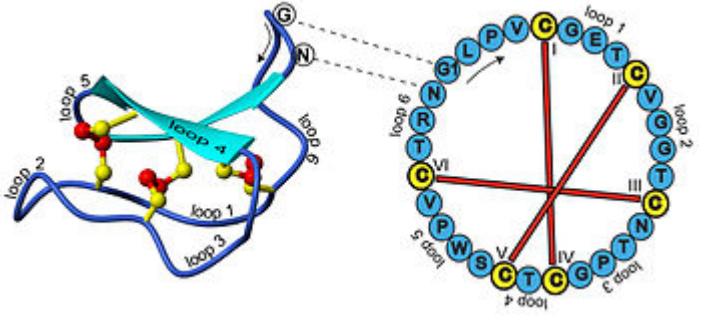
The second project was to synthesise AuNPs coated with tethered liposomes that can be used as alternative model membranes. The aim was to synthesise a three-dimensional analogue of the tBLM

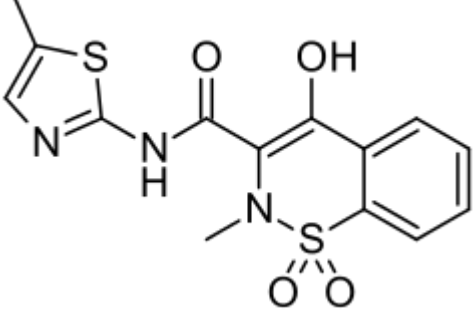
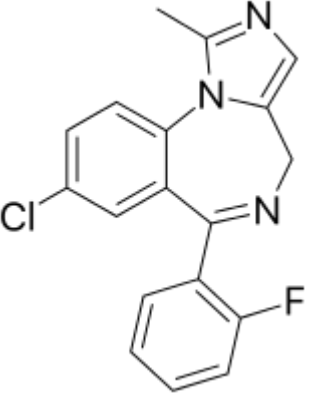
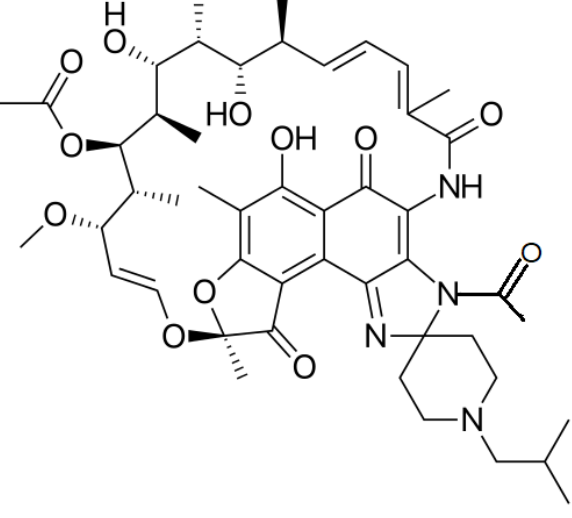
using thiolipids to anchor the liposomes to the AuNPs. The first stage was to functionalise gold nanoparticles with thiolipids. The second stage was to coat the functionalised nanoparticles with lipids by sonication or extrusion. Two methods of AuNP synthesis were tried, one producing nanoparticles stable in water but not in EtOH and the other producing nanoparticles stable in nonaqueous solvent. The AuNPs stable in nonaqueous solvent were then coated with two kinds of thiols, DDTh and HDFDTh. These thiols were used instead of thiolipid because they are commercially available compared to thiolipids which has to be synthesised in the laboratory. Finally, the thiolated nanoparticles were then coated with lipids by three different methods, extrusion, ultrasonication with ultrasonic cleaner and ultrasonication with ultrasonic probe. Ultrasonic probe method provided the strongest indication of liposome covering the HDFDTh coated AuNPs compared with the other two methods. Because thiol molecules were used to anchor the lipid to the nanoparticles the original goal of synthesising a tBLM-like nanoparticle was not achieved. Instead a HBM-like nanoparticle was synthesised. In addition, the aim of coating functionalised nanoparticles with lipids by ultrasonication was achieved. Although the stated aim cannot fully be achieved, this work still proved that a hybrid of tethered liposomes and gold nanoparticle is possible to synthesise. This is the contribution of this work to the development of new model membranes and also possible new drug carriers. Future direction of this research is to make a control experiment where the ZP of HDFDTh coated AuNP in nonaqueous solvent is measured. Further experiments are also necessary to ensure that the liposome covered one AuNP completely and not more than one AuNP is contained within one liposome. If the last step has been confirmed, then the next stage is to return to the original aim of this work. The first step in this future work will be to make AuNPs that are stable in the solvent for the thiolipids. It is better still to synthesise AuNPs that are stabilised by thiolipids. It will be good also to control the size of the nanoparticles to be no bigger than 200 nm. Next is the coating of the nanoparticles with lipids. This work has proven that ultrasonication can be used for this purpose. If the synthesised nanoparticles are small enough, the extrusion method may be used to coat the nanoparticles with lipids. Extrusion should provide better size distribution of the liposomes and the tethered liposome-AuNP hybrid. Once this construct has been made, it can be used in further research as a new model membrane or a new drug carrier.

APPENDIX: CHEMICAL COMPOUNDS AND THEIR CHEMICAL STRUCTURES

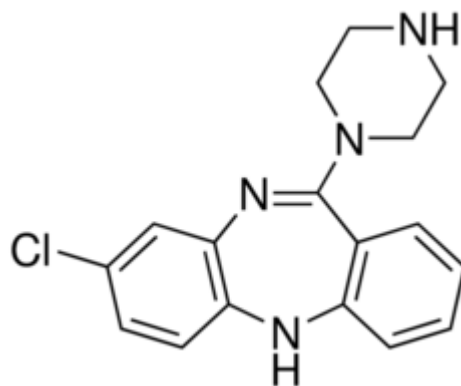
Chemical Compounds	Chemical Structures
(-)-OSU6162	
(-)-Sulpiride	
AGGKGF	RRGAGLGLALAKDGWALMLKLGFGRR
Amisulpride	
Amitriptyline	

<p>Amphotericin B (AmB, AmB-SCS, Fungizone)</p>	
<p>Asenapine</p>	
<p>Chlorpromazine (CPZ)</p>	
<p>Clozapine</p>	

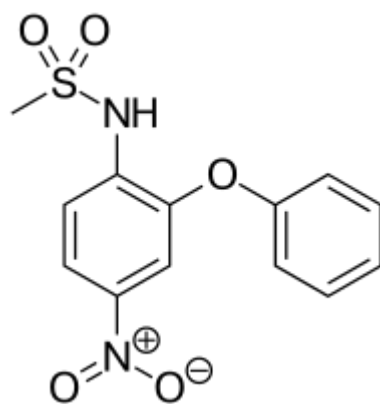
Daunorubicin	
FSKRGY	RRGFSCLKLALAKDGWALMLRLGYGRR
Haloperidol	
Indomethacin	
JNJ-37822681	 <p style="text-align: center;">HCl HCl</p>
Kalata	

<p>MagaininI (MagI)</p>	<p>H-Gly-Ile-Gly-Lys-Phe-Leu-His-Ser Ala-Gly-Lys-Phe-Gly-Lys-Ala-Phe Val-Gly-Glu-Ile-Met-Lys-Ser-OH</p>
<p>Meloxicam</p>	 <p>The structure of Meloxicam consists of a benzothiazine core. It features a methyl group at the 2-position, a methanesulfonyl group at the 4-position, and a 2-methyl-5-thiazolylamino group at the 6-position. A hydroxyl group is attached to the 7-position of the benzene ring.</p>
<p>Midazolam</p>	 <p>The structure of Midazolam is a 1,4-benzodiazepine derivative. It has a methyl group at the 2-position, a 5-chlorophenyl group at the 7-position, and a 2-fluorophenyl group at the 5-position.</p>
<p>N'-acetyl-rifabutin (RFB2)</p>	 <p>The structure of N'-acetyl-rifabutin (RFB2) is a complex polycyclic molecule. It features a central naphthalene-like core with multiple hydroxyl groups, a methoxy group, and a long side chain containing a double bond and a methyl group. The nitrogen atom is substituted with an acetyl group and a piperazine ring, which is further substituted with an isobutyl group.</p>

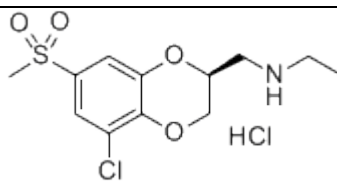
N-desmethylclozapine



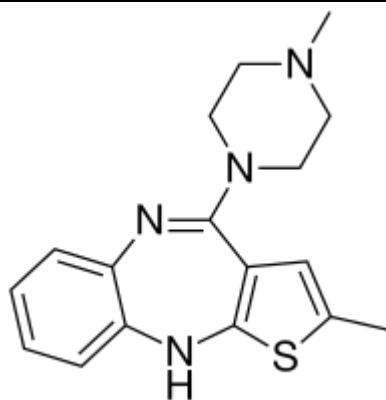
Nimesulide

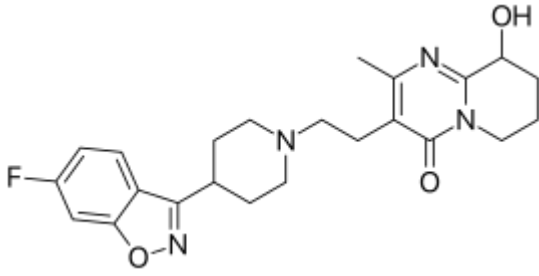
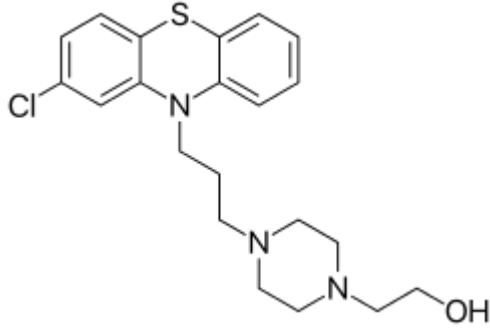
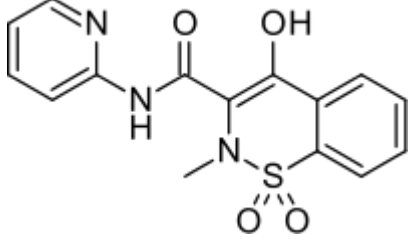
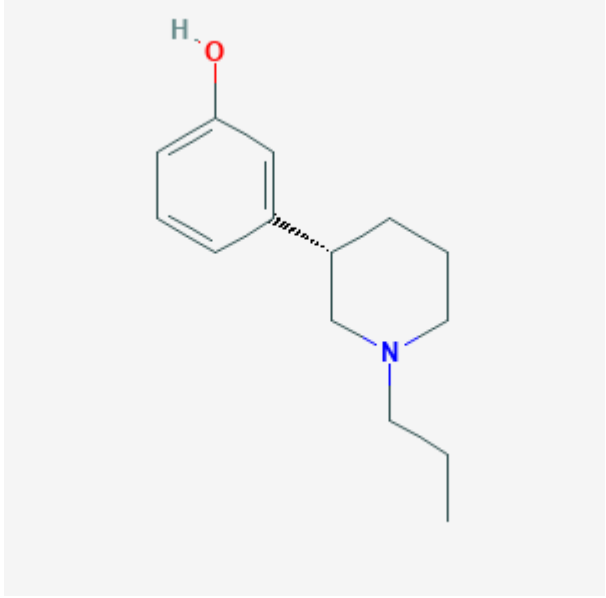


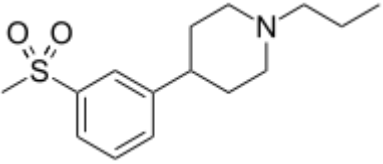
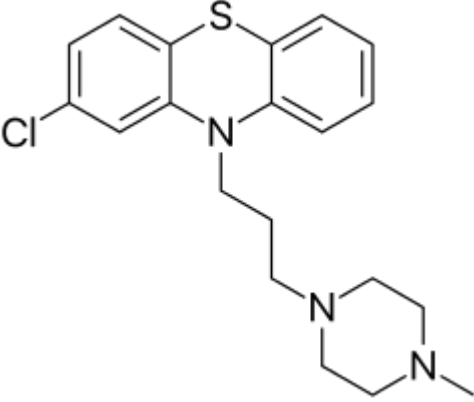
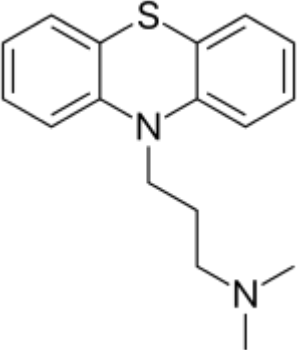
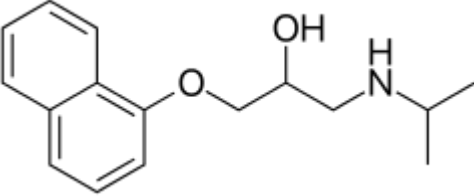
NS30678

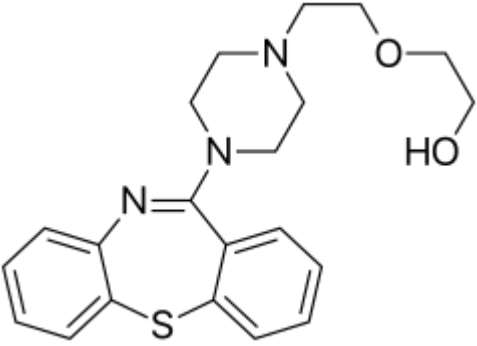
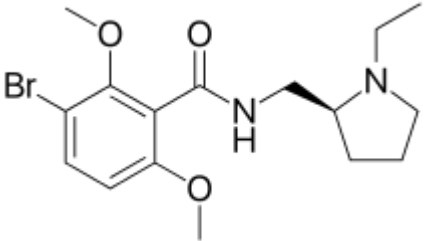
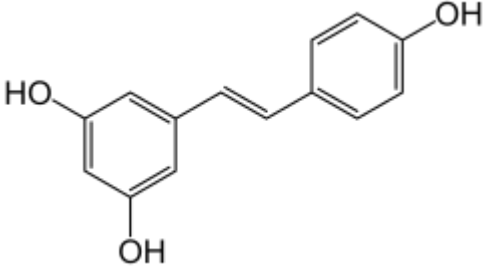
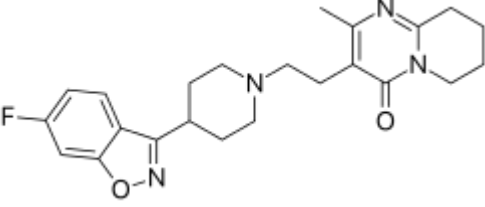
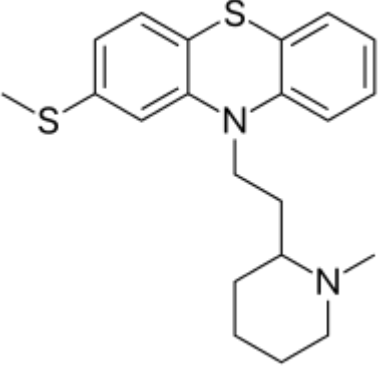


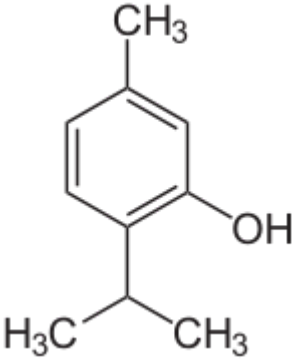
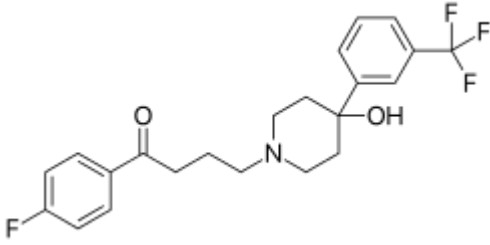
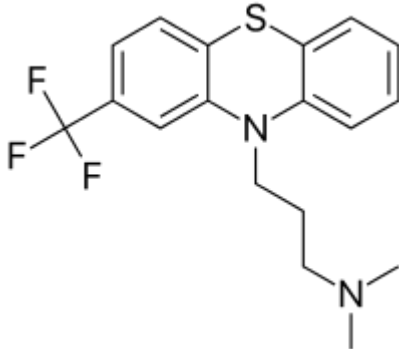
Olanzapine



Paliperidone	 <p>The chemical structure of Paliperidone consists of a piperidine ring connected via a propyl chain to a piperazine ring. The piperazine ring is further substituted with a methyl group and a hydroxyl group. The piperidine ring is attached to a benzimidazole ring system, which has a fluorine atom at the 6-position.</p>
Perfenazine/Perphenazine	 <p>The chemical structure of Perfenazine/Perphenazine features a central benzothiazine ring system. One of the nitrogen atoms in the benzothiazine is substituted with a propyl chain that leads to a piperazine ring. The piperazine ring is further substituted with a hydroxyethyl group. The benzothiazine ring system also has a chlorine atom at the 4-position.</p>
Piroxicam	 <p>The chemical structure of Piroxicam is a pyridine ring connected via an imidazole ring to a benzothiazine ring system. The benzothiazine ring system has a methyl group on the nitrogen and a sulfonamide group (SO₂NH₂) on the sulfur. The benzothiazine ring system also has a hydroxyl group at the 2-position.</p>
Preclamol ((-)-3PPP)	 <p>The chemical structure of Preclamol ((-)-3PPP) shows a benzene ring with a hydroxyl group at the 3-position. The benzene ring is connected via a dashed bond to a piperidine ring. The piperidine ring is further substituted with a propyl group on the nitrogen atom.</p>

Pridopidine (ACR16)	
Prochlorperazine	
Promazine	
Propranolol	

<p>Quetiapine</p>	 <p>The structure of Quetiapine consists of a benzothiazine core. The nitrogen at position 10 is substituted with a piperazine ring, which is further substituted at the 4-position with a 2-hydroxyethyl group. The sulfur atom at position 5 is bonded to a phenyl ring.</p>
<p>Remoxipride</p>	 <p>The structure of Remoxipride features a benzimidazole ring system. The benzimidazole ring has a bromine atom at position 6 and methoxy groups at positions 7 and 8. The nitrogen at position 2 is substituted with a propyl chain, which is further substituted with an ethyl group on a secondary amine.</p>
<p>Resveratrol</p>	 <p>The structure of Resveratrol is a stilbenoid, specifically a trans-stilbenol. It consists of two phenolic rings connected by a double bond. One ring has hydroxyl groups at the 3 and 4 positions, while the other has a hydroxyl group at the 4 position.</p>
<p>Risperidone</p>	 <p>The structure of Risperidone is a benzisoxazole derivative. It features a benzisoxazole ring system with a fluorine atom at position 6. The nitrogen at position 3 is substituted with a piperazine ring, which is further substituted with a propyl chain leading to a piperazine ring with a methyl group and a carbonyl group.</p>
<p>Thioridazine</p>	 <p>The structure of Thioridazine is a thienothiazine derivative. It features a thienothiazine ring system with a methylsulfanyl group at position 4. The nitrogen at position 10 is substituted with a propyl chain, which is further substituted with a piperazine ring with a methyl group.</p>

Thymol	
Trifluperidol	
Triflupromazine	

REFERENCES

1. Bolsover, S.R., et al., *Membranes and Organelles*. 2003, John Wiley & Sons, Inc.: Hoboken, NJ, USA. p. 51-63.
2. Tanaka, M. and E. Sackmann, *Polymer-supported membranes as models of the cell surface*. *Nature*, 2005. **437**(7059): p. 656-663.
3. Watson, H., *Biological membranes*. *Essays Biochem*, 2015. **59**: p. 43-69.
4. Yeagle, P.L., *The Membranes of Cells*. 1993, San Diego: Academic Press.
5. Bolsover, S.R., et al., *Membranes and Organelles*, in *Cell Biology*. 2003, John Wiley & Sons, Inc. p. 51-63.
6. Escribá, P.V., et al., *Membranes: a meeting point for lipids, proteins and therapies*. *Journal of cellular and molecular medicine*, 2008. **12**(3): p. 829-75.
7. Peetla, C., A. Stine, and V. Labhasetwar, *Biophysical interactions with model lipid membranes: applications in drug discovery and drug delivery*. *Molecular pharmaceutics*, 2009. **6**(5): p. 1264-1276.
8. Vereb, G., et al., *Dynamic, yet structured: The cell membrane three decades after the Singer-Nicolson model*. *Proceedings of the National Academy of Sciences of the United States of America*, 2003. **100**(14): p. 8053-8058.
9. Escribá, P.V., *Membrane-lipid therapy: a new approach in molecular medicine*. *Trends in molecular medicine*, 2006. **12**(1): p. 34-43.
10. Pinheiro, M., et al., *Drug-membrane interaction studies applied to N'-acetyl-rifabutin*. *European Journal of Pharmaceutics and Biopharmaceutics*, 2013. **85**(3): p. 597-603.
11. Pinheiro, M., et al., *The influence of rifabutin on human and bacterial membrane models: implications for its mechanism of action*. *The journal of physical chemistry. B*, 2013. **117**(20): p. 6187-6193.
12. Knobloch, J., et al., *Membrane-drug interactions studied using model membrane systems*. *Saudi J Biol Sci*, 2015. **22**(6): p. 714-8.
13. Köper, I., *Insulating tethered bilayer lipid membranes to study membrane proteins*. *Molecular BioSystems*, 2007. **3**(10): p. 651-657.
14. Mallaiya, K., et al., *Electrochemical impedance studies on the interaction of midazolam with planar lipid bilayer*. *Electrochimica Acta*, 2014. **138**(20): p. 360-366.
15. Sackmann, E., *Supported Membranes: Scientific and Practical Applications*. *Science*, 1996. **271**(5245): p. 43-48.
16. Rebaud, S., O. Maniti, and A.P. Girard-Egrot, *Tethered bilayer lipid membranes (tBLMs): Interest and applications for biological membrane investigations*. *Biochimie*, 2014. **107 Pt A**: p. 135-142.
17. Chan, Y.H.M. and S.G. Boxer, *Model membrane systems and their applications*. *Current opinion in chemical biology*, 2007. **11**: p. 581-587.
18. Yoshina-Ishii, C., et al., *General method for modification of liposomes for encoded assembly on supported bilayers*. *Journal of the American Chemical Society*, 2005. **127**(5): p. 1356-1357.
19. Yoshina-Ishii, C. and S.G. Boxer, *Arrays of Mobile Tethered Vesicles on Supported Lipid Bilayers*. *Journal of the American Chemical Society*, 2003. **125**(13): p. 3696-3697.
20. Oka, M. and H. Kamimori, *Lipid Membrane-Binding Properties of Amphotericin B Deoxycholate (Fungizone) Using Surface Plasmon Resonance*. *Analytical Sciences*, 2013. **29**(7): p. 697-702.

21. Nussio, M.R., et al., *Characterisation of the binding of cationic amphiphilic drugs to phospholipid bilayers using surface plasmon resonance*. ChemMedChem, 2007. **2**(3): p. 366-373.
22. Nussio, M.R., et al., *Kinetics membrane disruption due to drug interactions of chlorpromazine hydrochloride*. Langmuir : the ACS journal of surfaces and colloids, 2009. **25**(2): p. 1086-1090.
23. Bruinsma, R., a. Behrisch, and E. Sackmann, *Adhesive switching of membranes: experiment and theory*. Physical review. E, Statistical physics, plasmas, fluids, and related interdisciplinary topics, 2000. **61**(4 Pt B): p. 4253-67.
24. Wagner, M.L. and L.K. Tamm, *Reconstituted syntaxin1a/SNAP25 interacts with negatively charged lipids as measured by lateral diffusion in planar supported bilayers*. Biophysical journal, 2001. **81**(1): p. 266-75.
25. Vockenroth, I.K., *Investigations of tethered bilayer lipid membranes for their potential use in biosensing devices*, in Department of Chemistry. 2007, University of Bath: Bath.
26. Vockenroth, I.K., et al., *Formation of tethered bilayer lipid membranes probed by various surface sensitive techniques*. Biointerphases, 2009. **4**(2): p. 19-26.
27. Fischer, M., et al., *Design of biofunctional assemblies on solids through recombinant spherical bacterial protein lumazine synthase*. Chemphyschem : a European journal of chemical physics and physical chemistry, 2001. **2**(10): p. 623-7.
28. Berquand, A., et al., *Two-Step Formation of Streptavidin-Supported Lipid Bilayers by PEG-Trigged Vesicle Fusion. Fluorescence and Atomic Force Microscopy Characterization*. Langmuir, 2003. **19**(5): p. 1700-1707.
29. Knoll, W., et al., *Tethered bimolecular lipid membranes—A novel model membrane platform*. Electrochimica Acta, 2008. **53**(23): p. 6680-6689.
30. Wiltschi, B., W. Knoll, and E.-K. Sinner, *Binding assays with artificial tethered membranes using surface plasmon resonance*. Methods, 2006. **39**(2): p. 134-146.
31. Arslan Yildiz, A., et al., *Biomimetic membrane platform: fabrication, characterization and applications*. Colloids and surfaces. B, Biointerfaces, 2013. **103**: p. 510-516.
32. Rossi, C., et al., *Differential Mechanisms for Calcium-Dependent Protein/Membrane Association as Evidenced from SPR-Binding Studies on Supported Biomimetic Membranes*. Biochemistry, 2003. **42**(51): p. 15273-15283.
33. Naumann, R.L.C. and W. Knoll, *Protein tethered lipid bilayer: an alternative mimic of the biological membrane (Mini Review)*. Biointerphases, 2008. **3**(2): p. FA101-FA107.
34. Giess, F., et al., *The Protein-Tethered Lipid Bilayer: A Novel Mimic of the Biological Membrane*. Biophysical Journal, 2004. **87**(5): p. 3213-3220.
35. Hughes, L.D. and S.G. Boxer, *DNA-Based Patterning of Tethered Membrane Patches*. Langmuir, 2013. **29**(39): p. 12220-12227.
36. Homola, J., *Surface Plasmon Resonance Based Sensors*. Springer Series on Chemical Sensors and Biosensors. Vol. 4. 2006, Berlin, Heidelberg: Springer Berlin Heidelberg.
37. Homola, J., *Surface Plasmon Resonance Sensors for Detection of Chemical and Biological Species*. Chemical Reviews, 2008. **108**(2): p. 462-493.
38. Knoll, W., *Interfaces and thin films as seen by bound electromagnetic waves*. Annual review of physical chemistry, 1998. **49**: p. 569-638.
39. Horn, N. and M. Kreiter, *Plasmon Spectroscopy: Methods, Pitfalls and How to Avoid Them*. Plasmonics, 2010. **5**(4): p. 331-345.
40. Macdonald, J.R. and E. Barsoukov, *Impedance Spectroscopy*. 2005, Hoboken, NJ, USA: John Wiley & Sons, Inc.
41. *Understanding Electrochemical Cells*. 1997, Solartron Analytical. p. 1-32.

42. Cooger, N.D. and N.J. Evans, *An Introduction to Electrochemical Impedance Measurement*. 1999, Solartron Analytical.
43. *The Basics of Electrochemical Impedance Spectroscopy* Gamry Instruments. p. 1 -18.
44. *Basics of Electrochemical Impedance Spectroscopy*. Princeton Applied Research. p. 1-13.
45. Valincius, G., T. Meskauskas, and F. Ivanauskas, *Electrochemical impedance spectroscopy of tethered bilayer membranes*. *Langmuir*, 2012. **28**(1): p. 977-990.
46. *Zetasizer nano series user manual*. 2004, Malvern: Malvern Instruments. 14-1-14-5.
47. *Dynamic Light Scattering: An Introduction in 30 Minutes*. Malvern Instruments. p. 1-8.
48. *Zeta Potential An Introduction in 30 Minutes*. Malvern Instruments p. 1-6.
49. *Zetasizer Nano User Training Course Reliable Nano Particle Sizing*. 2017, ATA Scientific.
50. *Measuring Zeta Potential - Laser Doppler Electrophoresis*. Malvern Instruments. p. 1-2.
51. Stuart, B., *Infrared spectroscopy : fundamentals and applications*. 2004: Chichester, West Sussex, England ; Hoboken, NJ : J. Wiley, [2004] ©2004.
52. Alvarez-Ordóñez, A. and M. Prieto, *Fourier Transform Infrared Spectroscopy in Food Microbiology*. 1 ed. 2012: Springer US. VI, 55.
53. Williams, D.B. and C.B. Carter, *Transmission Electron Microscopy: A Textbook for Materials Science*. 2 ed. 2009, Springer US. LXII, 775.
54. Seydel, J.K., et al., *Drug Membrane Interaction and the Importance for Drug Transport, Distribution, Accumulation, Efficacy and Resistance*. *Archiv der Pharmazie*, 1994. **327**(10): p. 601-610.
55. Nunes, C., et al., *NSAIDs interactions with membranes: a biophysical approach*. *Langmuir : the ACS journal of surfaces and colloids*, 2011. **27**(17): p. 10847-10858.
56. Seydel, J.K. and M. Wiese, *Drug-Membrane Interactions*. *Methods and Principles in Medicinal Chemistry*. Vol. 15. 2002, Weinheim, FRG: Wiley-VCH Verlag GmbH & Co. KGaA.
57. Kamimori, H., et al., *Studies on the membrane interactions of the cyclotides kalata B1 and kalata B6 on model membrane systems by surface plasmon resonance*. *Analytical biochemistry*, 2005. **337**(1): p. 149-153.
58. Foglia, F., et al., *Neutron Scattering Studies of the Effects of Formulating Amphotericin B with Cholesteryl Sulfate on the Drug's Interactions with Phospholipid and Phospholipid–Sterol Membranes*. *Langmuir*, 2015. **31**(29): p. 8042-8051.
59. Neves, A.R., C.u. Nunes, and S. Reis, *New Insights on the Biophysical Interaction of Resveratrol with Biomembrane Models: Relevance for Its Biological Effects*. *Journal of Physical Chemistry B*, 2015. **119**(35): p. 11664-11672.
60. Ferreira, J.V.N., et al., *Mechanism of Action of Thymol on Cell Membranes Investigated through Lipid Langmuir Monolayers at the Air-Water Interface and Molecular Simulation*. *Langmuir*, 2016. **32**(13): p. 3234-3241.
61. Alves, A.C., et al., *The Daunorubicin interplay with mimetic model membranes of cancer cells: A biophysical interpretation*. *Biochim Biophys Acta*, 2017. **1859**(5): p. 941-948.
62. Lopes, D., et al., *Shedding light on the puzzle of drug-membrane interactions: Experimental techniques and molecular dynamics simulations*. *Prog Lipid Res*, 2017. **65**: p. 24-44.
63. Steinbrecher, T.B., et al., *Accurate Binding Free Energy Predictions in Fragment Optimization*. *J Chem Inf Model*, 2015. **55**(11): p. 2411-20.
64. Onishi, M. and H. Kamimori, *High-Throughput and Sensitive Assay for Amphotericin B Interaction with Lipid Membrane on the Model Membrane Systems by Surface Plasmon Resonance*. *Biological and Pharmaceutical Bulletin*, 2013. **36**(4): p. 658-663.
65. Nascimento, J.M., et al., *Evaluation of Magainin I interactions with lipid membranes: an optical and electrochemical study*. *Chemistry and physics of lipids*, 2012. **165**(5): p. 537-544.

66. Chang, W.K., et al., *Characterization of antimicrobial peptide activity by electrochemical impedance spectroscopy*. *Biochimica et biophysica acta*, 2008. **1778**(10): p. 2430-2436.
67. Shin, H. and J.-H. Song, *Antipsychotics, chlorpromazine and haloperidol inhibit voltage-gated proton currents in BV2 microglial cells*. *European journal of pharmacology*, 2014. **738**: p. 256-262.
68. Li, H.-J., et al., *Chlorpromazine confers neuroprotection against brain ischemia by activating BKCa channel*. *European journal of pharmacology*, 2014. **735**: p. 38-43.
69. Sahlholm, K., et al., *Typical and atypical antipsychotics do not differ markedly in their reversibility of antagonism of the dopamine D2 receptor*. *The international journal of neuropsychopharmacology / official scientific journal of the Collegium Internationale Neuropsychopharmacologicum (CINP)*, 2014. **17**(1): p. 149-155.
70. Parida, P., et al., *In-silico protein ligand interaction study of typical antipsychotic drugs against dopaminergic D2 receptor*. *International Journal of Pharmacy and Pharmaceutical Sciences*, 2013. **5**(2): p. 183-189.
71. Reismann, S. and G. Lee, *Assessment of a five-layer laminate technique to measure the saturation solubility of drug in pressure-sensitive adhesive film*. *J Pharm Sci*, 2012. **101**(7): p. 2428-38.
72. Cremers, T.I., et al., *Development of a Rat Plasma and Brain Extracellular Fluid Pharmacokinetic Model for Bupropion and Hydroxybupropion Based on Microdialysis Sampling, and Application to Predict Human Brain Concentrations*. *Drug Metab Dispos*, 2016. **44**(5): p. 624-33.
73. *Langmuir adsorption isotherm*. Available from: www.chemistrylearning.com/langmuir-adsorption-isotherm/.
74. Langmuir, I., *THE ADSORPTION OF GASES ON PLANE SURFACES OF GLASS, MICA AND PLATINUM*. *Journal of the American Chemical Society*, 1918. **40**(9): p. 1361-1403.
75. Baird, C.L., E.S. Courtenay, and D.G. Myszka, *Surface plasmon resonance characterization of drug/liposome interactions*. *Analytical Biochemistry*, 2002. **310**(1): p. 93-99.
76. A.V, Y., et al., *Stability Aspects of Liposomes*. *Indian Journal of Pharmaceutical Education and Research*, 2011. **45**(4): p. 402 - 413.
77. Crommelin, D.J.A., G.J. Fransen, and P.J.M. Salemink, *Stability of Liposomes on Storage*, in *Targeting of Drugs With Synthetic Systems*, G. Gregoriadis, J. Senior, and G. Poste, Editors. 1986, Springer US: Boston, MA. p. 277-287.
78. Hu, M., et al., *Design Principles for Nanoparticles Enveloped by a Polymer-Tethered Lipid Membrane*. *ACS Nano*, 2015. **9**(10): p. 9942-9954.
79. Kang, J.H. and Y.T. Ko, *Lipid-coated gold nanocomposites for enhanced cancer therapy*. *Int J Nanomedicine*, 2015. **10 Spec Iss**: p. 33-45.
80. McFarland, A.D., et al., *Color My Nanoworld*. *Journal of Chemical Education*, 2004. **81**(4): p. 544A-544A.
81. Zhao, P., N. Li, and D. Astruc, *State of the art in gold nanoparticle synthesis*. *Coordination Chemistry Reviews*, 2013. **257**(3-4): p. 638-665.
82. Sau, T.K., et al., *Size controlled synthesis of gold nanoparticles using photochemically prepared seed particles*. *Journal of Nanoparticle Research*, 2001. **3**(4): p. 257-261.
83. Kumar, A., et al., *Investigation into the Interaction between Surface-Bound Alkylamines and Gold Nanoparticles*. *Langmuir*, 2003. **19**(15): p. 6277-6282.